STUDIES OF THE CIRCULAR POLARISATION OF NUCLEAR GAMMA RAYS

Thesis

Submitted by

RONALD D.L. MACKIE, B.Sc.,

for the degree of

Doctor of Philosophy

University of Edinburgh,

September, 1968.

C O N T E N T S

C O N T E N T S (Contd.)

C O N T E N T S (Contd.)

C O N T E N T (Contd.)

INTRODUCTION

Study of the laws of the β-interaction has been intensive since Fermi's original theory formulated in 1934[1]. Since 1956, however, the overthrow of parity conservation in weak interactions has increased the number of β-decay observables, and the interaction has been established as being V - A. In particular, the correlation between the direction of a β-particle and the circular polarisation of a γ ray emitted after the β-decay has provided valuable information about the laws of β-decay.

With the basic form of the β-interaction established as V - A, it is now possible to use the measurements on β-decay to evaluate the nuclear matrix elements involved. The importance attached to work on β-decay has therefore swung away somewhat from the study of the basic β-interaction, towards the investigation of nuclear structure.

The purpose of this thesis is to investigate the measurement of the β-circularly polarised correlation by the transmission technique, in general, and, in particular, to measure this correlation for the highest energy β group emitted by Eu^{152}. The relevance of this measurement to the study of the structure of the Eu^{152} nucleus is discussed in Chapter 3, while Chapters 1 and 2 provide a brief theoretical background and the glossary of terms necessary to approach Chapter 3.

CHAPTER 1

A BRIEF SURVEY OF β-DECAY THEORY

1.1 The Fermi Theory of β-Decay

The phenomenon of β-decay is a weak interaction between four fermions, and its three observable effects ($\beta^{\pm}$ emission) and orbital electron capture) can be represented by the general equation

$$n + \nu \longleftrightarrow p + e^{-} \quad .$$

Although β radioactivity had been recognised at the close of the last century, the elucidation of the basic processes above required Pauli's neutrino hypothesis (1931) and the discovery of the neutron (1932). From this qualitative description Fermi developed in 1934[1] the standard theory of β-decay by analogy with quantum electrodynamics.

The electrodynamic interaction can be represented by a Hamiltonian energy density of the form

$$H_{e.m.} = j_{\alpha} A_{\alpha}$$

where A_{α} $(\bar{A}, \frac{i\phi}{c})$ is the four-vector potential of the electromagnetic field, and $j_{\alpha}(\bar{J}, ic\rho)$ is the four-vector current density interacting with A_{α}. Fermi, regarding β-decay as also stemming from the interaction of two polar four-vector currents, replaced A_{α} and j_{α} with j_{μ}, the lepton current, and J_{μ}, the nucleon current, in order to obtain the β-interaction Hamiltonian density

$$H_V = g_V(\bar{\psi}_P \gamma_\mu \psi_n)(\bar{\psi}_{e^-} \gamma_\mu \psi_\nu) + h.c.$$

where g_V is the coupling constant for the β-interaction (replacing the charge e in the electrodynamic case), the ψ's are the fermion wave functions

$\bar{\psi} = \psi^\dagger \gamma_4$ ($\psi^\dagger$ being the complex conjugate of ψ),

$\gamma_\mu(-i\beta\bar{\alpha}, \beta)$ are the usual Dirac matrix operators constructed from the Dirac matrices $\bar{\alpha}$ and β.

The hermitean conjugate term "h.c." represents positron emission.

Since Fermi's original paper, the theory of β-decay has widened to include all possible couplings of the fermion fields consistent with leading to a relativistically invariant theory. The most general Hamiltonian could then be expressed as a linear combination of contributions from the five possible couplings; scalar S, polar vector V, tensor T, axial vector A, and pseudoscalar P, each with its own complex coupling constant. Derivative couplings introduced by Konopinski in 1935[2,3] were soon found to give results which disagreed with experiment, and were discarded. The experimental work which followed was mainly concerned with finding the magnitudes of the coupling constants.

1.2 Modifications to Fermi's Theory

The suggestion of Lee and Yang in 1956[4] that parity is not conserved in weak interactions complicated the problem by allowing the introduction of pseudoscalar terms into the Hamiltonian, which became of the form

$$H_\beta = \sum_i C_i(\bar{\psi}_P O_i \psi_n)(\bar{\psi}_e O_i \psi_\nu) + \sum_i C_i'(\bar{\psi}_P O_i \psi_n) \cdot(\bar{\psi}_e O_i \gamma_5 \psi_\nu) + \text{h.c.}$$

where i = S, V, T, A, P.

C_i are the parity conserving coupling constants.

C_i' are the parity non-conserving coupling constants.

O_i are operators which can be expressed in terms of the γ's.

$\gamma_5 = \gamma_1\gamma_2\gamma_3\gamma_4$.

There now arises the possibility of interferences between the scalar and pseudoscalar terms in this Hamiltonian, giving rise to new observables.

The stimulus of Lee and Yang's startling suggestion led to great experimental activity which, as well as verifying the non-conservation of parity in weak interactions, whittled down the number of participating couplings to V and A within two or three years.

The interaction, then, has been found to be expressible as the coupling of two four-vector currents, and the essentials of Fermi's original formulation still hold. The

Hamiltonian density can be conveniently written

$$H_\beta(x) = \frac{G_\beta}{\sqrt{2}} \left[J_\mu(x)\, j_\mu(x) + \text{h.c.} \right]$$

G_β is a constant determining the strength of the coupling.

The experimental findings since Lee and Yang's parity non-conservation hypothesis have, however, led to modifications in the assumptions underlying Fermi's original theory. Key experiments, on the helicity of β particles, the electron-neutrino angular correlation, and the helicity of the neutrino, which had established that only V and A couplings need be considered, also showed that the particles participate in the β-interaction through their left-handed components only, and the antiparticles through their right-handed components. Any fermion state ψ can be resolved into its left-handed and right-handed components ϕ^+ and ϕ^- by means of the operators $\frac{1}{2}(1 + \gamma_5)$ and $\frac{1}{2}(1 - \gamma_5)$ respectively.

$$\psi = \phi^+ + \phi^- = \tfrac{1}{2}(1 + \gamma_5)\psi + \tfrac{1}{2}(1 - \gamma_5)\psi \ .$$

The lepton four-current j_μ then takes on the form

$$\bar{\psi}_e - \tfrac{1}{2}(1 + \gamma_5)\gamma_\mu \tfrac{1}{2}(1 + \gamma_5)\psi_\nu$$

which becomes

$$\bar{\psi}_e - \gamma_\mu \tfrac{1}{2}(1 + \gamma_5)\psi_\nu$$

when the properties of the γ matrices are taken into account. This lepton current contains equally strong polar

and axial vector parts, which can be considered to be a consequence of the two-component theory of the neutrino, which postulates only two (rather than four) neutral lepton states:- negative helicity (left-handed) neutrinos and positive helicity (right-handed) antineutrinos.

1.3 Nucleon Current

The nucleon current is so much more complicated in form due to the strong interactions experienced by these particles that an explicit expression for J_μ has not yet been obtained. It is convenient, however, to separate J_μ into its polar and axial vector parts:

$$J_\mu = J_\mu^{(V)} + J_\mu^{(A)} \quad .$$

The most general operators $O_\mu^{(V)}$ and $O_\mu^{(A)}$ which generate $J_\mu^{(V)}$ and $J_\mu^{(A)}$, and which lead to the correct Lorentz transformation properties of these currents, contain three terms in each. The three terms in $O_\mu^{(V)}$ are: the usual polar vector operator $i\gamma_\mu$, a "weak magnetism" term and an induced scalar term. $O_\mu^{(A)}$ consists of: the usual axial vector operator $i\gamma_\mu\gamma_5$, an induced pseudoscalar term and an induced tensor interaction.

When the β-decay Hamiltonian is constructed from these operators and the lepton current j_μ, noting that for β-decay the momentum transfer is small (a few $\frac{\text{MeV}}{c}$), it is found that all the operators except $i\gamma_\mu$ and

$i\gamma_\mu\gamma_5$ make very small contributions. Then separation of the temporal and spatial components of the currents leads to the following expression for the β^--decay Hamiltonian for a nucleus containing A nucleons:

$$H_{\beta^-} = \sqrt{2}\, G_\beta \sum_{a=1}^{A} \left\{ \left[C_V - C_A \gamma_5^a \right] j_4(x_a) - i \left[C_V \bar{\alpha}^a + C_A \bar{\sigma}^a \right] \cdot \bar{j}(x_a) \right\} \tau_a^+$$

where C_V and C_A are the relative strengths of the polar and axial vector couplings, $\bar{\sigma}$ is the spin operator $-\gamma_5\bar{\alpha}$, and τ_a^+ is the isospin ladder operator, which formally transforms the a-th nucleon from a neutron into a proton.

The hermitean conjugate of the above Hamiltonian expresses the β^+-decay interaction.

1.4 β-decay Matrix Elements

The β^--decay probability of a nucleus is proportional to the square of the matrix element

$$M_{\beta^-} = \langle \psi_f, \psi_{e^-}, \psi_{\bar{\nu}} \left| H_{\beta^-} \right| \psi_i \rangle$$

where ψ_i and ψ_f are the initial and final nuclear states. The leptonic part of M can be calculated with considerable precision, whereas inadequate knowledge of nuclear wave functions makes estimates of the nuclear part very uncertain. For this reason, the nuclear β moments are usually evaluated experimentally.

The lepton current appearing in M_{β^-} is evaluated

using, for the electron, solutions of the Dirac equation for a particle in a Coulomb field, and for the neutrino, free particle solutions of the Dirac equation. This current is usually expressed as a series expansion in powers of $\bar{p}.\bar{r}$, where $\bar{p}$ is the total lepton momentum, the coefficients involving the radial wave functions of the electron, which must be evaluated at the position of the transforming nucleon. Evaluating these wave functions at the nuclear radius, to avoid the singularity at $r = 0$, does not introduce appreciable errors, except in the case of heavy nuclei. Very accurate evaluations of the lepton current take account of finite nuclear size effects, and corrections to the simple Coulomb field of the nucleus due to screening by atomic electrons.

From the expansion of j_μ in powers of $\bar{p}.\bar{r}$, or $\frac{r}{\lambda}$ where λ is the lepton wave length, there arises a series of matrix elements of $H_{\beta-}$ between given initial and final nuclear states. Fortunately, however, the character of nuclei and leptons allows the termination of this series after a few terms to be a justifiable approximation. For nuclear β-decay, energy releases are such that the lepton wavelengths are considerably greater than the dimensions of nuclei; in fact $\frac{r}{\lambda}$ is of order $\frac{1}{10}$. Thus the terms in the expansion of j_μ rapidly decrease in magnitude.

As regards nuclear states, it is important to realise that the operators 1, $\bar{\sigma}$, $\bar{\alpha}$ and γ_5 produce matrix elements of order of magnitude 1, 1, v/c and v/c respectively, where v is the nucleon speed and usually of

order $\frac{c}{10}$.

The resulting matrix elements of H_β^- are then conveniently classed according to their order of magnitude and the selection rules for nuclear spin and parity which must be obeyed if they are to be non-zero. This classification leads naturally to lists of the matrix elements which can contribute to the various decays - allowed, first forbidden etc.

1.5 The Allowed Approximations

The matrix elements of H_{β^-} of largest magnitude arise from the operators of order unity, i.e. 1 and $\bar{\sigma}$, coupled with the term $(\frac{r}{\lambda})^0$ in the expansion of j_μ. The two matrix elements which survive in this approximation are:

Selection Rules.

$M_V^{(0)} = C_V \langle f | \sum_{a=1}^{A} \tau_a^+ | i \rangle$ often written $\int 1$ — $\Delta I = 0$; $\Delta \pi$ = no

$M_A^{(0)} = C_A \langle f | \sum_{a=1}^{A} \bar{\sigma}_a \tau_a^+ | i \rangle$ often written $\int \bar{\sigma}$ — $\Delta I = 0, \pm 1$; $\Delta \pi$ = no (no $0 \rightarrow 0$) .

These, then, are the matrix elements which can make the largest contribution to allowed β^--decay.

1.6 First Forbidden Transitions

The matrix elements of H_β- one order of magnitude lower than those of allowed decay can be similarly collected and tabulated.

Matrix Element	ΔJ	Order of Magnitude
$C_A \int \bar{\sigma}.\bar{r}$	0	αZ
$C_A \int i\gamma_5$	0	v_n/c
$C_V \int \bar{r}$	$0, \pm 1$ (no $0 \to 0$)	αZ (where α is the fine structure constant $\frac{1}{137}$.)
$C_V \int i\bar{\alpha}$		v_n/c
$C_A \int i\bar{\sigma}\times\bar{r}$		αZ
$C_A \int B_{ij} = C_A \int (\sigma_i r_j + \sigma_j r_i - \frac{2}{3}\delta_{ij}\bar{\sigma}.\bar{r})$	$0, \pm 1, \pm 2$ (no $0 \to 0$, $\frac{1}{2} \to \frac{1}{2}$, $1 \to 0$)	r

$\Delta\pi$ = yes for all elements.

1.7 The "Normal" Approximation

Order of magnitude estimates show that β-decay calculations which retain only the lowest contributing power of r/λ in the lepton current expansion should be adequate in most cases. This procedure is known as the normal approximation.

1.8 The Coulomb Approximation

For nuclei of large Z, the influence of the Coulomb field on the electron wave functions becomes important, and the magnitudes of the terms in the lepton current expansion can become determined by the term containing the largest power of the parameter $\xi = \frac{\alpha Z}{2R}$, which is a measure of the Coulomb energy of the electron as it leaves the nucleus of radius R. For a medium-heavy nucleus, ξ is of order 10, whereas the β end-point energy W_o is of the order of a few, and so the Coulomb energy ξ is much greater than the final lepton kinetic energy. The ξ, or Coulomb, approximation amounts to making the assumption $\xi \gg W_o$, which can also be written $\alpha Z \gg \frac{R}{\lambda}$, and thereafter discarding all but the highest power of ξ (ξ^2) which appears in the lepton functions. Weidenmüller[5] discusses the Coulomb approximation in full, and illustrates his arguments by giving expressions for the observables in the form of power series in ξ.

In this approximation, first forbidden decays with $\Delta J = 0, \pm 1$ are expected to display energy and angular characteristics identical with those of allowed decays. For example, the β-spectrum shape, for most first forbidden decays is indeed just the statistical shape of the allowed decays. The matrix element $\int B_{ij}$ does not contribute to a first forbidden decay for which the Coulomb approximation is valid; the other five matrix elements appearing in the form of two independent linear combinations

$$V = C_A \int i\gamma_5 + \xi C_A \int \bar{\sigma}.\bar{r} \quad , \text{ and}$$

$$Y = -C_V \int i\bar{\alpha} - \xi C_A \int i\bar{\sigma}\times\bar{r} + \xi C_V \int \bar{r} \quad .$$

Two measurements, for instance of ft value and β - circularly polarised γ angular correlation, give the magnitudes of these two combinations. The individual matrix elements cannot be measured in Coulomb approximation. To determine the matrix elements separately, therefore, the decays which show deviations from this approximation must be examined.

1.9 Deviations from the Coulomb Approximation

Several first forbidden decays with $\Delta J = 0$ or 1 deviate from the expectations of the Coulomb approximation by exhibiting characteristics of the unique ($\Delta J = 2$) first forbidden decays. Such decays have an abnormally high ft value, an energy dependent spectrum shape factor, and β-γ and β-circularly polarised γ angular correlations which are β energy dependent.

The validity of the approximation breaks down if the linear combinations of matrix elements appearing in the ξ^2 term in the lepton current expansion is small, or if the β end-point energy W_o is so large that ξ is no longer $\gg W_o$. The combinations of matrix elements may be small if either a) they almost cancel each other (the "cancellation effect") or b) the matrix elements corresponding to $\Delta J = 0$ and 1 are very much smaller than

the element $\int B_{ij}$ which is solely responsible for unique decays. To explain this behaviour, a nuclear model must be sought which introduces a selection rule inhibiting contributions from matrix elements other than $\int B_{ij}$. This is the so-called "selection rule effect".

1.10 Present Status of the Theory

When the many β-decay experiments are analysed according to the theory as outlined here, then there emerges strong evidence for the application of the following principles to β-decay.

		Consequences	
a)	Lepton conservation.	No neutrinoless double β-decay.	
b)	Two-component theory of the neutrino	Simplest description of neutrino behaviour	Zero neutrino mass
c)	Time-reversal invariance	Real coupling constants.	
d)	A V - A interaction only		
e)	Conserved vector current (CVC) hypothesis, $\frac{\partial J_\mu^{(V)}}{\partial x_\mu} = 0$		
f)	The interaction is local	No intermediate vector boson exists.	

The constants appearing in the theory have been measured to be

$$G_\beta C_V = (1.4149 \pm 0.0022) \times 10^{-49} \text{ erg. cm.}^3 ;$$

$$\frac{C_A}{C_V} = - 1.18 \pm 0.02 \quad .$$

The CVC theory (so-called by analogy with electromagnetic theory where the conservation of charge leads to the continuity equation $\frac{\partial(\bar{J}, ic\rho)_\mu}{\partial x_\mu} = 0$, where $(\bar{J}, ic\rho)$ is the four-current density) postulates that the vector coupling strength is conserved, even during virtual transitions of the β-transforming nucleons. In other words, the CVC theory implies a weak pion-lepton coupling. The fact that $|C_A| \neq |C_V|$, taken along with the CVC hypothesis, means that only the axial vector coupling has to be renormalised to take account of the strong nucleon-pion coupling.

An important deduction from CVC theory is that there is a relationship between the matrix elements $\int i\bar{\alpha}$ and $\int \bar{r}$, which reduces the number of such parameters involved in first forbidden β transitions from 6 to 5, in general.

CHAPTER 2

β-CIRCULARLY POLARISED γ CORRELATION

2.1 Definition of Photon Circular Polarisation

In the literature of physics there are two common ways of describing the circular polarisation of electromagnetic radiation, the choice of method usually depending upon the energy involved. At low energies, where the electromagnetic field description is largely according to the classical wave picture, and energy is measured by frequency or wavelength, circular polarisation is usually described as a rotation, about the direction of wave propagation, of the vector representing the electric field associated with the radiation. On the other hand, at the high energy end of the electromagnetic spectrum, it is more common and useful to use quantum concepts. Here, the important characteristics of electromagnetic radiation (or photon beam in quantum terminology) are momentum and angular momentum. That the circular polarisation of photons is associated with their angular momentum has been beautifully demonstrated experimentally in the optical region by Beth[6], who measured directly the angular momentum carried by a beam of circularly polarised light.

The circular polarisation of nuclear γ rays is usually described by considering the projection of the spin of the photon on to its direction of momentum; with right circular polarisation corresponding to parallel spin and momentum,

the projection $\mu = +1$, and left circular polarisation corresponding to anti-parallel spin and momentum, the projection $\mu = -1$. The photon, although having a spin of one, has only the two possibilities $\mu = \pm 1$; the projection $\mu = 0$ is ruled out by the transverse nature of its electromagnetic field. If I_R and I_L are the intensities of photons with right and left circular polarisation respectively, then the degree, P_c, of circular polarisation of the γ ray beam is given by

$$P_c = \frac{I_R - I_L}{I_R + I_L} \quad .$$

2.2 Production of Circularly Polarised Photons

The production of a circularly polarised γ ray beam requires a polarised source, and simple angular momentum considerations show that, in general, P_c depends upon the angle between the photon momentum and the polarisation axis of the source.

As a consequence of the non-conservation of parity in weak interactions, the leptons emitted in β-decay are longitudinally polarised, and, therefore, the recoiling daughter nuclei can be partially polarised relative to the direction of emission of the β particles. If these recoiling polarised nuclei emit γ rays, then these γ rays may be circularly polarised, with P_c depending, in general, upon the characteristics of the β and γ transitions, and upon the angle θ between the β and γ momenta.

If, as in allowed Fermi β-transitions, the lepton field carries off zero total angular momentum, then the recoil nuclei cannot have their angular momenta polarised. Any subsequent γ-ray cannot, therefore, be circularly polarised. In allowed Gamov-Teller transitions, however, the leptons carry off one unit of angular momentum, and since the leptons are longitudinally polarised, so also will be, in general, the daughter nuclei and any subsequent γ-rays. These simple deductions from the Law of Conservation of Angular Momentum are very clearly developed by Lipkin[7].

2.3 The β-circularly Polarised γ Correlation

The β-γ angular correlation observed with a γ detector that responds only to γ radiation of circular polarisation μ, can be written,

$$\omega(\theta, \mu) = \sum_k \mu^k A_k(\beta) A_k(\gamma) P_k(\cos\theta)$$

where the coefficients

$A_k(\beta)$ depend upon the details of the β process,

$A_k(\gamma)$ " " " " " γ " ,

the $P_k(\cos\theta)$ are Legendre polynomials,

the summation over k extends from zero up to $(2\ell+1)$ where ℓ is the order of forbiddenness of the β-decay.

The electromagnetic γ processes are well understood,

and so the $A_k(\gamma)$ are known. These coefficients depend upon the spins of the nuclear levels involved in the γ transition, the multipolarities of the emitted γ radiation, and the mixing ratio of the contributing multipoles. The coefficients $A_k(\beta)$, on the other hand, depend upon the β particle energy W, bilinear products of the nuclear matrix elements contributing to the β-decay, the radial wave functions of the β particle, the spins of the participating nuclear states, and the coupling constants of the β interaction.

Contracting the notation, the correlation can be written

$$\omega(\theta, \mu, W) = \sum_k \mu^k A_k(W) P_k(\cos\theta)$$

where the known $A_k(\gamma)$ are incorporated in the coefficients $A_k(W)$. For allowed β-decays the sum contains the two terms corresponding to $k = 0$ and $k = 1$, whereas for first forbidden decays the k summation contains the four terms from zero to three. The terms involving polynomials of odd degree are detected only when a γ detector which is sensitive to circular polarisation is used.

The degree of polarisation of the γ-rays then becomes

$$P_c(\theta, W) = \frac{\omega(\theta, +1, W) - \omega(\theta, -1, W)}{\omega(\theta, +1, W) + \omega(\theta, -1, W)}$$

$$= \frac{A_1(W)P_1(\cos\theta) + A_3(W)P_3(\cos\theta)}{A_0(W) + A_2(W)P_2(\cos\theta)}$$

$A_o(W)$ is simply the β-spectrum correction factor $C(W)$;
$A_2(W)$ is obtained from the β-γ directional correlation;
$A_1(W)$ and $A_3(W)$ are then obtained from measurements of P_c.

The coefficients $A_k(W)$ are bilinear functions of the nuclear matrix elements contributing to the β-decay. In particular, $A_2(W)$ can be expressed in terms of ε, the anisotropy coefficient of the β-γ directional correlation, and $A_3(W)$ is a function of the matrix element $\int B_{ij}$. However, first forbidden decays exhibiting the allowed spectrum shape lead to little or no anisotropy ε in their direction correlation, and have a negligible contribution from $\int B_{ij}$. In these cases, therefore, the correlation function ω has an angular dependence which is similar to that of allowed decays.

On the other hand, P_c for a β decay which involves the maximum change of angular momentum allowable in any class of forbiddenness, e.g. $\Delta I = \pm 1$ for allowed and $\Delta I = \pm 2$ for first forbidden decays, does not depend upon the matrix elements, and can therefore be calculated exactly. The reason for this is that only one matrix element makes a significant contribution to such a decay ($\int \vec{\sigma}$ in allowed, and $\int B_{ij}$ in first forbidden), and this matrix element cancels throughout the expression for P_c.

2.4 Perturbed Angular Correlations

Angular correlations can be perturbed if the intermediate nuclear state (in the case of $\omega(\theta, \mu, W)$ this is the β-decay excited daughter nucleus) has a sufficiently strong interaction with extra-nuclear fields through its magnetic dipole moment or electric quadrupole moment. This attenuation of the correlation is appreciable when the lifetime, τ, of the intermediate state is long, and when the interaction energy, ΔE, in this state is large. A rough criterion for the threshold of importance of this effect is given by

$$\Delta E \,.\, \tau > \hbar ,$$

although the critical value of $\Delta E.\tau$ will depend upon the sensitivity of the particular apparatus used.

CHAPTER 3

NUCLEAR MATRIX ELEMENTS IN FIRST FORBIDDEN β-DECAYS

3.1 General

Beta-decay observables are analytically expressed by homogeneous bilinear functions of the nuclear matrix elements. As has been pointed out in Chapter 1, accurate theoretical calculations of these matrix elements are usually impossible because of the lack of precise knowledge of the nuclear wave functions. These matrix elements are, therefore, usually treated as parameters to be evaluated experimentally.

Since only two matrix elements contribute significantly to allowed β-decays, their values for a particular transition are obtained relatively easily by means of a few (at least two) well chosen experiments. For a first forbidden decay, however, up to six matrix elements can be important, in general; and so their evaluation requires the careful measurement of several (six or more) β-decay observables. Unique transitions, however, depend upon only one matrix element.

3.2 Non-unique First Forbidden Decays

Most non-unique first forbidden β transitions exhibit features similar to those of allowed transitions; including a statistical spectrum shape and a small β-γ directional

correlation coefficient. This behaviour has been theoretically described by the Coulomb approximation. Since, in this approximation, the matrix elements appear only in the linear combinations

$$V = C_A \int i\gamma_5 + \xi C_A \int \underline{\sigma}.\underline{r} \quad \text{for rank 0}$$

and $$Y = -C_V \int i\underline{\alpha} - \xi C_A \int i\underline{\sigma} \times \underline{r} + \xi C_V \int \underline{r} \quad \text{for rank 1}$$

(the matrix element $\int B_{ij}$ is rendered insignificant by this approximation), it is impossible to measure them individually.

Several non-unique first forbidden decays, however, display spectra which deviate from the statistical shape, and when these β transitions are followed by a γ ray, the $\beta - \gamma$ directional correlation shows a large anisotropy. These decays are also characterised by an abnormally high log ft value which ran range from about 9 to 12, compared with the more usual log ft values of about 7 for non-unique and about 8 to 10 for unique first forbidden transitions.

Considerable research work has been devoted to measuring nuclear matrix elements, in order to test proposed nuclear models, and in the case of first forbidden β-decays attention has been focussed on the $\Delta I = 1$ transitions which show the above behaviour. The reasons for this concentration of effort are that in these decays only four matrix elements (those of ranks 1 and 2) can contribute

and also, because the Coulomb approximation appears to be invalid for these transitions, the possibility arises of evaluating individual matrix elements. The four observables usually used in the measurement of these four matrix elements are the comparative half-lives of the transitions, the energy dependence of the spectrum shape factors, the energy dependence of the $\beta - \gamma$ directional correlations and the energy or angular dependence of the β-circularly polarised γ correlations.

The proposed explanation of the fact that these transitions have nearly a "unique" behaviour is that there is either a relative predominance of the second rank matrix element $\int B_{ij}$, due to some selection rule effect, or else there takes place a cancellation of some linear combination of the matrix elements of tensor rank 1. Kotani[7] has discussed these possibilities, and has drawn attention to the fact that a measurement of the angular or energy dependence of the β-circularly polarised γ correlation is one of the most sensitive ways of distinguishing between the occurrence of the selection rule and cancellation effects. It was to help to clarify this point that the present experiment on circular polarisation was undertaken.

3.3 The Nuclide Eu^{152}

The highest energy β group in 12.4 year Eu^{152} was chosen for this study because it is a first forbidden,

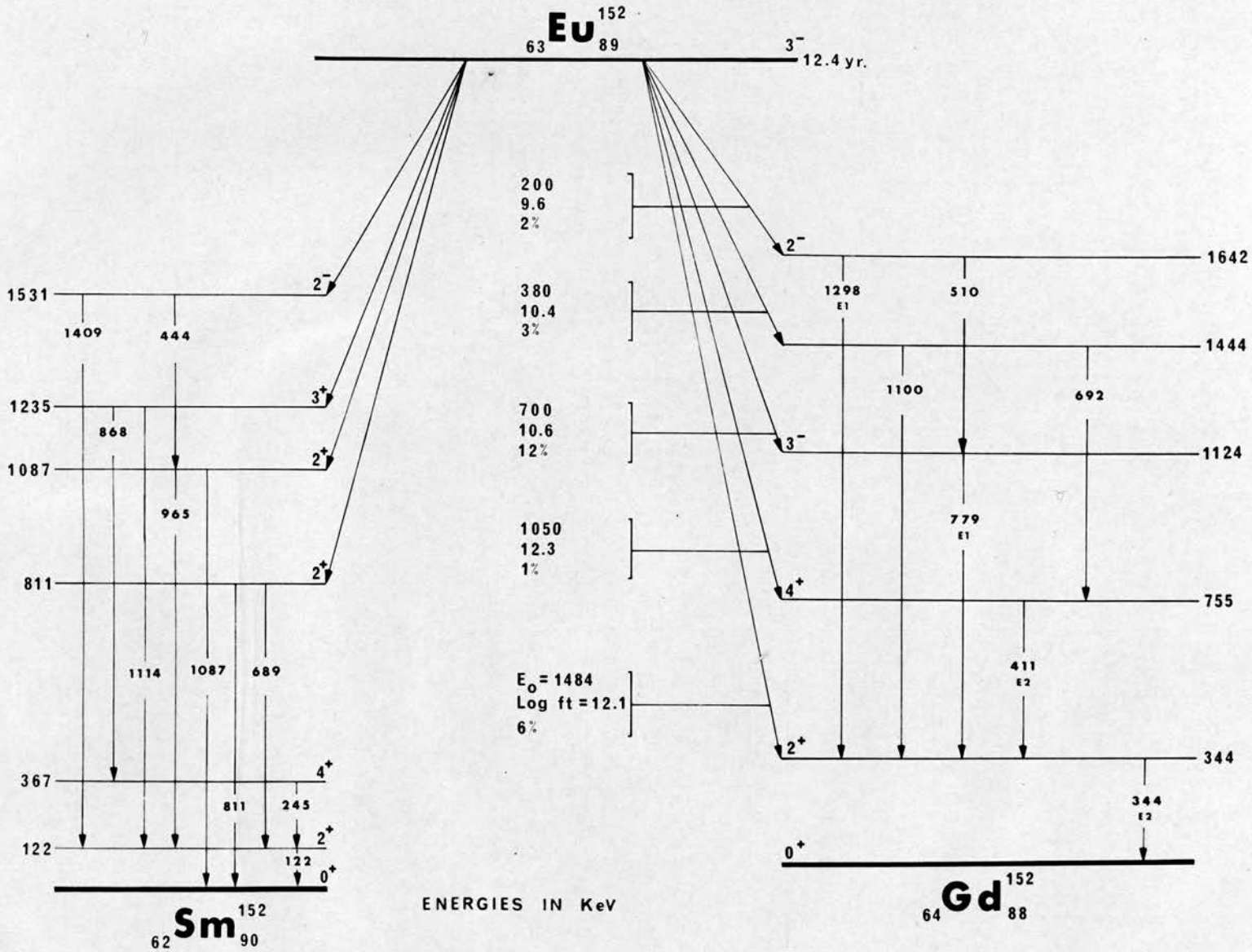
Eu 152
63 89
3⁻
12.4 yr.
200
9.6
2%
380
10.4
3%
700
10.6
12%
1050
12.3
1%
E0 = 1484
Log ft = 12.1
6%
2⁻
1642
1298
E1
510
1444
1100
692
3⁻
1124
779
E1
4⁺
755
411
E2
2⁺
344
344
E2
0⁺
1531
2⁻
1409
444
1235
3⁺
868
1087
2⁺
965
811
2⁺
1114
1087
689
367
4⁺
811
245
122
2⁺
122
0⁺
Sm 152
62 90
ENERGIES IN KeV
Gd 152
64 88

FIGURE 3.1

non-unique, $\Delta I = 1$, transition which is not satisfactorily described by the Coulomb approximation, although in this case $\xi = {}^{\alpha Z}/_{2R}$ is 14.1. The decay scheme[8] is shown in Fig. 3.1. It is a well studied transition, and from measurements, of the four usual observables, Lipnik and Sunier[9] and Alexander and Steffen[10] have calculated values for the matrix elements involved. It is found that the values of all four are inhibited, with the tensor-type element $\int B_{ij}$ much less inhibited than the other three matrix elements, which are of vector-type.

Lipnik and Sunier find that the experimental evidence collected for Eu^{152} is consistent with a theoretical description of this decay based on the so-called "Modified B_{ij} Approximation", in which only the parameters Y and $\int B_{ij}$ are retained. In addition, the values of the matrix elements extracted by Alexander and Steffen show that, since all the vector-type elements are reduced more than the tensor type element $\int B_{ij}$, a "selection rule effect" must be operating to favour the emission of a lepton field which carries away two units of angular momentum, at the expense of emission of a field carrying one unit of angular momentum.

The slowness of the decay of Eu^{152} can be explained when one examines the level schemes of its daughters. The level scheme of Gd^{152} is characteristic of vibrational states of a spherical nucleus, and so the equilibrium shape of the Gd^{152} nucleus is almost certainly spherical;

whereas, on the other hand, the level scheme of Sm^{152}, is typical of a deformed nucleus. So it appears that the nuclei Sm^{152}, Eu^{152} and Gd^{152} are in a transition region where the nature of the levels is changing rapidly from nuclide to nuclide, which will lead to a poor overlap of the wave functions appearing in the nuclear matrix elements. These matrix elements will therefore be small, and the corresponding transitions slow; which is shown by the fact that the log ft values for <u>all</u> the transitions from the ground state of Eu^{152} are abnormally large.

This quantitative discussion gives a plausible explanation of how it is that all the nuclear matrix elements for β transitions from Eu^{152} are reduced; it cannot supply reasons for the relative dominance of the $\int B_{ij}$ matrix element. To explain this "selection rule effect", a more detailed knowledge of the structure of the ground state of Eu^{152} is necessary.

CHAPTER 4

MEASUREMENT OF THE CIRCULAR POLARISATION OF GAMMA RAYS

4.1 Introduction

Although the measurement of the circular polarisation of γ rays provided important evidence for the non-conservation of parity in β-decays, the technique had been developed for other purposes in the years immediately preceeding the Lee and Yang hypothesis of 1956. Several sources of polarised γ-rays were known, and several measurements were made.

O. Halpern[11] in 1951 suggested that the circular polarisation of the γ-rays from polarised n - γ reactions could be measured using Compton scattering. Clay and Hereford[12] in 1952 used Compton scattering from ferromagnetic foils to study the polarisation of annihilation photons; and in 1955 Wheatley et al.[13] measured the circular polarisation of γ-rays emitted from a Co^{60} source polarised at very low temperatures.

The measurement of the circular polarisation of γ-rays is usually performed by scattering the γ-rays from polarised electrons. This technique relies upon the existence in the cross-section for Compton scattering of a term which depends upon the relative orientation of the spins of the γ-ray and the scattering electron. The total Compton cross-section can be written

$$\sigma = \sigma_0 + \sigma_0 \cos \psi$$

where

$$\frac{\sigma_o}{2\pi r_o^2} = \frac{1 + k_o}{k_o^2}\left\{\frac{2 + 2k_o}{1 + 2k_o} - \log\frac{1 + 2k_o}{k_o}\right\} + \frac{\log(1 + 2k_o)}{2k_o} - \frac{1 + 3k_o}{(1 + 2k_o)^2}$$

is the well known expression for unpolarised photons and electrons,

$$\frac{\sigma_o}{2\pi r_o^2} = \frac{1 + 4k_o + 5k_o^2}{k_o(1 + 2k_o)^2} - \frac{(1 + k_o)\log(1 + 2k_o)}{2k_o^2}$$

is the part of the cross-section sensitive to γ-ray circular polarisation and electron spin;

ψ is the angle between the momentum of the incident photon and the spin of the scattering electron;

r_o is the classical radius of the electron $= \frac{e^2}{mc^2}$;

k_o is the energy of the incident photon in units of mc^2.

Fig. 4.1 shows $\sigma_c / 2\pi r_o^2$ as a function of k_o.

This polarisation-sensitive phenomenon has been developed into a measuring technique in a few different geometrical arrangements. One of the major difficulties of applying this phenomenon to the measurement of circular polarisation is obtaining a sufficiently dense assembly of polarised electrons to act as an efficient scatterer. Magnetised iron is a possible scatterer, although its polarisation detecting efficiency is low because only two of its twenty six electrons are polarised at saturation.

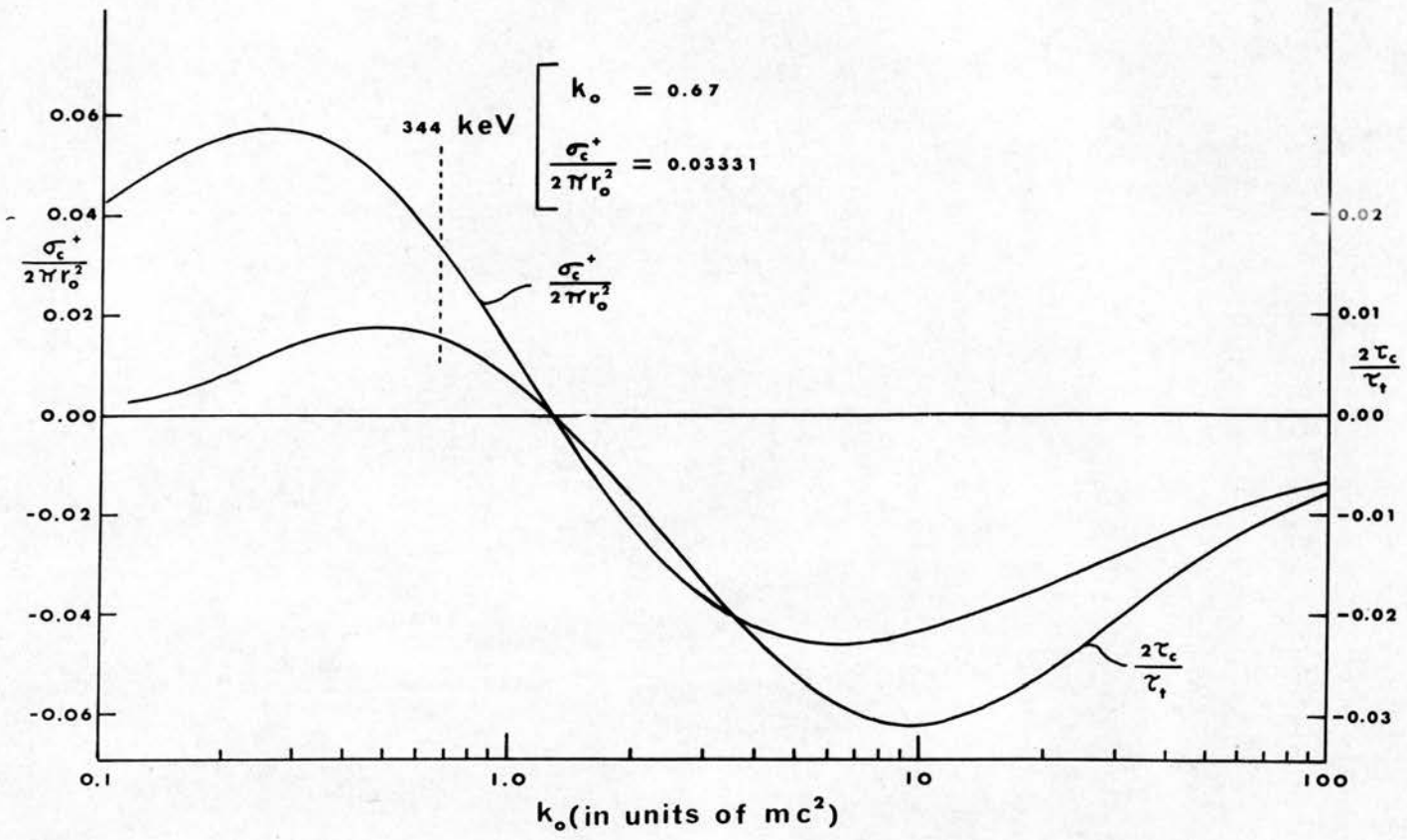
$k_o = 0.67$
$\frac{\sigma_c^+}{2\pi r_o^2} = 0.03331$
344 keV
$\frac{\sigma_c^+}{2\pi r_o^2}$
$\frac{2\tau_c}{\tau_t}$
0.06
0.04
0.02
0.00
-0.02
-0.04
-0.06
0.02
0.01
0.00
-0.01
-0.02
-0.03
0.1
1.0
10
100
k_o(in units of mc^2)

FIGURE 4.1

4.2 Forward Scattering Method

Forward scattering of γ-rays from magnetised iron is a well established technique for measuring circular polarisation, and the general features of a typical apparatus for investigating a $\beta - \gamma$ circular polarisation correlation are shown in Fig. 4.2. The asymmetry in the coincidence counting rate as the magnetisation $\bar{M}$ is reversed gives a measure of the circular polarisation of the γ-rays. The details of such a measurement will be given later when the experimental set-up used in the present work is described.

The first measurement of a $\beta - \gamma$ circular polarisation correlation was performed by Schopper[14] using this technique. The method has the advantage of providing a large solid angle for the γ-rays, but has the disadvantage that it is difficult to vary the angle between the β- and γ-rays. (See, for instance, Saigntignon[15]). Schopper has given full details of performing such an experiment, and has included a discussion of the corrections necessary to take account of finite geometry, photon absorption in the iron, and plural scattering.

4.3 Transmission Method

The measurement of the circular polarisation of γ-rays can also be carried out by transmitting them through magnetised iron. The first use of a transmission magnet was by Gunst and Page[16], who, in 1953, measured σ_c for

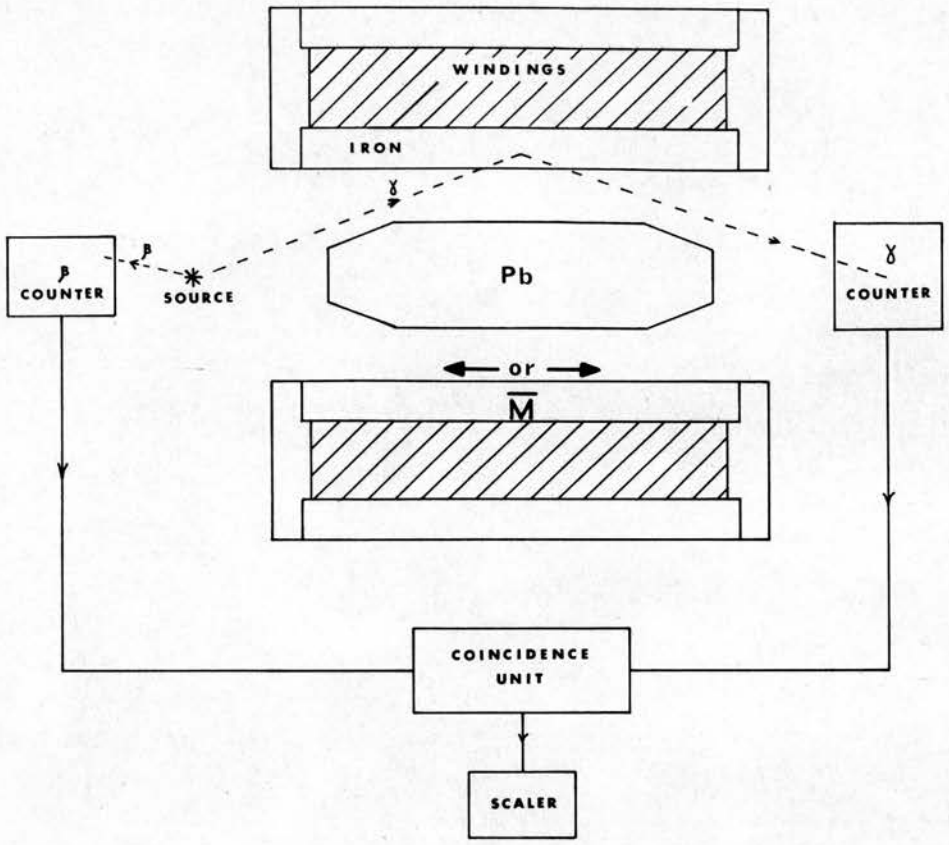

FIGURE 4.2

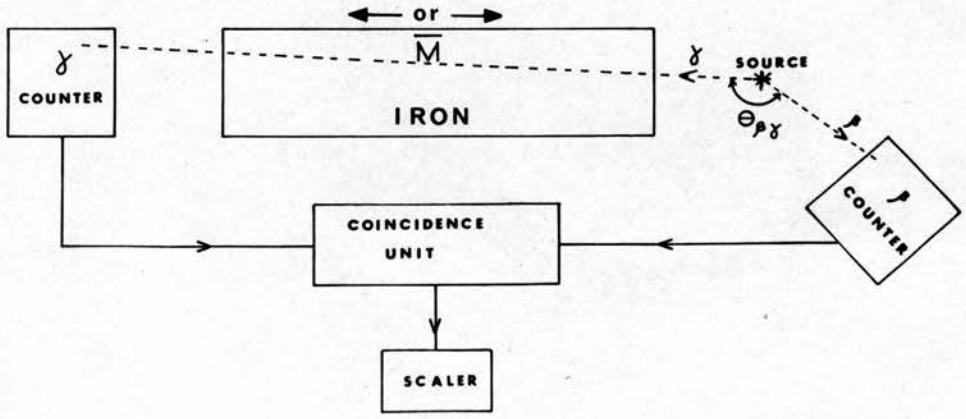

FIGURE 4.3

2.62 MeV γ-rays. Lundby et al.[17] were the first to apply this method to the measurement of a $\beta - \gamma$ circular polarisation correlation, and their results were published, only a few months after those of Schopper. Fig. 4.3 shows a simplified lay-out of a correlation experiment using the transmission method. As in the forward scattering technique, the measurement of the polarisation of the γ-rays consists of a determination of the asymmetry in the coincidence counting rate as the magnetisation is reversed.

The advantages of the transmission method over the forward scattering method are that the γ energy discrimination is superior (the γ lines are considerably broadened by scattering), and that the angle between the β- and γ-rays is more easily varied.

Since this was the technique chosen for the present work, it will be described in some detail.

4.4 Theory of the Transmission Method

Consider a beam of photons, of energy k_o, propagating along the x direction. If the beam consists of N^+ photons with spin parallel to momentum and N^- with spin and momentum antiparallel, then the circular polarisation P_c of the beam is given by

$$P_c = \frac{N^+ - N^-}{N^+ + N^-} \quad .$$

Let the transmission iron contain n^+ electrons per unit volume with their spins parallel to the x direction, and

n^- electrons per unit volume with their spins in the opposite direction. Due to end effects, the magnetisation of the iron will not be uniform, and the behaviour of $\bar{M}$ is indicated in Fig. 4.4. However, the spin of a polarised electron is antiparallel to $\bar{M}$, and so the angle ψ between the photon momentum and the electron spin is obviously a function of x.

If the Compton cross-section is written as

$$\sigma = \sigma_o + \sigma_c \cos\psi$$

the absorption of the photon beam can be expressed as

$$N^+(x+dx) = N^+(x) - (n^+ + n^-)\sigma_o N^+ dx - n^+\sigma_c \cos\psi(x) N^+ dx - n^-\left[-\cos\psi(x)\right]\sigma_c N^+ dx ,$$

$$N^-(x+dx) = N^-(x) - (n^+ + n^-)\sigma_o N^- dx - n^-\sigma_c \cos\psi(x) N^- dx - n^+\left[-\cos\psi(x)\right]\sigma_c N^- dx .$$

These equations can be contracted by introducing

$$N = N^+ + N^- \qquad P = N^+ - N^-$$

$$n = n^+ + n^- \qquad p = n^+ - n^- .$$

Therefore

$$\frac{dN}{dx} = -\sigma_o n(x) N(x) - \sigma_c \cos\psi(x) p(x) P(x)$$

$$\frac{dP}{dx} = -\sigma_c \cos\psi(x) p(x) - \sigma_o n(x) P(x) .$$

The only properties of the photon beam of interest here are

its intensity N and its circular polarisation $P_c = P/N$, and so the beam can be represented by the Stokes vector $\binom{N}{P}$, from which the linear polarisation components have been omitted. With this notation

$$\frac{d}{dx}\binom{N}{P} = -A(x)\binom{N}{P}$$

where $A(x)$ is the matrix $\sigma_o n(x)\begin{pmatrix}1 & 0\\ 0 & 1\end{pmatrix} + \sigma_c \cos\psi(x)\, p(x)\begin{pmatrix}0 & 1\\ 1 & 0\end{pmatrix}$.

The equation for solution is now

$$\frac{d}{dx}\binom{N}{P} + A(x)\binom{N}{P} = 0 ,$$

which can be solved by introducing the integrating factor $e^{\int A(x)\,dx}$. Then

$$\frac{d}{dx}\left[e^{\int A(x)\,dx}\binom{N}{P}\right] = 0 \quad \text{integrates to}$$

$$e^{\int A(x)\,dx}\binom{N}{P} = \text{constant} = \binom{N_o}{P_o} , \quad \text{the original beam.}$$

$$\therefore \binom{N}{P} = e^{-\int A(x)\,dx}\binom{N_o}{P_o}$$

with $$\int A(x)\,dx = \begin{pmatrix}1 & 0\\ 0 & 1\end{pmatrix}\int_o^L \sigma_o n(x)\,dx + \begin{pmatrix}0 & 1\\ 1 & 0\end{pmatrix}\int_o^L \sigma_c \cos\psi(x)\, p(x)\, dx ,$$

where L is the length of the magnet. However $n(x)$, the number of electrons per unit volume of iron, may be assumed to be independent of x; and so

$$\int_o^L \sigma_o n(x)\, dx = \sigma_o nL .$$

Defining the magnetic length, L_m, of the magnet by

$$\sigma_c \, p \, L_m = \int_0^L \sigma_c \, p(x) \cos \psi(x) \, dx \quad ,$$

where p is the value of p(x) where the iron is saturated, leads to

$$\begin{pmatrix} N \\ P \end{pmatrix} = e^{-\left[\sigma_o nL \begin{pmatrix} 1 & 0 \\ 0 & 1 \end{pmatrix} + \sigma_c p L_m \begin{pmatrix} 0 & 1 \\ 1 & 0 \end{pmatrix}\right]} \begin{pmatrix} N_o \\ P_o \end{pmatrix} \quad .$$

The matrices can be removed from the exponents by realising that since

$$\mathbf{I} = \begin{pmatrix} 1 & 0 \\ 0 & 1 \end{pmatrix} = I^2 = I^3 = \text{etc.}$$

then $e^{-\sigma_o nLI} = Ie^{-\sigma_o nL}$.

Similarly, if $J = \begin{pmatrix} 0 & 1 \\ 1 & 0 \end{pmatrix}$, then $J^2 = I$, $J^3 = J$, etc., and so

$$e^{-\sigma_c pL_m \begin{pmatrix} 0 & 1 \\ 1 & 0 \end{pmatrix}} = \mathbf{I} - \sigma_c pL_m J + \frac{(\sigma_c pL_m)^2}{2!} I - \frac{(\sigma_c pL_m)^3}{3!} J \quad \text{etc.}$$

$$= \left[\cosh(\sigma_c pL_m)\right] I - \left[\sinh(\sigma_c pL_m)\right] J \quad .$$

Introducing

$\frac{p}{n} = s$, the electron polarisation at saturation

$\sigma_o n = \alpha_o$, $\sigma_c n = \alpha_c$

$\checkmark = \frac{sL_m}{L}$, the effective electron polarisation,

simplifies the equation expressing the behaviour of the photon beam to

$$\begin{pmatrix} N \\ P \end{pmatrix} = e^{-\alpha_o x} \begin{pmatrix} \cosh \alpha_c \sqrt{L} & -\sinh \alpha_c \sqrt{L} \\ -\sinh \alpha_c \sqrt{L} & \cosh \alpha_c \sqrt{L} \end{pmatrix} \begin{pmatrix} N_o \\ P_o \end{pmatrix} .$$

It is now very easy to calculate the asymmetry in transmission through the magnetised iron when the magnetisation is reversed. With the magnetisation in such a direction that $\underline{s} \parallel \underline{k}_o$ ($\sqrt{}$ positive)

$$N = N^{\uparrow} = e^{-\alpha_o L} (N_o \cosh \alpha_c \sqrt{L} - P_o \sinh \alpha_c \sqrt{L}) .$$

And with $\underline{s}$ antiparallel to $\underline{k}_o$ ($\sqrt{}$ negative)

$$N = N^{\downarrow} = e^{-\alpha_o L} (N_o \cosh \alpha_c \sqrt{L} + P_o \sinh \alpha_c \sqrt{L}).$$

Therefore, the asymmetry

$$E = \frac{N^{\uparrow} - N^{\downarrow}}{N^{\uparrow} + N^{\downarrow}} = - P_c \tanh \alpha_c \sqrt{L} .$$

In practice, $\alpha_c \sqrt{L}$ is of order 10^{-2}, and so to within about 0.1% one may write

$$E = - P_c \alpha_c \sqrt{L} .$$

It is worth pointing out here than many authors, including Schopper[18], quote the asymmetry as

$$E = - \tanh P_c \alpha_c \sqrt{L} .$$

Although this is wrong theoretically, due to an over-simplified scattering model which neglects the change in polarisation of the photon beam as it proceeds through the magnet, in practice $P_c \tanh \alpha_c \sqrt{L}$ is very close to $\tanh P_c \alpha_c \sqrt{L}$ because $\alpha_c \sqrt{L}$ is so small and $|P_c|$ is, of

course, no greater than unity.

In fact, $\left| P_c \tanh \alpha_c \sqrt{L} \right| \ll \left| \tanh P_c \sqrt{\alpha_c} \; L \right|$, the equality occurring when $L = 0$ or $|P_c| = 1$. The inequality of the two expressions is greatest for small P_c; but for any measurable value of P_c, the disparity is less than 1% for values of $\alpha_c \sqrt{L}$ less than about 0.2, which corresponds in an iron transmission magnet to a length of less than about 40 cm. As L tends to infinity, the two expressions for the asymmetry E tend to different asymptotic values; the expression derived here tends to $-P_c$, while that quoted by Schopper tends to ∓ 1, the sign depending upon whether P_c is positive or negative.

This estimate of the length of magnet which will produce a 1% difference between the two expressions for E depends, of course, on the magnitude of σ_c, which is a function of the photon energy. It must also be pointed out that the plot of $\frac{\sigma_{c-}}{2\pi r_o^2}$ versus k_o quoted by Schopper[18] is in error in two respects. Firstly, σ_{c-} should be negative at small photon energies; and secondly, the magnitude of $\frac{\sigma_{c-}}{2\pi r_o^2}$ is too large by a factor of two (Schopper is possibly plotting $\frac{\sigma_{c-}}{\pi r_o^2}$ rather than $\frac{\sigma_{c-}}{2\pi r_o^2}$) A correct plot of σ_c is given by Gunst and Page[16], and also in Fig. 4.1.

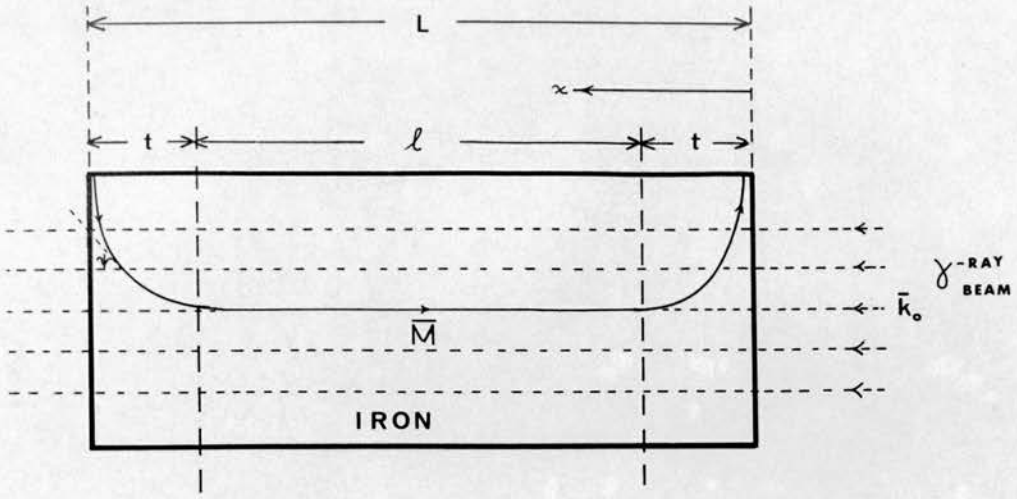

FIGURE 4.4

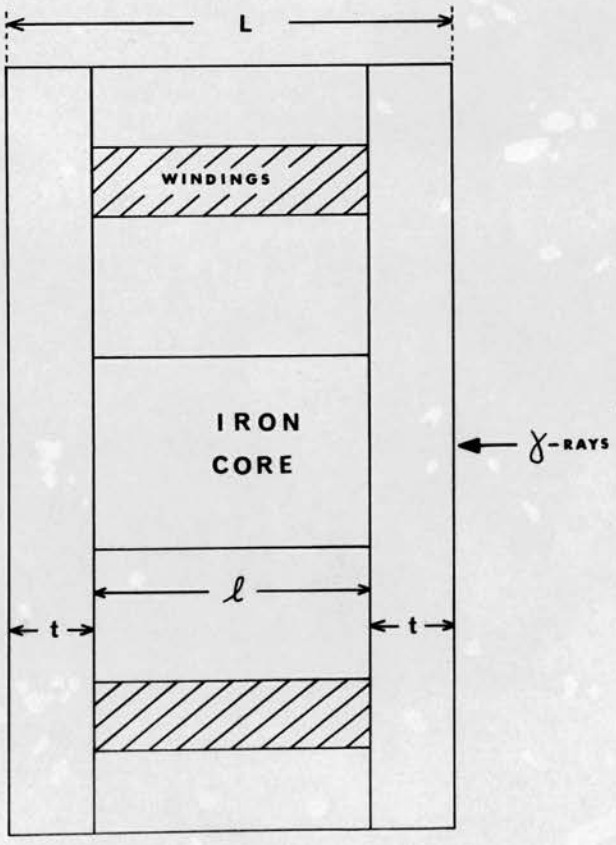

FIGURE 4.5

4.5 The Polarisation-Detection Efficiency of a Transmission Magnet

The properties of the transmission magnet relevant to this experiment are contained in the factor $a_c\sqrt{L}$. However, the calculation of this expression for a particular case gives rise to considerable difficulty, because of the uncertainty in the distribution of magnetisation throughout the magnet. Chesler[19] has discussed the polarisation detection efficiency of transmission magnets, and in the interpretation of his illustrative experiments he had to introduce an empirical factor, C, into his magnetic length to take account of end effects.

The geometry of Chesler's magnet is shown in Fig. 4.5, and in the analysis he assumed that the end effects are confined to the cheek plates of thickness t. He then put the effective magnetic length of each end plate equal to $Ca_c st$, where C is some factor < 1, and found that his theory and experiments agreed if $C = 0.17$. Simple geometrical considerations led him to expect C to be about $\frac{1}{4}$; and perhaps it is not surprising that the experimental C was somewhat lower than this, when one considers that the end effects were unlikely to be confined solely to the end plates. His magnets had $\frac{2t}{\ell}$ of the order of a half, and so the importance of this factor C in determining his final result was considerable.

It is one of the aims of this present work to attempt to measure the polarisation-detection efficiency of the transmission magnet used.

4.6 Optimum Length of Magnet

Although the counting rate asymmetry E increases as L increases, the γ counting rate decreases by absorption, and so there results a greater statistical uncertainty, ΔE, in E. An optimum value of L can therefore be found which leads to a minimum fractional statistical uncertainty, $\Delta E/E$, for a given counting time.

Assuming that the counting rates, $N_\gamma^{\pm}$, obey Poisson statistics:

$$\frac{\Delta E}{E} \approx \frac{\sqrt{2}\sqrt{N_\gamma^{\pm}}}{N_\gamma^{+} - N_\gamma^{-}} \quad \begin{pmatrix} \text{since } N_\gamma^{+} \text{ is almost equal} \\ \text{to } N_\gamma^{-} \end{pmatrix},$$

and using the interaction matrix for the magnet

$$e^{-\alpha_o L} \begin{pmatrix} \cosh \alpha_c\sqrt{L} & -\sinh \alpha_c\sqrt{L} \\ -\sinh \alpha_c\sqrt{L} & \cosh \alpha_c\sqrt{L} \end{pmatrix}$$

$$\left|\frac{\Delta E}{E}\right| = \frac{\sqrt{2}e^{\frac{-\alpha_o L}{2}}\left[N_o \cosh\alpha_c\sqrt{L} - P_o \sinh \alpha_c\sqrt{L}\right]^{\frac{1}{2}}}{2e^{-\alpha_o L} P_o \sinh \alpha_c\sqrt{L}} .$$

Since $P_o/N_o = P_c$, and $P_o \sinh \alpha_c\sqrt{L} \ll N_o \cosh\alpha_c\sqrt{L}$,

$$\left|\frac{\Delta E}{E}\right| = \frac{e^{\alpha_o L/2}}{\sqrt{2}\sqrt{N_o} P_c \sinh \alpha_c\sqrt{L}}$$

$$\approx \frac{e^{\alpha_o L/2}}{\sqrt{2}\sqrt{N_o} P_c \alpha_c\sqrt{L}} \quad (\text{since } \alpha_c\sqrt{L} \ll 1)$$

$$= \frac{e^{\alpha_o L/2}}{\sqrt{2}\sqrt{N_o} P_c \sigma_c n s L_m} .$$

If the magnet geometry is as in Fig. 4.5, then assuming that end effects (non-uniform $\bar{M}$) are confined to the two regions of length t, as L is varied, only ℓ changes. Then $L = \ell + 2t$, and $L_m = \ell + 2tC$, where C is Chesler's constant. In addition, a fixed counting time means a constant N_o.

Then

$$\left|\frac{\Delta E}{E}\right| = \frac{e^{\alpha_o t} \cdot e^{\alpha_o \frac{\ell}{2}}}{\sqrt{2}\sqrt{N_o} P_c \sigma_c n s (\ell + 2tC)} .$$

For minimum $\left|\frac{\Delta E}{E}\right|$; $\frac{\partial}{\partial \ell}\left(\frac{\Delta E}{E}\right) = 0$

$$\therefore \quad \text{constant}\left[e^{\alpha_o \frac{\ell}{2}}\left\{\frac{\alpha_o}{2(\ell + 2tC)} - \frac{1}{(\ell + 2tC)^2}\right\}\right] = 0$$

giving $(\ell + 2tC) = \frac{2}{\alpha_o} = 2\lambda$, where λ is the mean free path.

In other words $L_m = 2\lambda$.

But $$\frac{L}{L_m} = \frac{\ell + 2t}{\ell + 2tC} > 1$$

$$\therefore \quad \text{Optimum } L = \frac{1 + \frac{2t}{\ell}}{1 + \frac{2tC}{\ell}} 2\lambda ,$$

and using Chesler's values for $\frac{2t}{\ell}$ and C, a practical condition on L is

$$L \approx 3\lambda .$$

If $L_m = 2\lambda$, then the counting asymmetry, E_m, becomes

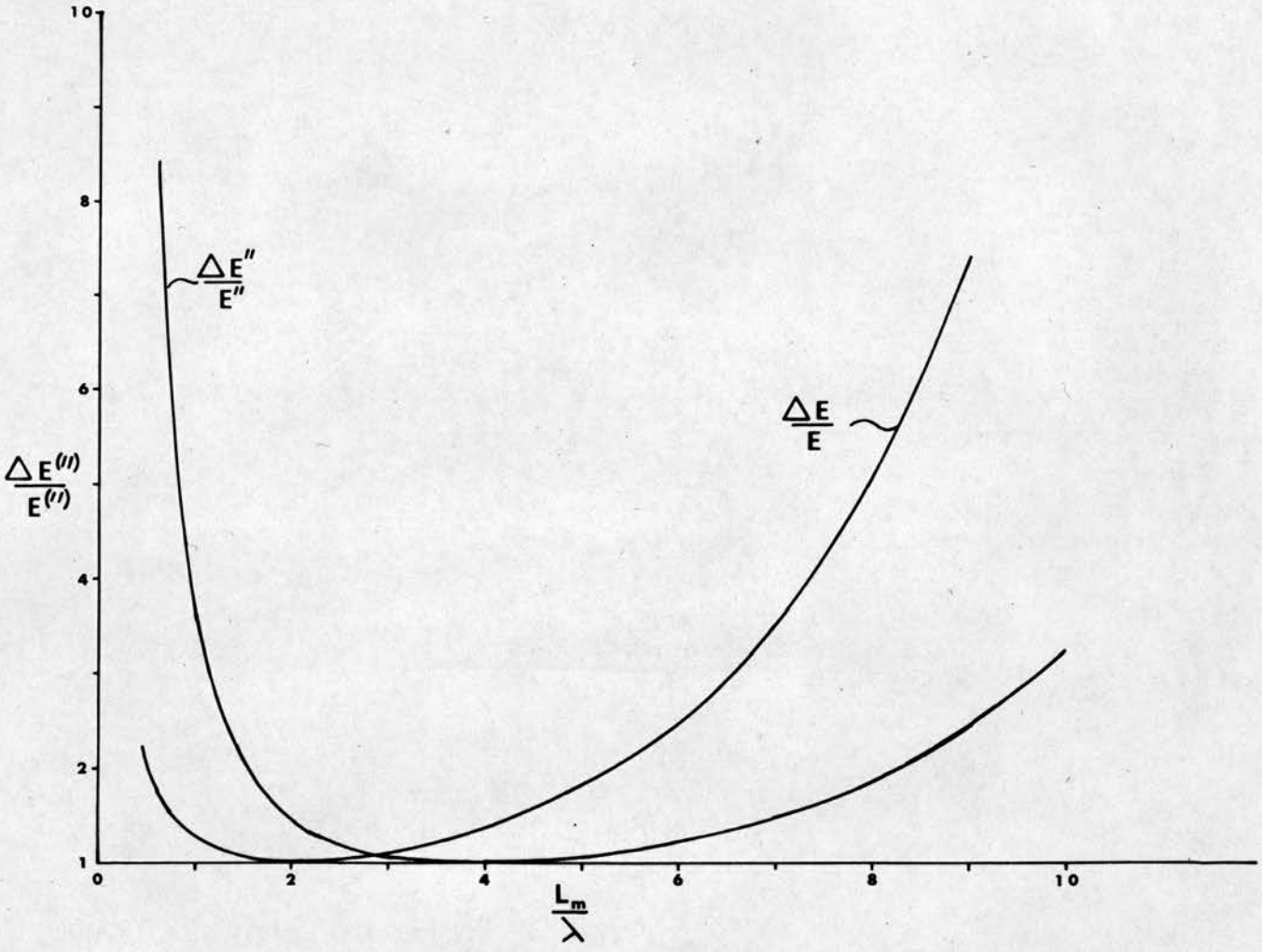
10
8
6
4
2
1
0
2
4
6
8
10
$\frac{\Delta E''}{E''}$
$\frac{\Delta E}{E}$
$\frac{\Delta E^{(n)}}{E^{(n)}}$
$\frac{L_m}{\lambda}$

FIGURE 4.6

$E_m = - \frac{2P_c \tau_c}{\tau_t}$, where τ_c is the polarisation dependent part of the Compton cross-section per atom, and τ_t is the total absorption cross-section per atom (including photoelectric effect and pair production). The dependence of $2\tau_c/\tau_t$ on k_o is shown in Fig. 4.1, where it can be seen that, for a completely polarised γ-ray beam, the maximum asymmetry E_m is of the order of three percent.

Fig. 4.6 shows that the minimum value of $\frac{\Delta E}{E}$ occurring at $L_m = 2\lambda$ is not a sharp minimum, and so the accuracy of a measurement of E does not depend critically upon the length of the magnet, provided $0.5 < \frac{L_m}{\lambda} < 5$, or so.

4.7 Scattering Corrections

The above analysis of transmission rate asymmetries assumes that only the transmitted beam is detected. In practice, to obtain reasonably high γ counting rates, the discriminator in the γ channel must be set to accept a finite range of γ counter pulse height, and so photons scattered through small angles may also be counted. Chesler[19] has investigated this problem, and has extended his calculations to include 5 scatterings. His calculations show that the asymmetry produced by circularly polarised photons scattered in the forward direction is, in general, relatively large and may differ in sign from the asymmetry produced by unscattered photons. The effect of scattered

photons must, therefore, be taken into account when using the transmission method. Chesler gives the multiple scattering corrections to be applied to the pure transmitted asymmetry for various values of photon energy, magnet length, magnet to γ counter separation and γ discriminator setting.

The corresponding correction to be applied to the circular polarisation results of the forward scattering technique has been experimentally investigated by Schopper[20] and found to be small (about a few percent), even although the intensity of multiply scattered γ-rays may be greater than 30% of the total γ intensity reaching the detector.

4.7b. Single Scattering Correction Calculation

Chesler's scattering corrections, computed by a Monte Carlo type calculation, are quoted only for a few geometries and energy discrimination levels, and so the results cannot be directly applied accurately to other geometries. Because it is expected that, for a narrow window in the γ analyser, single scattering will make the largest contribution to the scattering correction, it would be useful to calculate an analytic expression for the single scattering correction which can be applied to any particular apparatus.

Let the γ-ray beam be scattered through an angle θ having traversed a distance x in the magnet (see Fig. 4.7). The scattered beam is represented by a Stokes vector[21]

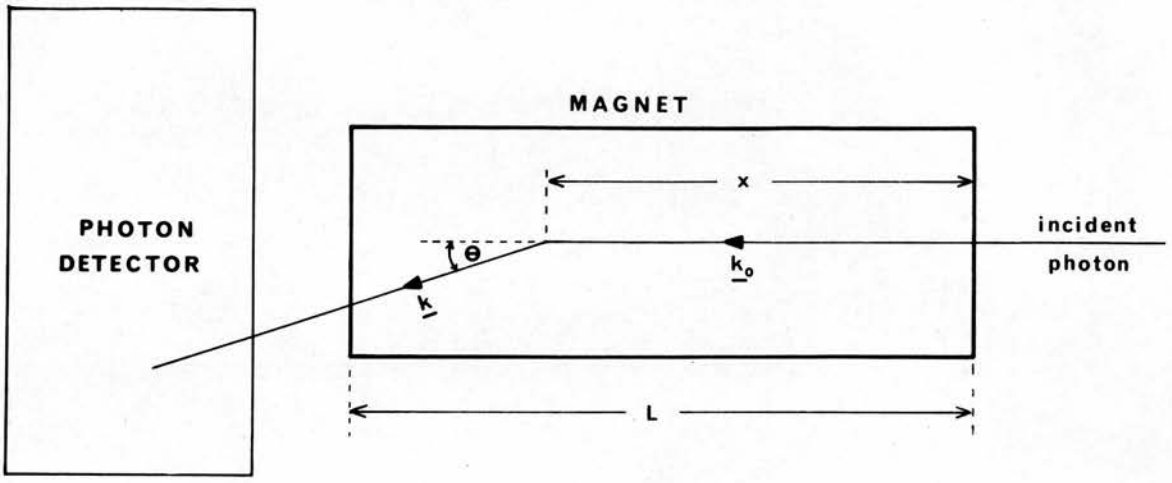
MAGNET
PHOTON
DETECTOR
x
incident
photon
θ
$\underline{k}$
$\underline{k}_o$
L

FIGURE 4.7

$$\begin{pmatrix} N \\ P \end{pmatrix}_{\substack{\text{scattered} \\ \text{at } x}} = \tfrac{1}{2} r_o^2 \left(\frac{k}{k_o}\right)^2 \begin{pmatrix} a & b \\ c & d \end{pmatrix} d\Omega \begin{pmatrix} N \\ P \end{pmatrix}_{\text{incident at } x}$$

where $a = 1 + \cos^2\theta + (k_o - k)(1 - \cos\theta)$

$b = -(1 - \cos\theta)(\underline{k}_o \cos\theta + \underline{k}).\underline{S}$

$c = -(1 - \cos\theta)(\underline{k}\cos\theta + \underline{k}_o).\underline{S}$

$d = 2\cos\theta + (k_o - k)(1 - \cos\theta)\cos\theta$

$d\Omega$ = is the element of solid angle into which the beam is scattered.

The beam has therefore travelled a distance x before scattering, and a further $(L - x)\sec\theta$ before emerging from the iron. Neglecting magnetic end effects, the spin-dependent cross-section for the scattered beam is $a_c \cos\theta$, since the angle between $\underline{k}$ and $\underline{s}$ is θ. The Stokes' vector of the beam which is scattered at x to the detector is then

$$\begin{pmatrix} N \\ P \end{pmatrix}_{\substack{\text{scattered at} \\ x \text{ to detector}}} = \begin{pmatrix} \text{Transmitted} \\ \text{from x to L} \end{pmatrix} \begin{pmatrix} \text{Scattered} \\ \text{at x} \end{pmatrix} \begin{pmatrix} \text{Transmitted} \\ \text{to x} \end{pmatrix} \begin{pmatrix} N_o \\ P_o \end{pmatrix}$$

$$= e^{-a_o(k)(L-x)\sec\theta} \begin{pmatrix} \cosh(a_c(k)\sqrt{(L-x)\sec\theta}) & -\sinh(\text{same}) \\ -\sinh(\text{same}) & \cosh(\text{same}) \end{pmatrix}$$

$$\times \tfrac{1}{2} r_o^2 \left(\frac{k}{k_o}\right)^2 d\Omega\, n\, dx \begin{pmatrix} a & b \\ c & d \end{pmatrix} e^{-a_o(k_o)x} \begin{pmatrix} \cosh a_c(k_o)\sqrt{x} & -\sinh(\text{same}) \\ -\sinh(\text{same}) & \cosh(\text{same}) \end{pmatrix} \begin{pmatrix} N_o \\ P_o \end{pmatrix}$$

To calculate the total beam scattered into the detector through an angle θ, the above expression must be integrated over x from 0 to L. The following approximations are made to facilitate the integration:

$$a_o(k) = a_o(k_o), \qquad a_c(k) = a_c(k_o).$$

These are justified by the fact that α_o and α_c vary fairly slowly with energy, and in most experimental situations $\frac{k_o - k}{k_o}$ is of the order of 10-20% only.

$$\therefore \begin{pmatrix} N \\ P \end{pmatrix} = e^{-\alpha_o L} \; e^{\alpha_o L(1-\sec\theta)} \; e^{-\alpha_o x(1-\sec\theta)} \tfrac{1}{2} r_o^2 \left(\frac{k}{k_o}\right)^2 d\Omega \, n \, dx$$

$$\times \begin{pmatrix} \cosh \alpha_c\sqrt{}(L-x) & - \sinh(\text{same}) \\ -\sinh(\text{same}) & \cosh(\text{same}) \end{pmatrix} \begin{pmatrix} a & b \\ c & d \end{pmatrix} \begin{pmatrix} \cosh \alpha_c\sqrt{}x & - \sinh \alpha_c\sqrt{}x \\ -\sinh \alpha_c\sqrt{}x & - \cosh \alpha_c\sqrt{}x \end{pmatrix} \begin{pmatrix} N_o \\ P_o \end{pmatrix}$$

These matrices do not commute, and in order to juxtapose the matrices with hyperbolic elements the following relation is used:

$$\begin{pmatrix} \cosh X & - \sinh X \\ -\sinh X & \cosh X \end{pmatrix} \begin{pmatrix} a & b \\ c & d \end{pmatrix} = \begin{pmatrix} a & b \\ b & a \end{pmatrix} \begin{pmatrix} \cosh X & - \sinh X \\ -\sinh X & - \cosh X \end{pmatrix}$$

$$+ \begin{pmatrix} (b-c)\sinh X & (a-d)\sinh X \\ -(b-c)\cosh X & -(a-d)\cosh X \end{pmatrix}$$

For small X, this last matrix has much smaller elements than the elements in the product matrix which is the first term on the right hand side. This small matrix is associated with photon spin-flipping, and will be neglected. The matrix triple product now becomes

$$\begin{pmatrix} a & b \\ b & a \end{pmatrix} \begin{pmatrix} \cosh\alpha_c\sqrt{}(L-x) & - \sinh(\text{same}) \\ -\sinh(\text{same}) & \cosh(\text{same}) \end{pmatrix} \begin{pmatrix} \cosh\alpha_c\sqrt{}x & - \sinh \alpha_c\sqrt{}x \\ -\sinh\alpha_c\sqrt{}x & \cosh \alpha_c\sqrt{}x \end{pmatrix}$$

$$= \begin{pmatrix} a & b \\ b & a \end{pmatrix} \begin{pmatrix} \cosh \alpha_c\sqrt{}L & - \sinh \alpha_c\sqrt{}L \\ -\sinh \alpha_c\sqrt{}L & \cosh \alpha_c\sqrt{}L \end{pmatrix}$$

which is independent of x.

The integral over x is then simply

$$\int_0^L e^{-\alpha_o x(1-\sec\theta)}\, dx$$

$$= \frac{1 - e^{-\alpha_o L(1 - \sec\theta)}}{\alpha_o(1 - \sec\theta)}$$

Collection of all L-dependent factors gives the factor

$$Le^{-\alpha_o L}\left\{\frac{1 - e^{-\alpha_o L(\sec\theta - 1)}}{\alpha_o L(\sec\theta - 1)}\right\}$$

$$= Le^{-\alpha_o L}\, \phi(\alpha_o L, \sec\theta)$$

where $\phi(\alpha_o L, \sec\theta) = \dfrac{1 - e^{-\alpha_o L(\sec\theta - 1)}}{\alpha_o L(\sec\theta - 1)}$.

To obtain the total scattered beam, an integration over solid angle, Ω , must be performed. This integral is

$$\int_0^{\Omega_{max}} \tfrac{1}{2} r_o^2 \left(\frac{k}{k_o}\right)^2 nLe^{-\alpha_o L}\, \phi(\alpha_o L, \sec\theta) \begin{pmatrix} a & b \\ b & a \end{pmatrix} \begin{pmatrix} \cosh\alpha_c\sqrt{}L & -\sinh\alpha_c\sqrt{}L \\ -\sinh\alpha_c\sqrt{}L & \cosh\alpha_c\sqrt{}L \end{pmatrix} d\Omega$$

$$= nLe^{-\alpha_o L} \begin{pmatrix} \bar{a} & \bar{b} \\ \bar{b} & \bar{a} \end{pmatrix} \begin{pmatrix} \cosh\alpha_c\sqrt{}L & -\sinh\alpha_c\sqrt{}L \\ -\sinh\alpha_c\sqrt{}L & \cosh\alpha_c\sqrt{}L \end{pmatrix}$$

where $\begin{pmatrix} \bar{a} \\ \bar{b} \end{pmatrix} = \tfrac{1}{2} r_o^2 \int_0^{\Omega_{max}} \left(\frac{k}{k_o}\right)^2 \phi(\alpha_o L, \sec\theta)\, d\Omega \begin{pmatrix} a \\ b \end{pmatrix}$

These integrals can be easily calculated on a computer, using the relations:

$$k = \frac{k_o}{1 + k_o(1 - \cos\theta)} \quad ; \quad \text{let} \quad \omega = \frac{\Omega}{2\pi} = (1 - \cos\theta)$$

$$\therefore \quad \sec\theta - 1 = \frac{\omega}{1-\omega} \quad ; \quad \frac{k}{k_o} = \frac{1}{1 + k_o\omega}$$

$$\omega_{max} = \frac{1}{k_{min}} - \frac{1}{k_o}$$

where k_{min} is the minimum photon energy accepted by the photon detector.

The scattered beam can now be written

$$\binom{N}{P}_{scatt.} = e^{-\alpha_o L} \begin{pmatrix} \bar{a}Ln & \bar{b}Ln \\ \bar{b}Ln & \bar{a}Ln \end{pmatrix} \begin{pmatrix} \cosh\alpha_c\sqrt{L} & -\sinh\alpha_c\sqrt{L} \\ -\sinh\alpha_c\sqrt{L} & \cosh\alpha_c\sqrt{L} \end{pmatrix} \begin{pmatrix} N_o \\ P_o \end{pmatrix}$$

The total beam arriving at the detector is then:

$$\binom{N}{P}_{total} = \binom{N}{P}_{transmitted} + \binom{N}{P}_{scattered}$$

$$= e^{-\alpha_o L} \begin{pmatrix} \left[(1 + \bar{a}Ln)\cosh\alpha_c\sqrt{L} - \bar{b}Ln\sinh\alpha_c\sqrt{L}\right] & \text{same} \\ \left[-(1+\bar{a}Ln)\sinh\alpha_c\sqrt{L} + \bar{b}Ln\cosh\alpha_c\sqrt{L}\right] & \text{same} \end{pmatrix}$$

Substituting $$\frac{\bar{b}Ln}{\sqrt{(1 + \bar{a}Ln)^2 - (\bar{b}Ln)^2}} = \sinh\psi'$$

and $$\frac{1 + \bar{a}Ln}{\sqrt{(1 + \bar{a}Ln)^2 - (\bar{b}Ln)^2}} = \cosh\psi'$$

$$\binom{N}{P}_{total} = e^{-\alpha_o L}\sqrt{(1+\bar{a}Ln)^2-(\bar{b}Ln)^2} \begin{pmatrix} \cosh(\alpha_c\sqrt{L}-\psi') & -\sinh(\alpha_c\sqrt{L}-\psi') \\ -\sinh(\alpha_c\sqrt{L}-\psi') & \cosh(\alpha_c\sqrt{L}-\psi') \end{pmatrix}$$

Therefore the corrected transmission rate asymmetry

$$E_{cor.} = -\tanh(\alpha_c\sqrt{L} - \psi') \quad \text{for} \quad P_c = +1$$

where $\tanh\psi' \approx \psi' = \dfrac{\bar{b}Ln}{(1 + \bar{a}Ln)}$ is the single scattering correction.

The justification for neglecting the spin-flipping terms lies in the fact that the ratio of the magnitudes of the elements in the matrix expressing spin-flipping to the elements of the matrix representing single scattering is of order ω^2 ; ω_{max} being < 0.2, and often much smaller. This approximation is therefore more valid the smaller ω_{max} is, i.e. the higher the energy and the smaller the window in the photon energy analyser.

The calculated single scattering corrections to be applied to the pure transmission asymmetry are shown in Fig. 4.8, and the transmission asymmetries corrected for single scattering are shown in Fig. 4.9, where it is immediately seen that this correction is a very important one - amounting to about 10 to 20% for typical experimental conditions. Under certain conditions - photon energies around 600 keV, or high photon energy coupled with a wide γ analyser window - the correction can be much greater than 20%.

The curves shown in Fig. 4.8 and Fig. 4.9 were computed on a PDP-8 computer; the calculations using the γ-ray absorption coefficients for iron tabulated by Davisson[25], and the following constants:

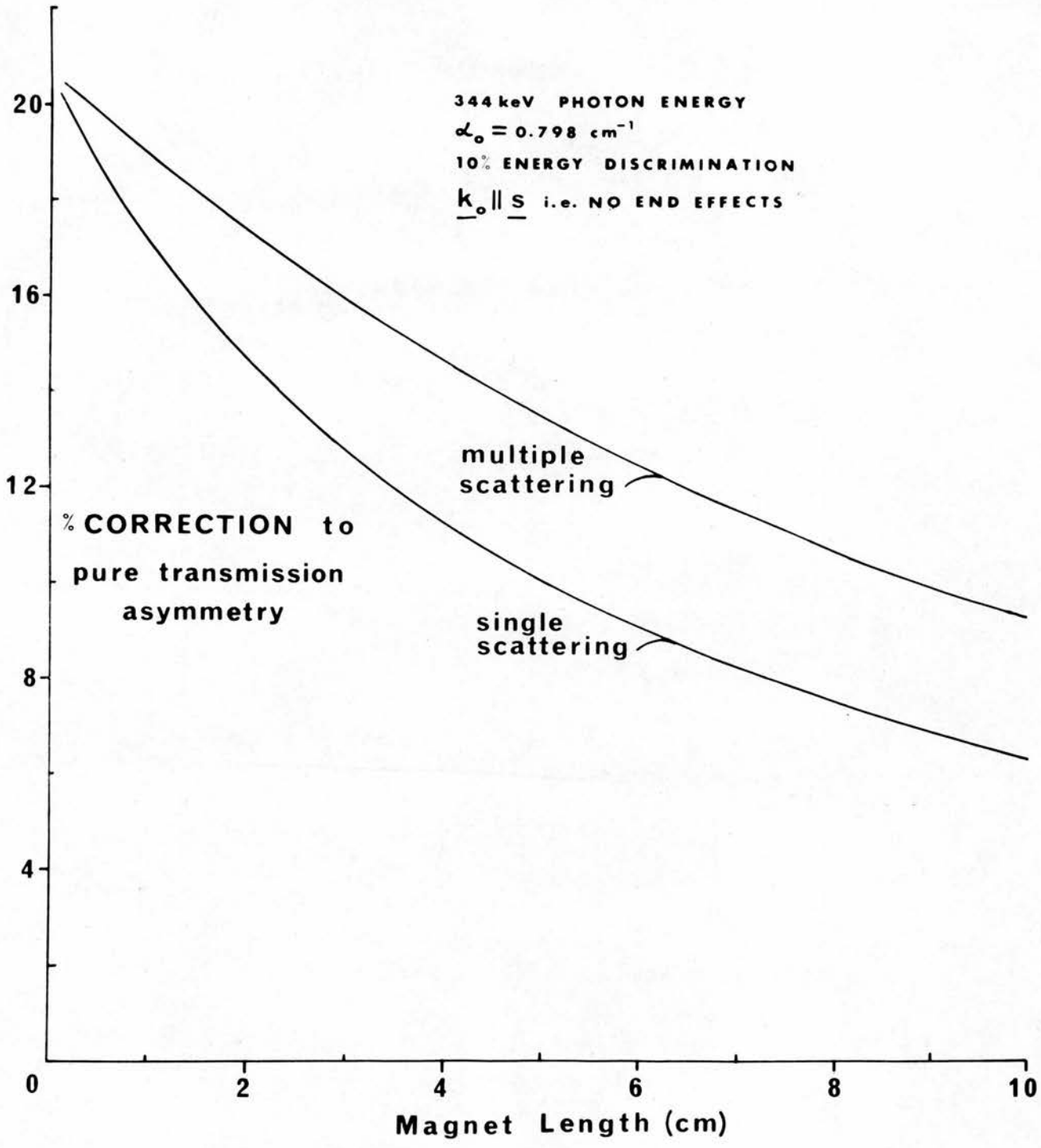
344 keV PHOTON ENERGY
$\alpha_o = 0.798\ cm^{-1}$
10% ENERGY DISCRIMINATION
$\underline{k}_o \| \underline{S}$ i.e. NO END EFFECTS
multiple scattering
single scattering
% CORRECTION to pure transmission asymmetry
20
16
12
8
4
0
2
4
6
8
10
Magnet Length (cm)

FIGURE 4.8

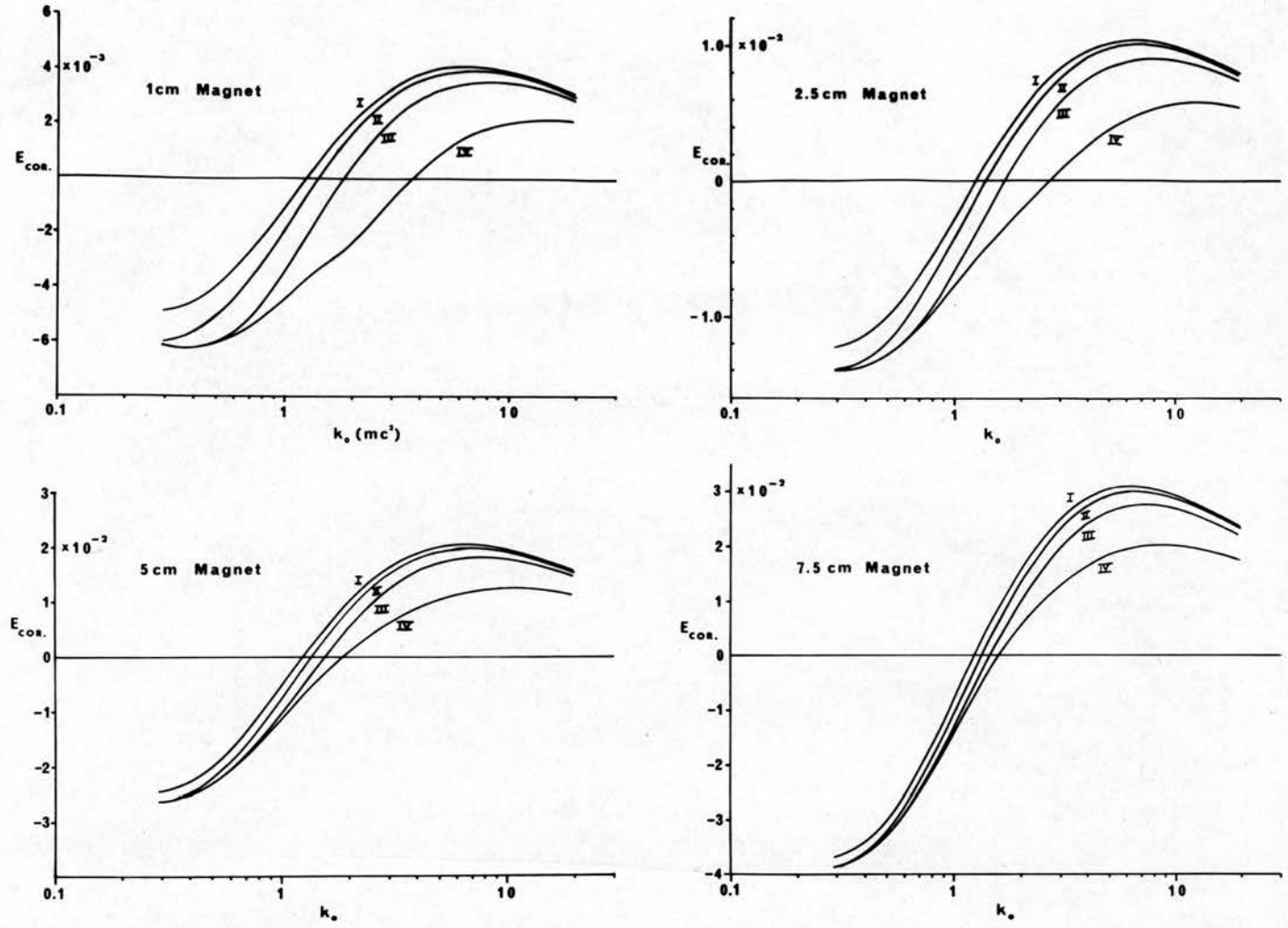

CURVES I, II, III, IV, ARE FOR PURE TRANSMISSION, 15%, 30%, 60% ENERGY DISCRIMINATION RESPECTIVELY. $P_c = +1$.

FIGURE 4.9

density of iron = $7.86\ g/cm^3$

$|S|$ = 0.08

n = 2.2×10^{24} electrons/cm^3

$2\pi r_o^2$ = $0.499 \times 10^{-24}\ cm^2$.

P_c = +1

The single scattering corrected curves in Fig. 4.9 show very similar characteristics to those of Chesler[19], even although Chesler includes multiple scattering up to fifth order. This agreement justifies an attempt to extend these calculations to include multiple scattering, to improve the calculation by removing the approximation $a_o(k) = a_o(k_o)$, to include the photon spin-flipping terms, and to take account of finite detector size (which makes ω_{max} a function of both x and photon energy discrimination level). Such calculations are at present being carried out, and preliminary results including multiple scattering (of all orders) are shown in Fig. 4.8. So far, the calculations have given corrections which are slightly in excess of Chesler's values, but it is expected that agreement will be improved when all the above refinements have been incorporated.

The multiple scattering correction which has to be applied to the polarisation-detection efficiency of a transmission magnet can be calculated with greater accuracy than can the corresponding correction to a forward scattering magnet, because of the rather complicated averaging over geometry which is involved in the latter[18, 20].

On the other hand, the forward scattering technique does not run into the non-uniform magnetisation difficulties which limit the accuracy of the transmission method.

4.8 Measurement of the Magnetic Length of the Magnet

The distribution of the magnetisation $\bar{M}$ within the core of the transmission magnet is difficult to calculate, especially near the ends of the core, and especially near saturation where the relative permeability of the iron is low. This leads to one of the major difficulties of the measurement of γ-ray circular polarisation using this technique, namely the calculation of the magnetic length of the core,

$$L_m = \frac{1}{p\sigma_c} \int_0^L \sigma_c \, p(x) \cos \psi(x) \, dx \, .$$

As already mentioned, even Chesler's thorough calculations of the asymmetries expected from his transmission magnets assumed uniform $\bar{M}$, and end effects were accounted for by introducing the empirical constant C, which was adjusted to bring about the best agreement between theory and experiment. The corrections to the pure transmission asymmetries to take account of end effects were large, and could amount to about 20%.

This difficulty of calculating L_m suggests seeking a method of measuring it, and it is one of the purposes of the present work to investigate the possibility of devising a technique for measuring magnetic lengths of transmission

magnets. If such a measurement can be made, then the measurement of γ-ray circular polarisation is independent of assumptions concerning the behaviour of the magnetisation within the core of the magnet.

Many workers make relative measurements by calibrating their polarimeters with γ sources of known polarisation. However, because the polarisation detection efficiency is, in general, a function of photon energy, this calibration must be interpolated or extrapolated to the energy of the γ-ray of unknown polarisation. This introduces a further source of uncertainty, which could be eliminated if absolute measurements of circular polarisation could be made using transmission magnets with measured magnetic lengths.

In fact, the first experiment using a γ transmission magnet, by Gunst and Page[16], measured its magnetic length. This seems to have been overlooked by later users of such magnets, and it seems very worthwhile examining its possibilities.

If N denotes the number of γ-rays transmitted when the magnetic field is off, then

$$N = e^{-a_o L} N_o$$

and the a symmetry $E'' = \dfrac{N - \left(\frac{N^{\uparrow} + N^{\downarrow}}{2}\right)}{N + \left(\frac{N^{\uparrow} + N^{\downarrow}}{2}\right)}$

$$= \frac{1 - \cosh a_c \sqrt{L}}{1 + \cosh a_c \sqrt{L}} = - \tanh^2\left(\frac{a_o \sqrt{L}}{2}\right)$$

$$\approx - \left(\frac{a_c \sqrt{L}}{2}\right)^2 .$$

It is, in theory, then possible to obtain a direct measurement of the polarisation detection efficiency of transmission magnets, and it remains to estimate the feasibility of such measurements in practice.

4.9 Feasibility of Measuring Magnetic Lengths

Putting practical values into the expression for E" gives the order of magnitude expected for this asymmetry. For low photon energies, corresponding to positive σ_c^+, $|E''|$ is of order 10^{-5}; and for higher energies, E" can attain a magnitude of about 10^{-4}.

This is obviously a very small effect, and the feasibility of measuring it in the presence of statistical uncertainty and competing asymmetries must be examined. This examination will be carried out under the following headings:

(i) Statistics.

(ii) Thermal expansion effects.

(iii) Magnetostriction.

(iv) Instrumental asymmetries due to stray magnetic fields.

i) Statistics

Optimum Length of Magnet for Measurement of $a_c\sqrt{L}$

It has already been shown that

$$E'' = -\left(\frac{a_c\sqrt{L}}{2}\right)^2 ,$$

and for a given counting time (N_o fixed) it is required to

minimise $\frac{\Delta E''}{E''}$, where $\Delta E''$ is the statistical uncertainty in E".

Because N, $N^{\uparrow}$ and $N^{\downarrow}$ are very similar in magnitude

$$\frac{\Delta E''}{E''} \approx \frac{\sqrt{6}\ \sqrt{N}}{2N - (N^{\uparrow} + N^{\downarrow})}$$

$$= - \frac{\sqrt{6}\ e^{\alpha_o L/2}}{\sqrt{N_o}\ (\alpha_c \sqrt{L})^2} \quad , \text{ neglecting } P_o \sinh \alpha_c \sqrt{L} \text{ compared with unity.}$$

Assuming, as in the calculation of the minimum $\frac{\Delta E}{E}$, that $L = \ell + 2t$ and $L_m = \ell + 2tC$, the analysis proceeds as before ; giving the minimum fractional statistical uncertainty $\frac{\Delta E''}{E''}$ when

$$L_m = 4\lambda \quad .$$

Fig. 4.6 shows that the minimum in $\frac{\Delta E''}{E''}$ is not at all sharp; L_m may lie between 1.5 and 8 mean free paths without serious degradation of the accuracy of a measurement of E".

In practice, however, $\alpha_c \sqrt{L}$ is a very small quantity of order 10^{-2}, and so $(\alpha_c \sqrt{L})^2$ is of order 10^{-4}. This means that the asymmetry E" is very small, and its measurement requires a very large number of counts if any degree of accuracy is to be attained. Moreover, in an absolute measurement of γ-ray circular polarisation, the magnetic length expression, $\alpha_c \sqrt{L}$, must be measured to at least as high an accuracy as the polarisation expression, $P_c \alpha_c \sqrt{L}$, which is of order 2×10^{-3}. It is, however,

possible to match the accuracy of these two measurements because, whereas $P_c a_c \sqrt{L}$ is determined from fairly low coincidence counting rates, $(a_c \sqrt{L})^2$ is measured using relatively fast γ single counting. To measure the magnetic length to at least the same accuracy as the circular polarisation expression requires

$$\sqrt{\frac{N_\gamma}{N_c}} \geqslant \frac{2\sqrt{3}\, P_c}{a_c \sqrt{L}}$$

where N_γ and N_c are γ and coincidence counting rates respectively. In practice, this condition can be fulfilled.

(ii) Thermal Effects

About 200 watts are dissipated in the magnet windings, and so as the magnetising current is switched off and on, some thermal cycling of the magnet core is expected.

If $N = N_o e^{-a\rho L}$ where a = total absorption coefficient. cm^2/gm

ρ = electron density/cm^3

then $\frac{dN}{N} = -a\rho L \left[\frac{dL}{L} + \frac{d\rho}{\rho}\right]$

$= -a\rho L \left[\frac{dL}{L} - \frac{dV}{V}\right]$; (since $\frac{dV}{V} = -\frac{d\rho}{\rho}$) .

If α = coefficient of linear expansion/^oC

$\frac{dL}{L} = \alpha$; $\frac{dV}{V} = 3\alpha$

$\therefore \frac{dN_{Th}}{N} = 2a\rho L\alpha/^oC = E_{Th}$, say

TABLE 4.1

E_γ (MeV)	$\left\lvert\frac{E''}{E_{Th}}\right\rvert = \frac{a_c^2 \sqrt{2}}{8 a \rho \alpha} \frac{L}{\Delta T}$	L required to make $\left\lvert\frac{E''}{E_{Th}}\right\rvert = 10$ (mean free paths/°C)	$\left\lvert\frac{E''}{E_m}\right\rvert = \frac{a_c^2 \sqrt{2}}{4 \times 10^{-5} a \rho} L$ (per cm.)	L required to make $\left\lvert\frac{E''}{E_m}\right\rvert = 10$ (mean free paths)
0.133	$0.16 \times \frac{L}{\Delta T}$	83	0.32	44
0.25	0.22 "	45	0.44	23
0.344	0.14 "	57	0.28	29
2.6	0.7 "	4.3	1.4	2.2
5.0	0.8 "	2.5	1.6	1.3

In practice, since L_m L, the required lengths L are slightly larger than those quoted above.

In practice $a\rho L \approx$ a few, say 3 or 4

$\alpha \approx 10^{-5}/^{\circ}C$ for soft iron,

and so

$$\frac{dN_{Th}}{N} \approx + 10^{-4}/^{\circ}C$$

This effect increases $|E''|$, and since the magnet becomes rather warm during operation, the temperature may well cycle by a degree or two.

Table 4.1 compares the magnitude of E_{Th} and E'' for a temperature change $\Delta T^{\circ}C$, assuming $L_m = L$.

(iii) Magnetostriction

The dimensions of a bar of iron change as its state of magnetisation alters, and as this occurs in the transmission magnet, an asymmetry in the counting rate is expected. As in (ii), if $N = N_o e^{-a\rho L}$, then

$$\frac{dN}{N} = -a\rho L \left[\frac{dL}{L} - \frac{dV}{V}\right] .$$

Stoner[22] gives the following magnetostrictive properties of polycrystalline iron

$$\frac{dL}{L} \approx -1 \times 10^{-5} \text{ at saturation}$$

$$\max \frac{dV}{V} \approx + 1.6 \times 10^{-7} .$$

For optimum statistical accuracy, $a\rho L$ will be of order 3 or so,

giving $$\frac{dN_m}{N} \approx + 3 \times 10^{-5} = E_m$$

This effect, like the thermal effect, increases $|E''|$. See Table (4.1) for a comparison of $|E''|$ and $|E_m|$.

(iv) Instrumental Asymmetries due to Stray Magnetic Fields

As the magnetisation of the core is cycled, so also is its stray field; the photomultiplier tube in the γ counter resides, therefore, in a cycling magnetic field. Since the gain of a photomultiplier tube can depend upon the magnetic field in which it is located, the gain of the γ counter may cycle with the experimental cycle. An instrumental asymmetry in the counting rates can then arise.

It is impossible to make an a priori estimate of the sign and magnitude of this effect; all that can be done is to take the precautions of removing the photomultiplier tube as far as possible from the magnet by means of a light pipe, and surrounding the tube with magnetic shields and a bucking coil whose current is bled from the magnet supply.

A more sophisticated approach would be to hold the magnetic field at the photomultiplier tube constant using a bucking coil whose current is the output of a servo amplifier which has as input the signal from a magnetic field probe placed close to the tube. An attempt to produce such a servo is described in Chapter 5. A suitable system, capable of stabilising the magnetic field to within 10^{-8} weber/sq. m., is described by Graham and Geiger[23].

Other workers (including Saigntignon[15], Lundby et. al.[17] and Mann et al.[24]) using magnetic shields,

bucking coils and light pipes, have reported a residual γ counting rate asymmetry of order 10^{-4} due to stray magnetic fields. It would appear that very elaborate precautions are necessary to reduce this effect further.

Conclusion

When these different asymmetries are compared, it is seen that at low γ energies the asymmetry E" is completely masked by the much larger thermal and magnetostrictive effects - not to mention an asymmetry due to stray magnetic fields which is unknown in sign and likely to have a magnitude of about ten times that of E" ! And even although $|E"|$ is proportional to L^2, whereas $\frac{dN_{Th}}{N}$ and $\frac{dN_m}{N}$ are proportional to L, increasing L in order to make $|E"|$ comparable with the thermal and magnetostrictive effects is likely to introduce statistical accuracy problems due to the resulting low counting rates. This is especially true for low energy γ's whose mean free path is short; see Table (4.1).

Therefore, in view of the presence of these very large instrumental asymmetries, it seems to be impossible to measure the magnetic length of a transmission magnet, by the above technique, for low energy γ rays.

For high energy (greater than about 2 MeV) γ-rays, however, provided elaborate precautions are taken to minimise stray magnetic fields at the photomultiplier tube

and temperature changes in the magnet core, the magnetic length can be measured by this method, if the transmission magnet is sufficiently long.

Although Gunst and Page[16] give little quantitative discussion of the feasibility of their measurement of σ_c, they must have performed such an analysis. This is obvious from the details of their experiment: namely their choice of γ-ray energy, 2.62 MeV; their specially wound magnetising coil, ensuring constant power dissipation; and the length of their magnet, 12 inches or 8 mean free paths.

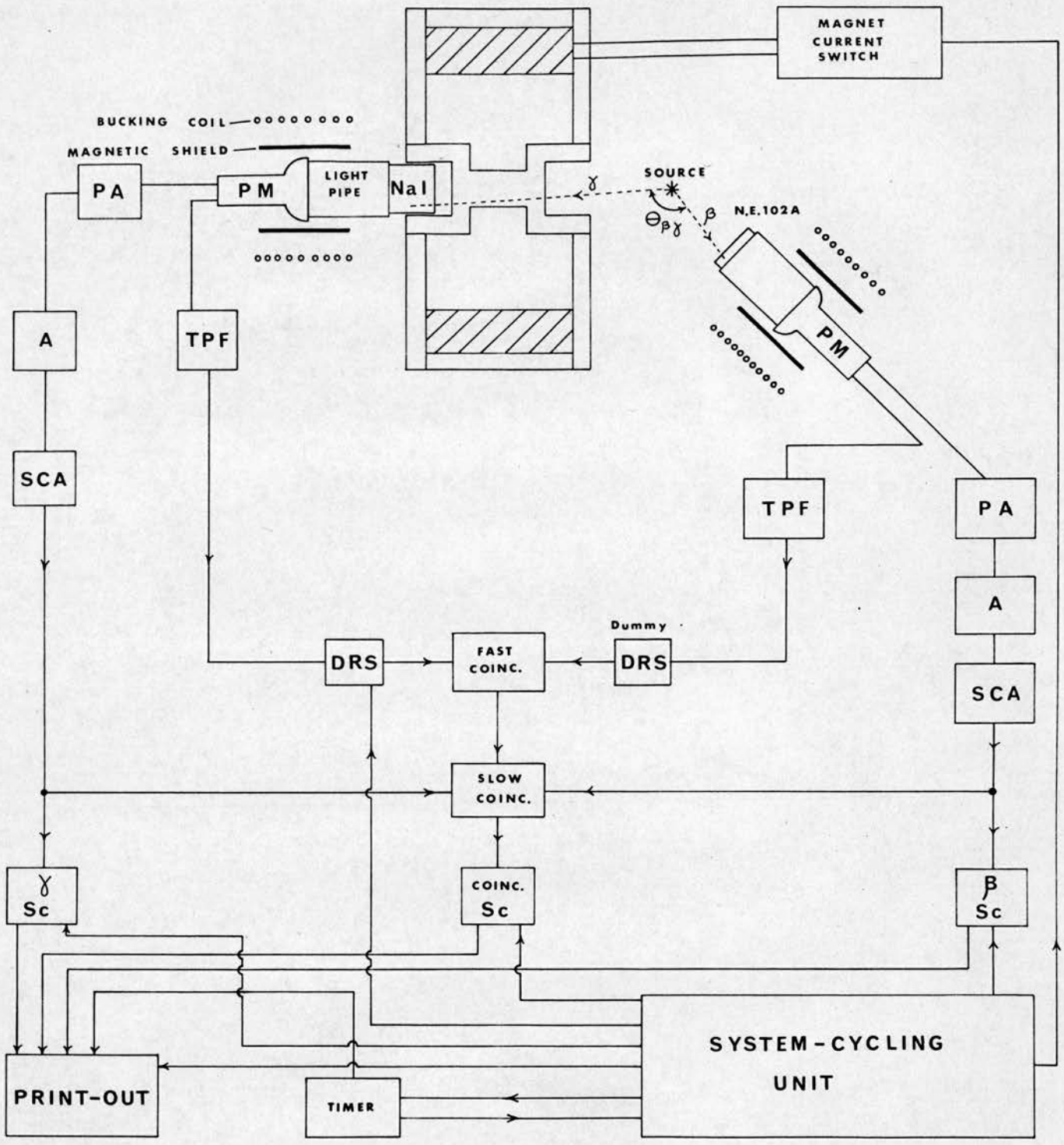

PM : photomultiplier

PA : preamplifier

A : amplifier

SCA: single channel analyser

FIGURE 5.1

Sc : scaler

TPF : timing pulse former

DRS : delay-routing switch

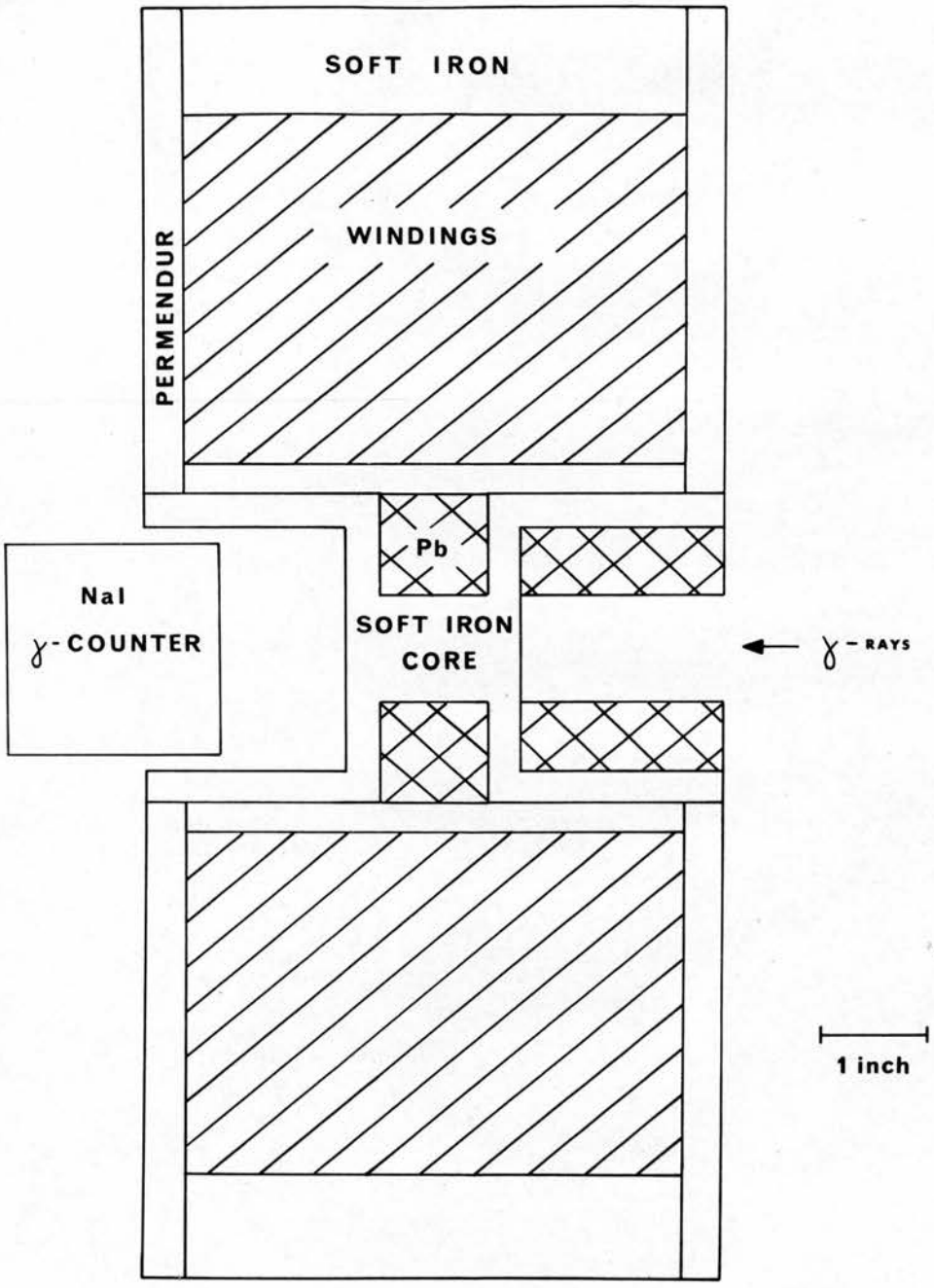
SOFT IRON
WINDINGS
PERMENDUR
Pb
NaI
γ-COUNTER
SOFT IRON
CORE
γ - RAYS
1 inch

FIGURE 5.2

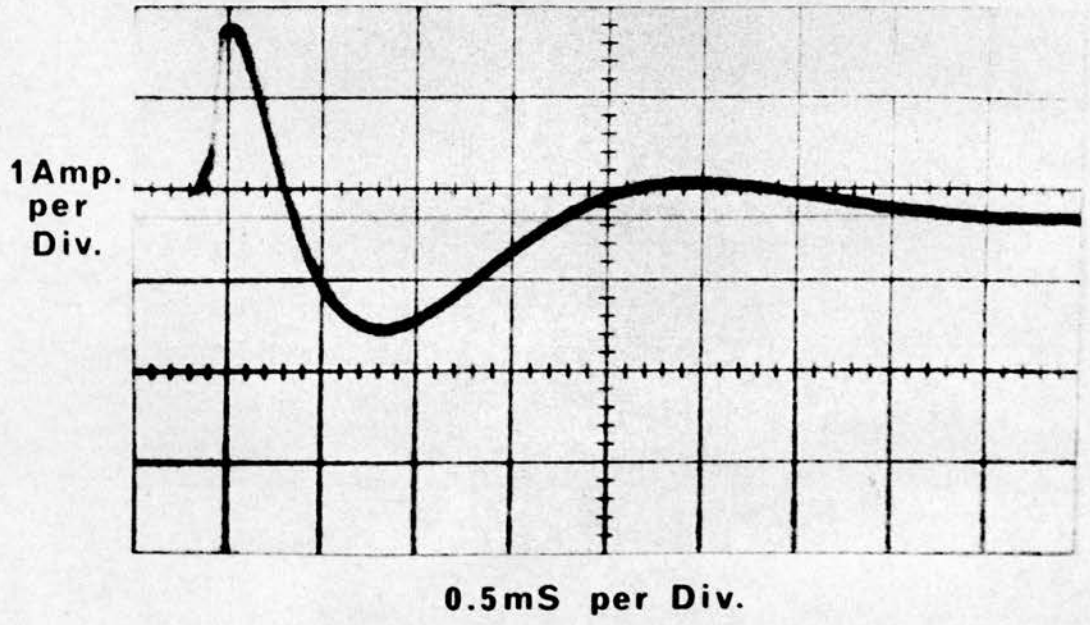

FIGURE 5.3

CHAPTER 5

THE APPARATUS

Figure 5.1 shows a schematic diagram of the complete apparatus, which is, obviously, complicated by the presence of so many electronic units. To help clarify the system, the mechanical and electronic details will be described separately.

5.1 The Transmission Magnet

The geometry of the transmission magnet is shown in Figure 5.2. The core of the magnet is made of soft magnetic iron (trade name Super Hiperm) of purity in excess of 99.8°/o. The saturation flux density is of the order of 2.1 webers/sq.cm., the specific gravity is 7.866 and the coefficient of linear expansion is $10.2 \times 10^{-6}/°C$. The outer cylindrical magnetic return path is also made of this material. The end-plates, however, are made of the soft iron-cobalt-vanadium magnetic alloy, Permendur, which has a very high saturation flux density (2.36 webers/sq.m.), and high permeability, at flux densities of the order of 2.1 webers/sq. m.. These properties allow the end-plates to be thin without serious increase in the magnetic reluctance of the complete circuit. It seems reasonable to assume that the ratio $2t/\ell$ (see Fig. 4.5) will decrease with decreasing end-plate thickness, provided that the material of these

plates does not saturate in the vicinity of the core.

The magnetising windings contain 7085 turns and carry a current of 1.4 amps. Because the reluctance of the magnetic circuit is low, this magnetomotive force is more than sufficient to saturate the iron core. A 1μF capacitor is connected across the magnet windings, partly to help to suppress the transient voltage spikes which occur on switching off the magnet, and partly to introduce some ringing of the winding current so that the magnetisation of the core is cycled to zero when the current is switched off. Fig. 5.3 shows a photograph of an oscilloscope trace of the behaviour of the current in the windings after switching off. It is seen that only a very limited amount of ringing occurs, because the Q of the circuit consisting of the windings and the parallel capacitor is low.

The D.C. supply for the magnetising coil is derived from the departmental rectifier at 240 volts, 100 volts of which is dropped across two lamps and a rheostat in series. These lamps fulfil two functions; they limit the surge current flowing into the shunting 1μF capacitor at switch on, and they conveniently indicate whether the magnet is on or not. The rheostat provides fine control of the magnet current to allow for supply voltage fluctuations. The total magnetomotive force in the magnetic circuit is so high, however, that, although the current

through the windings may vary by about 10°/o due to supply variations and thermal variations in the resistance of the coil, the core of the magnet remains saturated.

5.2 The Particle Detectors

The β and γ counters are both scintillation detectors, and are similar except for the scintillators. The β counter has a disc of NE102A plastic scintillator 7 mm. thick and 6 cm. in diameter, coated with magnesium oxide reflector paint on all surfaces except that coupled to the light pipe, while the γ counter uses a NaI crystal 2" by 2". The entrance window on the β counter is 0.001" aluminium foil which has a superficial density of about 7 mg./sq. cm., and the γ entrance window consists of 0.025" thick aluminium.

In each counter the light from the scintillator is fed to the photomultiplier tube (E.M.I. type 9578A) through a 12 inch long by 2½ inch diameter perspex light pipe; the interfaces being optically coupled by silicone grease. Both counters are in the form of demountable assemblies comprising scintillator, light pipe, photomultiplier-tube with mumetal shield, and preamplifier, and were supplied by Nuclear Enterprises (G.B.) Ltd.

Around the photomultipliers further magnetic shielding and bucking coils were placed. The screening consisted of three layers of thin Super Radiometal sheet, and the bucking coils were wound in such a way as to annul the divergent stray field of the magnet. The current for the

bucking coils (about 100 mA) was bled from the magnet current supply.

A spectrometer table was converted to serve as β counter support, in such a way that as the table is rotated, the angle between the longitudinal axis of the β counter and the longitudinal axis of the apparatus (the mean direction of the counted γ-ray beam) can be varied and measured. The source was mounted on the axis of rotation of the table (for method, see paragraph 6.1) to ensure a constant solid angle for γ-ray collection. The magnet, γ counter, and β counter on turntable are supported on cradles which slide along two horizontal parallel brass rails, and their alignment is made possible by adjusting screws (see Fig. 5.4).

5.3 Electronics

The electronics will be described from the particle detectors outwards.

i) Photomultiplier Dynode Resistor Chain

Two outputs are taken from the photomultiplier tubes - a timing pulse from the anode and a pulse for energy selection purposes from a dynode. Because the timing-pulse forming circuit is directly coupled to the anode of the photomultiplier tube, this end of the dynode resistor chain has to be near earth potential, and the photocathode, therefore, held at high negative potential.

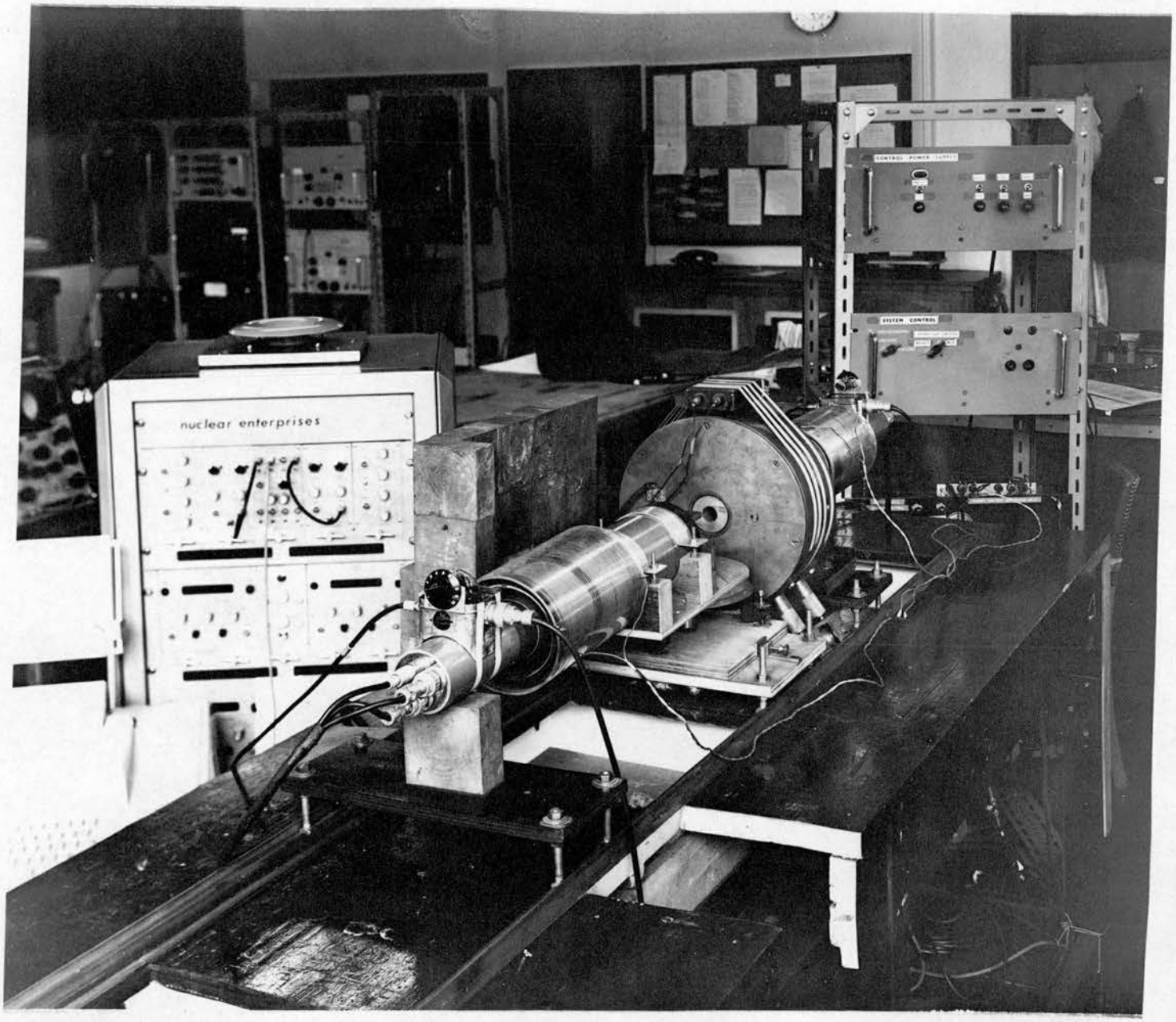

FIGURE 5.4

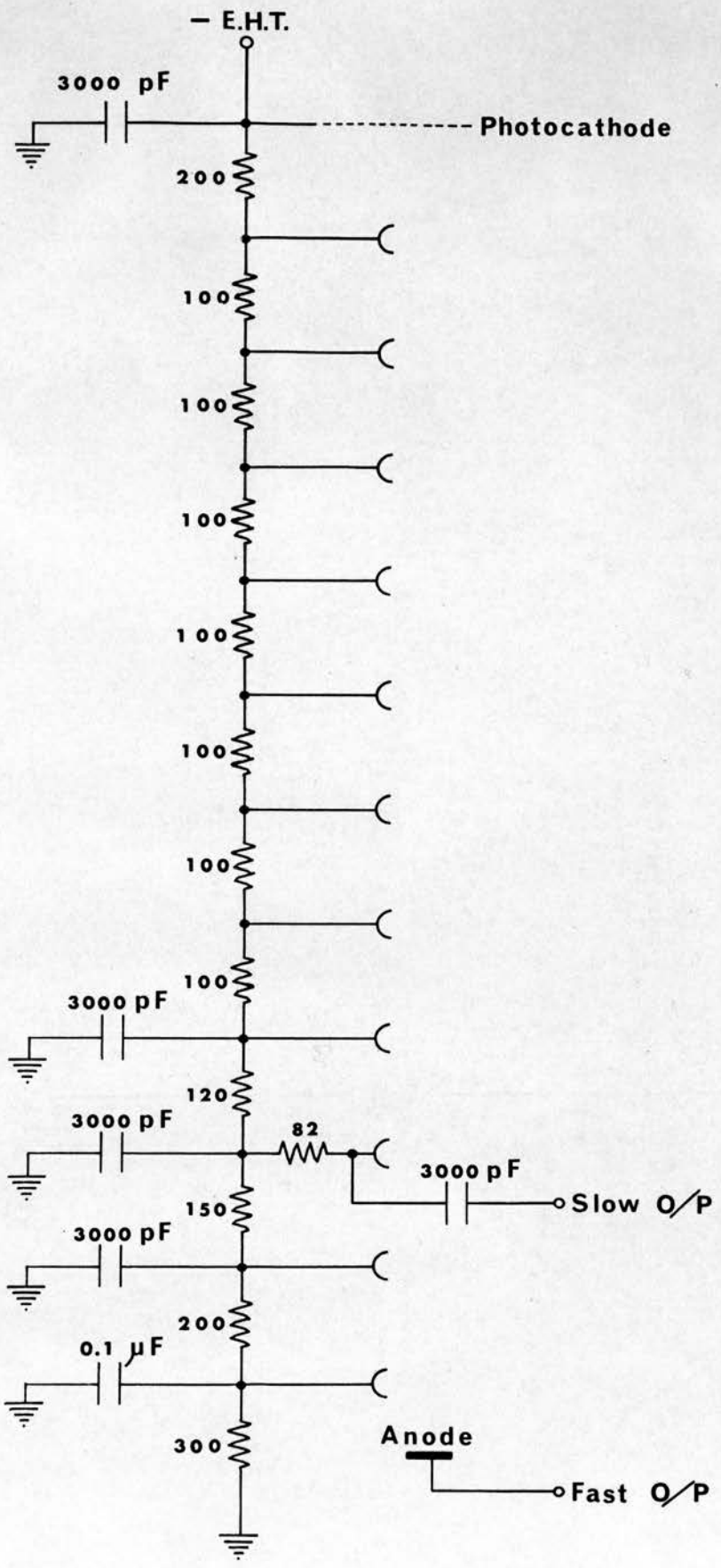

All resistors in kilohms.

FIGURE 5.5

To avoid the injection of spurious noise into the photocathode - first dynode region by high electric fields developed across the glass envelope of the tube, the outside surface of the tube in this region was coated with cold-setting solder (Eccobond 57C), and this conducting coating is maintained at photocathode potential. The solder is insulated from the rest of the counter assembly by P.V.C. tape. This treatment ensures that there are no high electric fields set up in the glass of the tube envelope at the photocathode end.

The dynode resistor chain is shown in Fig. 5.5.

ii) The Timing-Pulse Limiting Amplifier

The output pulses from the photomultiplier tube anode are fed to the input of the discriminator and limiting amplifier shown in Fig. 5.6. The tunnel diode 1N3149 acts as a pulse shaper and as a current discriminator whose threshold is set by the 1K potentiometer. This part of the circuit is developed from a time-maker circuit published by Larsen and Shera[26]. The half volt negative pulses from this tunnel diode are amplified by the limiting amplifier Tr 2 into fast rising (3n S rise time) flat topped positive pulses, which are differentiated by the 100 pF output capacitor. The resulting pulses, when examined at the far end of a terminated 100Ω cable, are 2.5 volts in size and of 50 nS duration.

To avoid degradation of the rise time and shape of the photomultiplier pulses due to the effects of stray

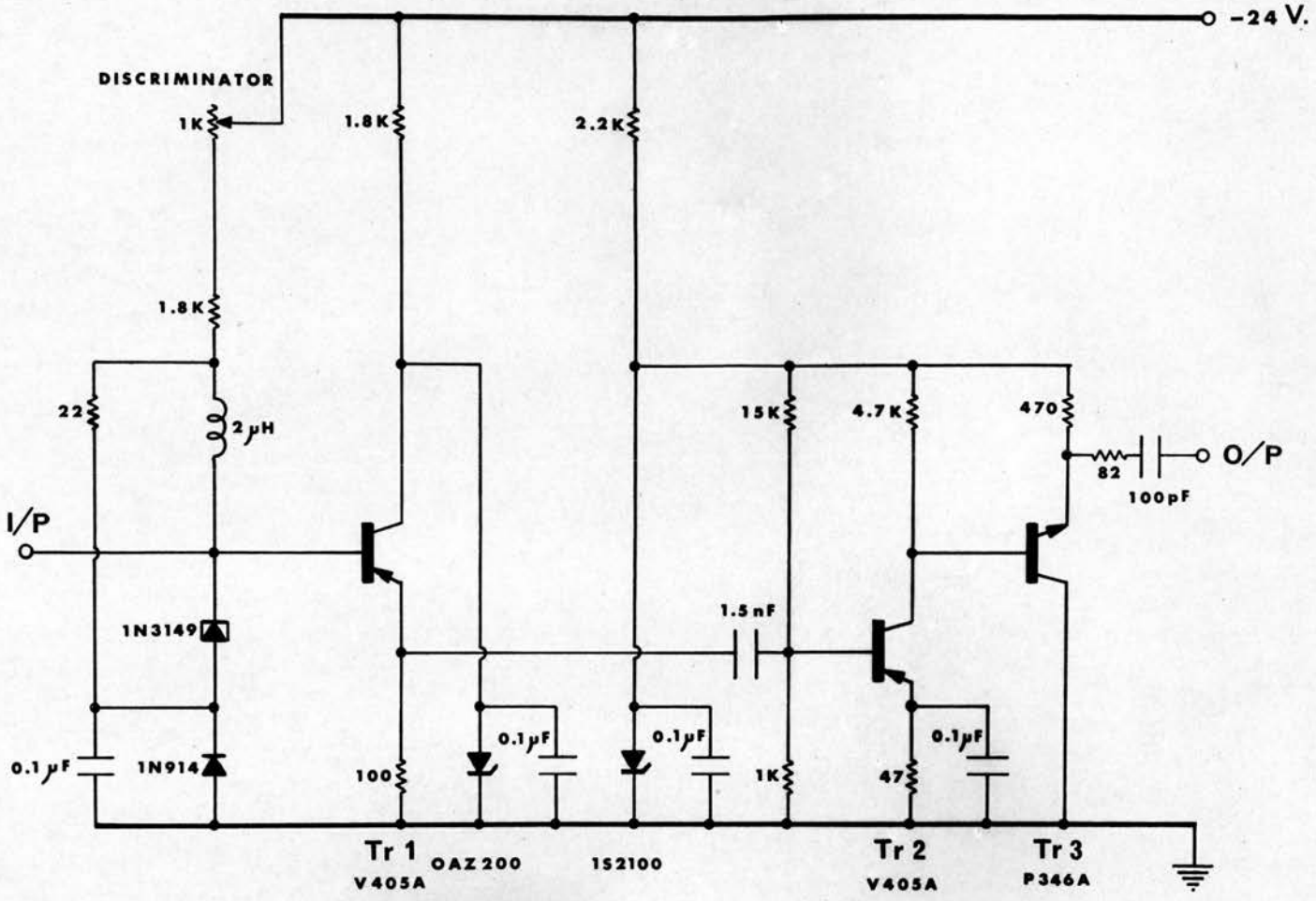
-24 V.
DISCRIMINATOR
1K
1.8K
2.2K
1.8K
22
2 μH
15K
4.7K
470
82
100pF
O/P
I/P
1N3149
1.5 nF
0.1 μF
1N914
0.1 μF
0.1 μF
0.1 μF
100
1K
47
Tr 1
V405A
OAZ 200
1S2100
Tr 2
V405A
Tr 3
P346A

FIGURE 5.6

capacitance, these timing circuits are mounted as closely as possible to the dynode resistor chains. The interconnecting cables are less than three inches long.

These circuits are capable of operating at pulse repetition rates slightly in excess of 1 MHz.

iii) The Fast Coincidence Unit

The pulses from the β limiting amplifier are fed to one input of the fast coincidence unit, while the timing pulses are fed to the other input to the coincidence unit via a delay routing circuit which will be described shortly. At each coincidence input the pulses are standardised by a fast monostable circuit adapted from a design by Righini[27]. This monostable circuit with associated pulse amplifier and line driver is shown in Fig. 5.7. The negative-going output pulses from this pulse standardiser have a very fast rise time (less than 2nS) and a duration of about 40 nS. They are, therefore, very suitable for shaping into pulses of about 10 nS duration by means of a short-circuited clipping cable. The line driver transistor, Tr 5, has a very low output impedance, and to match its output to the clipping stub and signal cable, a series resistor R is inserted as shown in Fig. 5.8. The pulses from the signal cable are of the form shown in Fig. 5.9, and the cleanest shape for coincidence adding corresponds to $B/A = 1$. The value of this ratio was measured for a few combinations

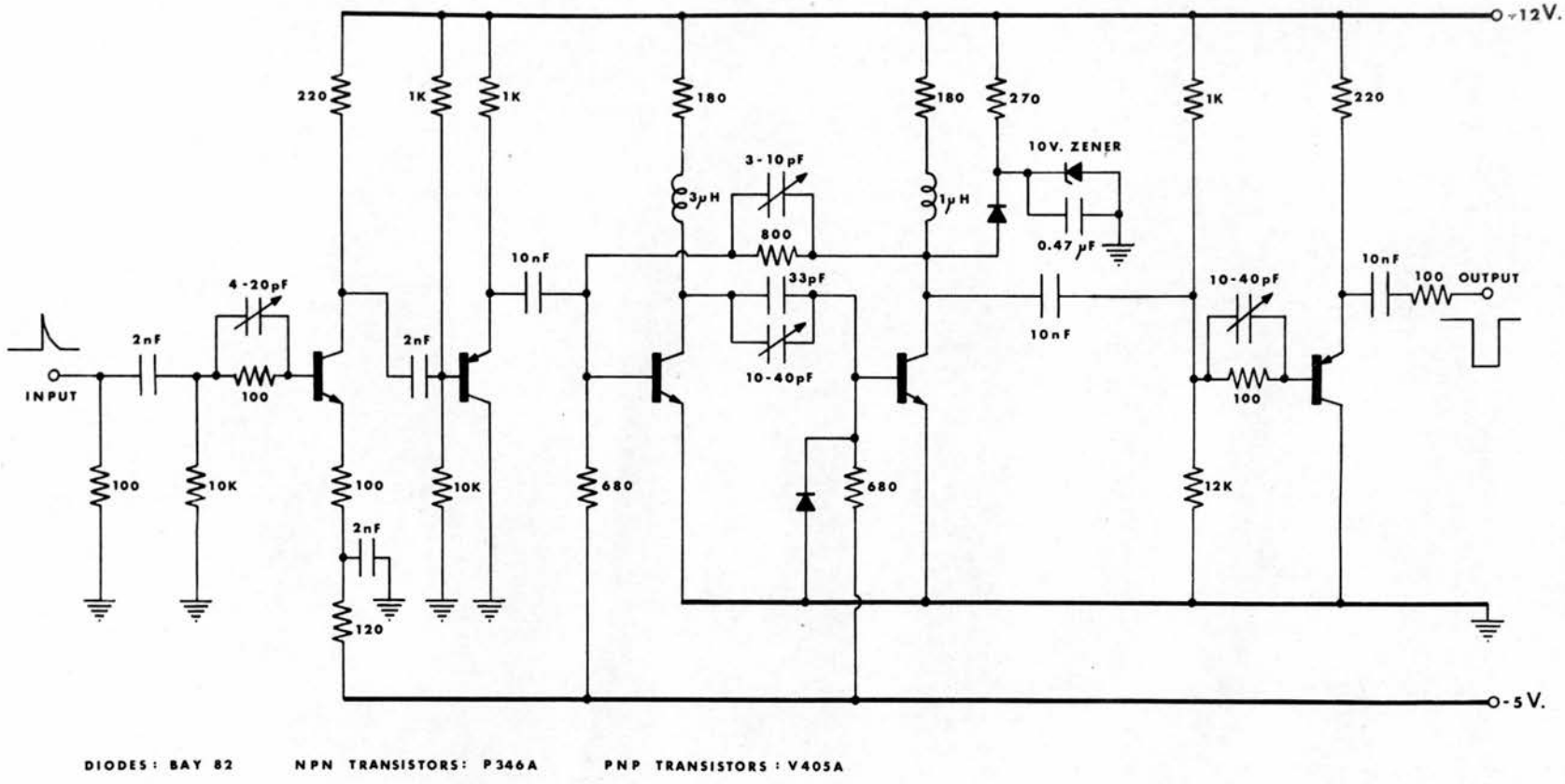
+12V.
220
1K
1K
180
180
270
1K
220
10V. ZENER
3-10pF
3μH
1μH
0.47μF
800
10nF
33pF
10nF
10-40pF
10nF
100 OUTPUT
4-20pF
2nF
2nF
INPUT
100
10-40pF
100
100
10K
100
10K
680
680
12K
2nF
120
-5V.
DIODES: BAY 82
NPN TRANSISTORS: P346A
PNP TRANSISTORS: V405A

FIGURE 5.7

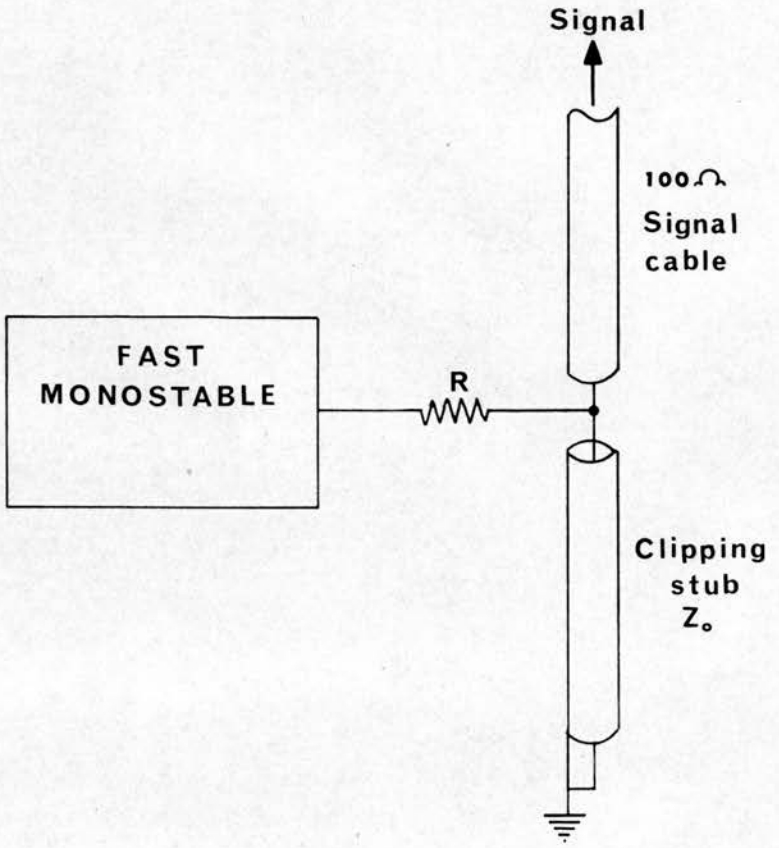

FIGURE 5.8

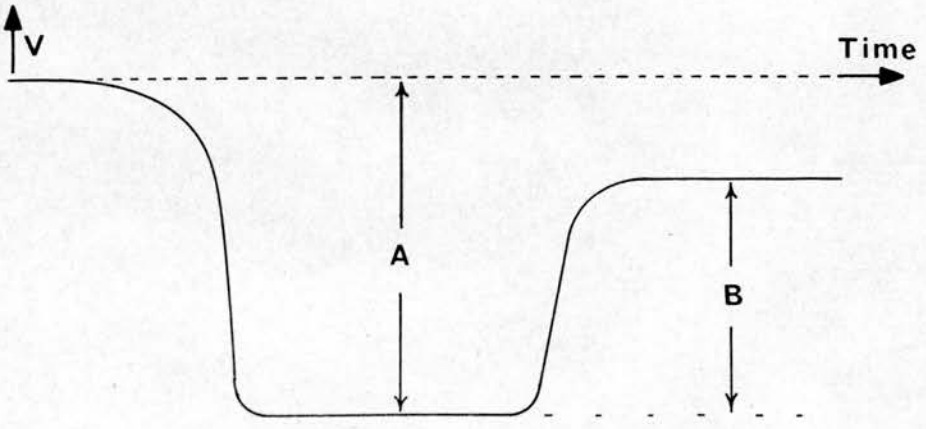

FIGURE 5.9

of R and Z_o, and the results are given in Table 5.1.

Table 5.1

Series resistor R (ohms)	Impedance of stub (ohms)	$\frac{B}{A}$
47	100	0.5
100	100	0.6
100	75	0.7
100	50	0.75

Apparently, optimum clipping occurs when the pulses reflected back from the short-circuited end of the clipping stub meet no impedance discontinuity at the mixing point.

The output pulses, suitably clipped, from the fast monostable circuits are then added at the simple diode adding gate via inputs (1) and (2); see Fig. 5.10. If these pulses overlap in time, the 2N501A transistor, operating in the avalanche mode, will trigger. This produces a very fast rising (rise time less than 1 nS) 20 volt positive pulse at the transistor collector, which is then differentiated and attenuated by the 0.5 nF capacitor and the resistors in the output circuit. The trigger threshold of this avalanche transistor (and, therefore, to some extent the coincidence resolving time) can be adjusted by varying the positive bias on its base by means of the 100K potentiometer. If this bias is removed

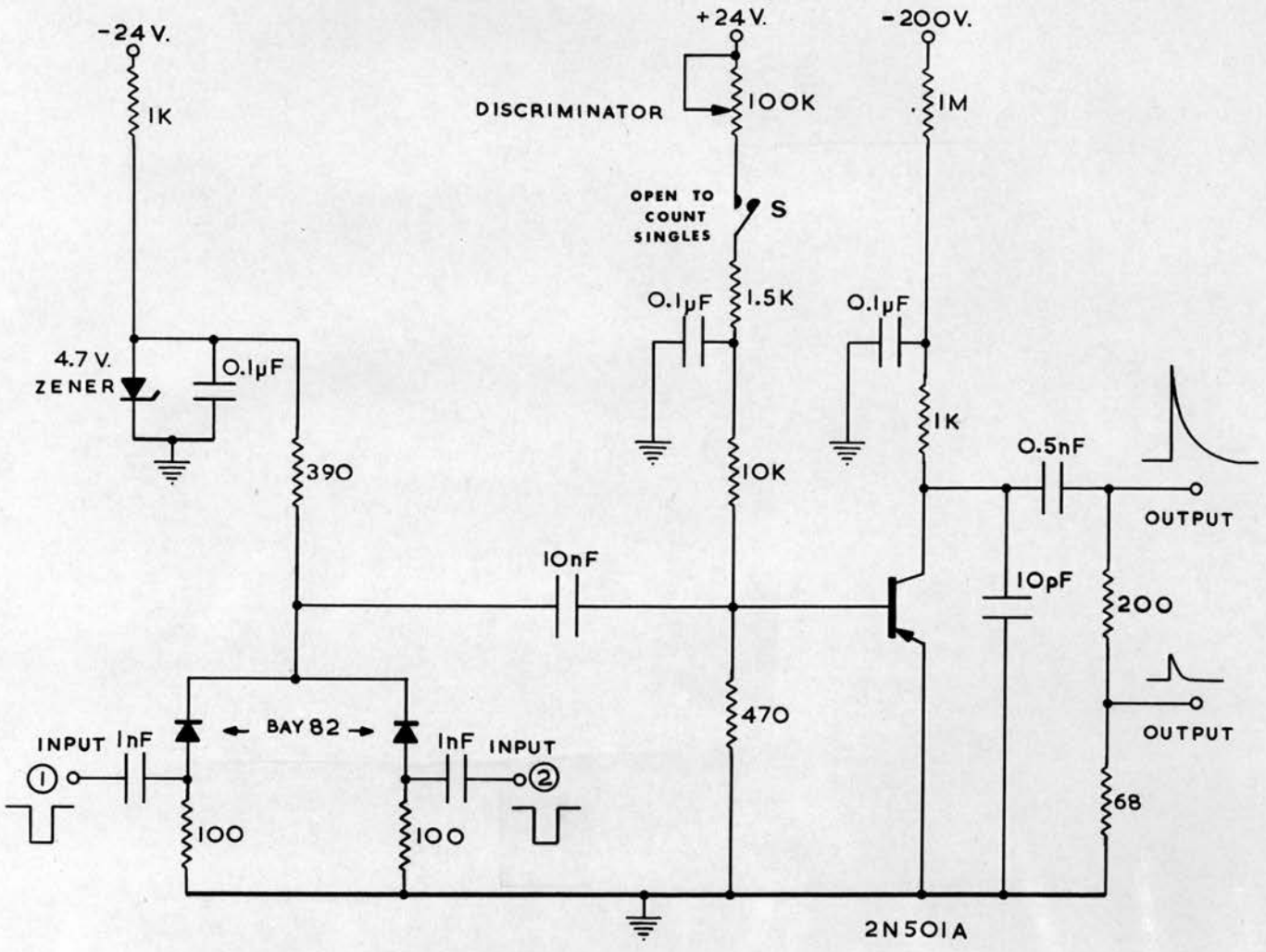
-24 V.
1K
+24 V.
-200V.
DISCRIMINATOR
100K
1M
OPEN TO COUNT SINGLES
S
0.1μF
1.5K
0.1μF
4.7 V. ZENER
0.1μF
390
10K
1K
0.5nF
OUTPUT
10nF
10pF
200
470
OUTPUT
INPUT
1nF
BAY 82
1nF
INPUT
1
2
100
100
68
2N501A

FIGURE 5.10

completely by opening the switch S, then the avalanche transistor will trigger on single input pulses, thus providing a simple monitor of the single input rates.

The variation of coincidence resolving time with discriminator level was investigated by recording the random coincidence counting rate, N_{RC}, at various settings of the discriminator. The fast input rates, N_γ and N_β, were each measured, and the resolving time, 2τ, was calculated from

$$N_{RC} = 2\tau N_\gamma N_\beta \quad .$$

The time correlation between the two input pulse trains was destroyed by inserting a 100 nS delay cable into one of the channels.

This calibration of the discriminator, using 10nS pulse-clipping stubs, is shown in Fig. 5.11.

The avalanche transistor pulses are then fed to a circuit which produces both a prompt output and a delayed output. This latter facility is necessary in a fast-slow coincidence system to allow time for the relatively slow-acting pulse height analysers to operate. This output circuitry is shown in block diagram form in Fig. 5.12.

iv) <u>The Delay Routing Switch</u>

It is standard practice to measure the random coincidence rate in a coincidence system by inserting a time delay, of duration much greater than the resolving time, into one input channel. The time correlation between the

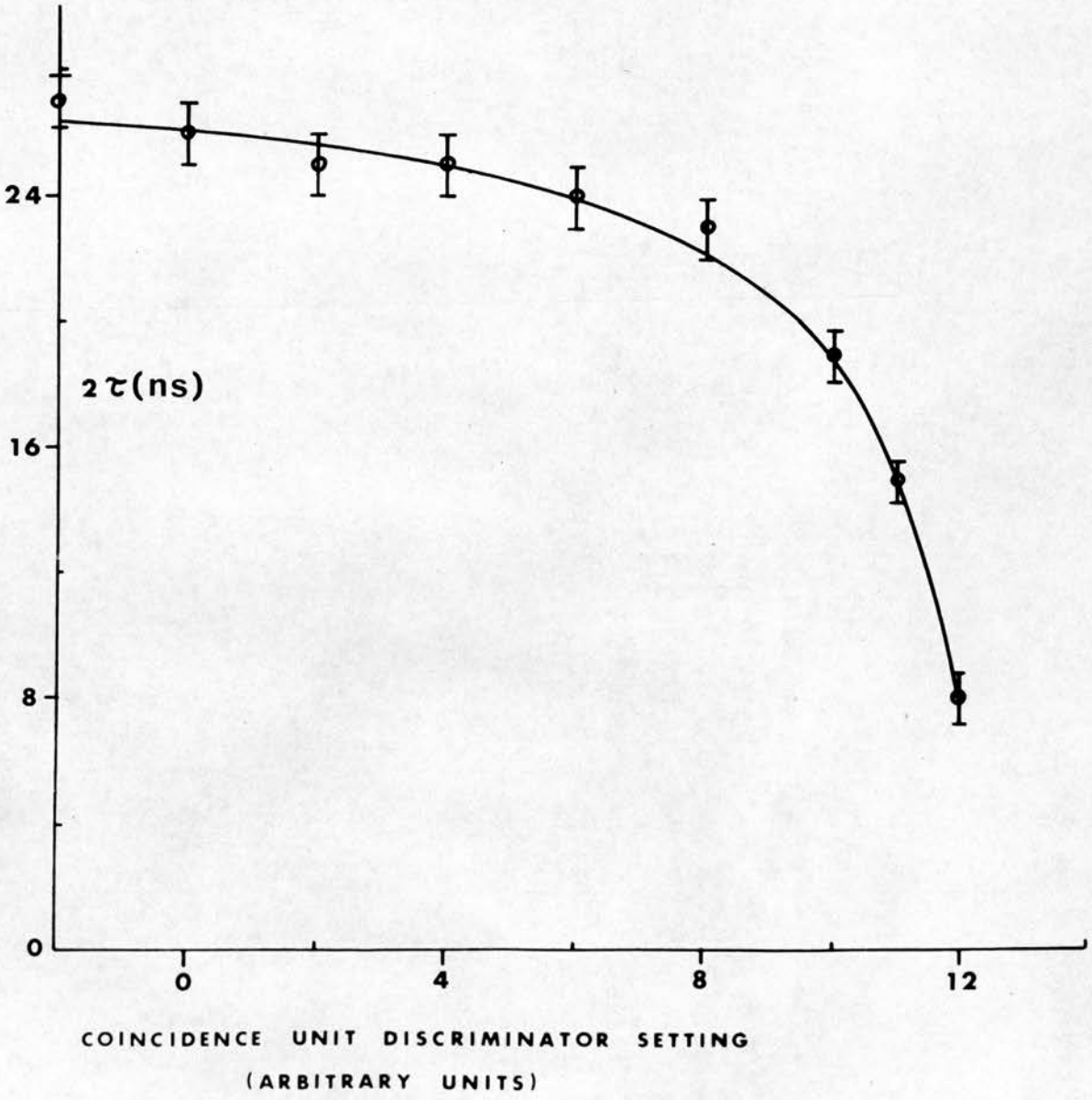
24
16
8
0
2τ(ns)
0
4
8
12
COINCIDENCE UNIT DISCRIMINATOR SETTING
(ARBITRARY UNITS)

FIGURE 5.11

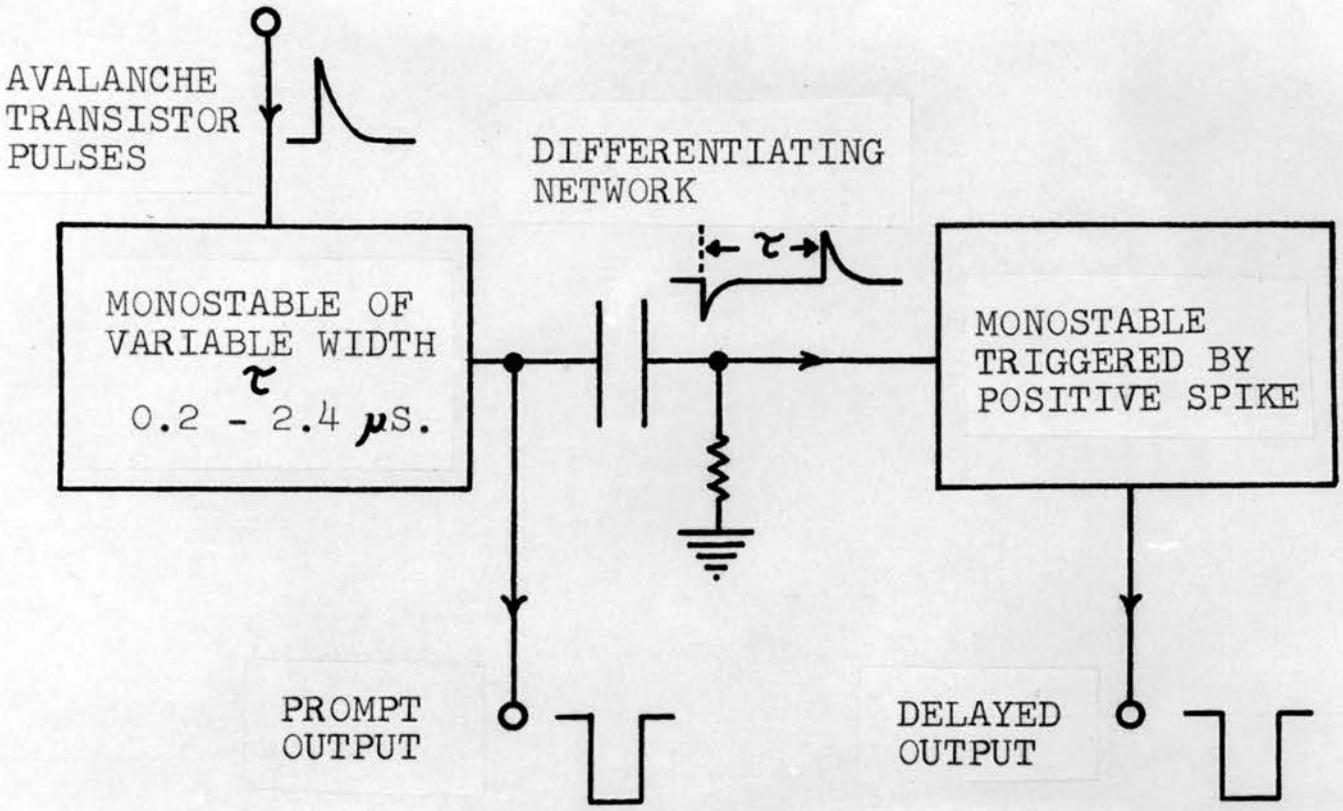
AVALANCHE
TRANSISTOR
PULSES
DIFFERENTIATING
NETWORK
τ
MONOSTABLE OF
VARIABLE WIDTH
τ
0.2 - 2.4 μs.
MONOSTABLE
TRIGGERED BY
POSITIVE SPIKE
PROMPT
OUTPUT
DELAYED
OUTPUT

FIGURE 5.12

two inputs is then lost. In the present case, it is convenient to do this automatically by means of the system control unit at every second phase of a full counting cycle. The pulse routing circuit is shown in Fig. 5.13, where (S) and (T) refer to points labelled on the control circuit diagram, Fig. 5.14.

When the magnet current is switched on, the fast γ pulses are routed through the 2nS cable, and when the magnet is off, the pulses pass through the 100 nS delay cable. Thus the coincidence counting rate recorded when the magnetic field is switched off is a measure of the random coincidence counting rate. Errors due to slow drifts in the coincidence resolving time are therefore eliminated.

The fast β pulses are not sent through a randomising delay switch, but, for symmetry, are passed during all phases of the counting cycle through a circuit identical to that traversed by the fast γ pulses when routed via the 2nS cable.

v) The Slow Electronics

Most of the rest of the electronics was purchased from Nuclear Enterprises (G.B.) Ltd. from their Edinburgh Series range of units. The following units are used:

Preamplifiers	NE5281	Timer	NE5053
Amplifiers	NE5256	Print control unit	NE6304
Single channel analysers	NE5153	E.H.T. Supplies	NE5353

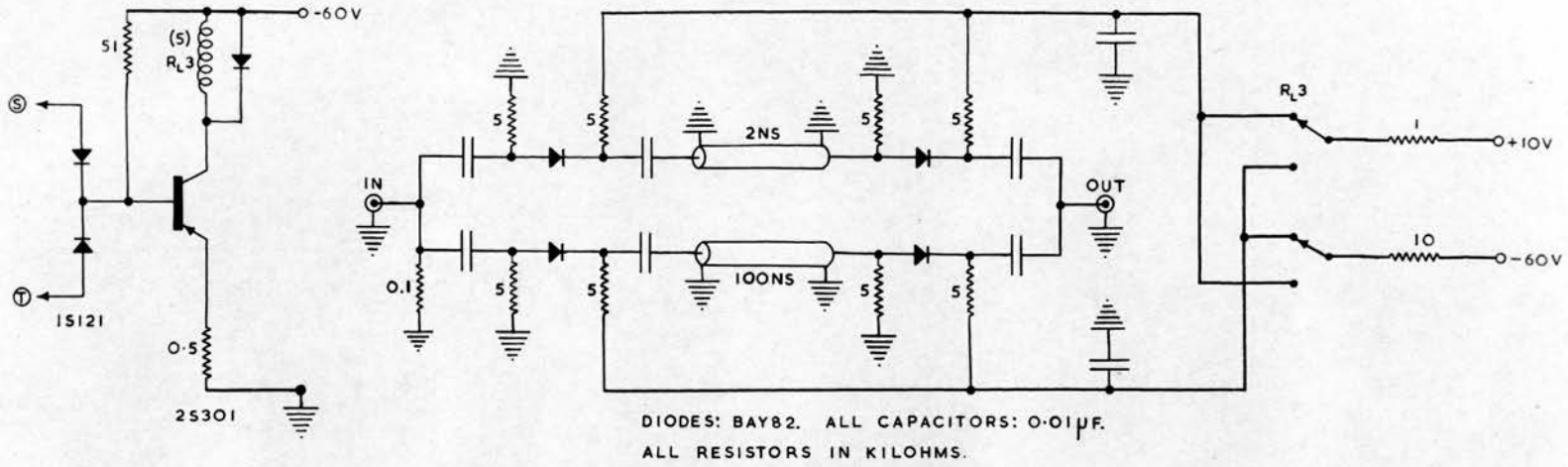
-60V
51
(S)
R_L3
S
T
15121
0·5
25301
IN
0.1
5
2NS
100NS
OUT
R_L3
1
+10V
10
-60V
DIODES: BAY82. ALL CAPACITORS: 0·01μF.
ALL RESISTORS IN KILOHMS.

FIGURE 5.13

Slow Coincidence Unit	NE5704	L.T. Supply	NE5384
Scalers	NE5073		

The Edinburgh Series scalers, timer and print control unit are particularly suitable for the present work, because they can be stopped, started and reset by remote control electrical pulses. This is an essential feature for use in an experiment where frequent data sampling necessitates an automatic system.

Because the β counting rates are very high in this experiment, it was necessary to build a prescaler to divide the scaler input by 16 in order to avoid overflowing of the β scaler's store of 10^6. A prescaler, operating by binary division, was constructed around an integrated circuit SN7493N.

The print-out is a record of the three scaler counts and the elapsed counting time measured by the timer, and is simultaneously presented in both typewritten and punched tape form by an ASR 33 page printer, which has been modified to accept the output of the NE6304 print-control unit.

vi) <u>The Automatic Data Sampling System</u>

The counting rate asymmetries to be measured in the present work are very small ($\approx 10^{-2}$), and therefore instrumental asymmetries due to electronic drifts must be kept to a minimum by sampling the data at time intervals which are short compared with the electronic drifting

time. In practice, with the present apparatus, the sampling time must be no longer than about 100 seconds, and for a total counting time of several weeks, several tens of thousands of samples require to be recorded. Under these circumstances, it is obvious that the system must be automated.

The Counting Cycle

An automatic system control unit has been built which provides the following cycle of operations, suitable for a β-γ circular polarisation correlation experiment:

a) Switch magnetic field
b) Reset scalers and timer
c) Start scalers and timer
d) Stop scalers and timer
e) Print-out scalers and timer
f) Switch magnetic field, i.e. back to phase a).

There are short delays of about 1 second incorporated between steps (a) and (b), and between (b) and (c). The delay between steps (a) and (b) is to allow any ringing in the magnet circuit to decay. If the magnet used is a large energy store, then switching surges may feed through to the scalers as control pulses, with the result that one or more scalers may start prematurely at the instant of magnet switching, introducing a spurious asymmetry into the counting rates.

When this trouble was experienced, it was overcome by reversing the order of functions (b) and (c); i.e. the scalers and timer start then reset without stopping. The counting time therefore starts with the resetting of the scalers and timer.

The duration of each sample of the counting rates (the time between (c) and (d)) is set either by a pre-set time or by a pre-set number of counts in one scaler; this latter procedure automatically normalises the samples to a selected count.

Function (a) has two possible sequences. The magnetic field can simply reverse when switched, or it can follow the cycle:

field on in one direction - field off - field on in the opposite direction - field off.

The use of the zero field phase in the cycle is that the single rates can provide a measurement of the analysing efficiency of the magnet as described in Chapter 4.

The Operation of the Circuit

The complete circuit is shown in Fig. 5.14, and a block diagram in Fig. 5.15. The five bistable circuits are similar, and so the component values are given only once. For clarity in these circuits, the resistance values are given in units of kilohms and the capacitors in microfarads. The two magnet switching relays each have two mercury make contacts and an energising coil resistance of 2K.

FIGURE 5.14

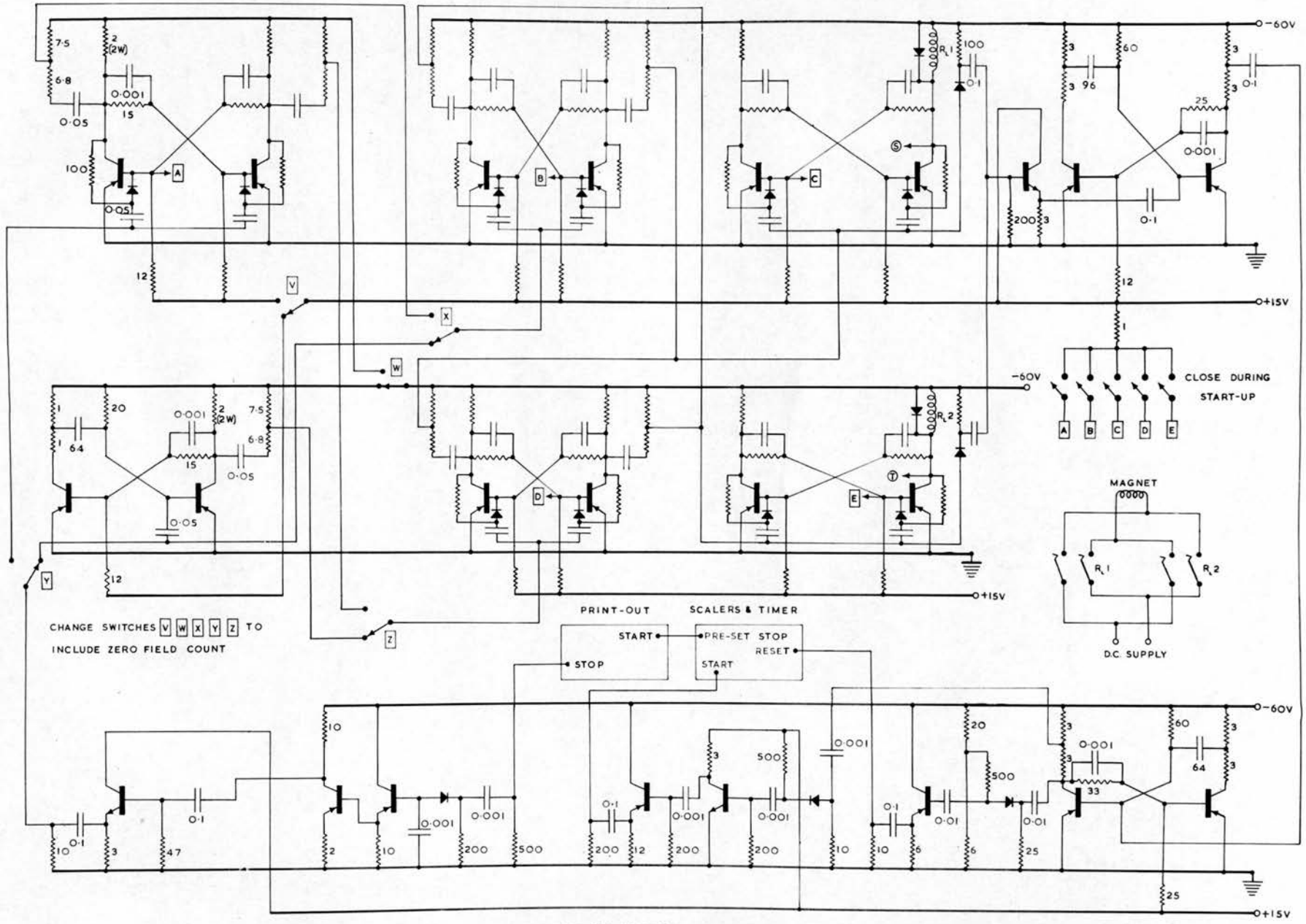

DIODES: IS121. P-N-P TRANSISTORS: 2S301. N-P-N TRANSISTORS: 2N1304. RESISTORS IN KILOHMS. CAPACITORS IN MICROFARADS.

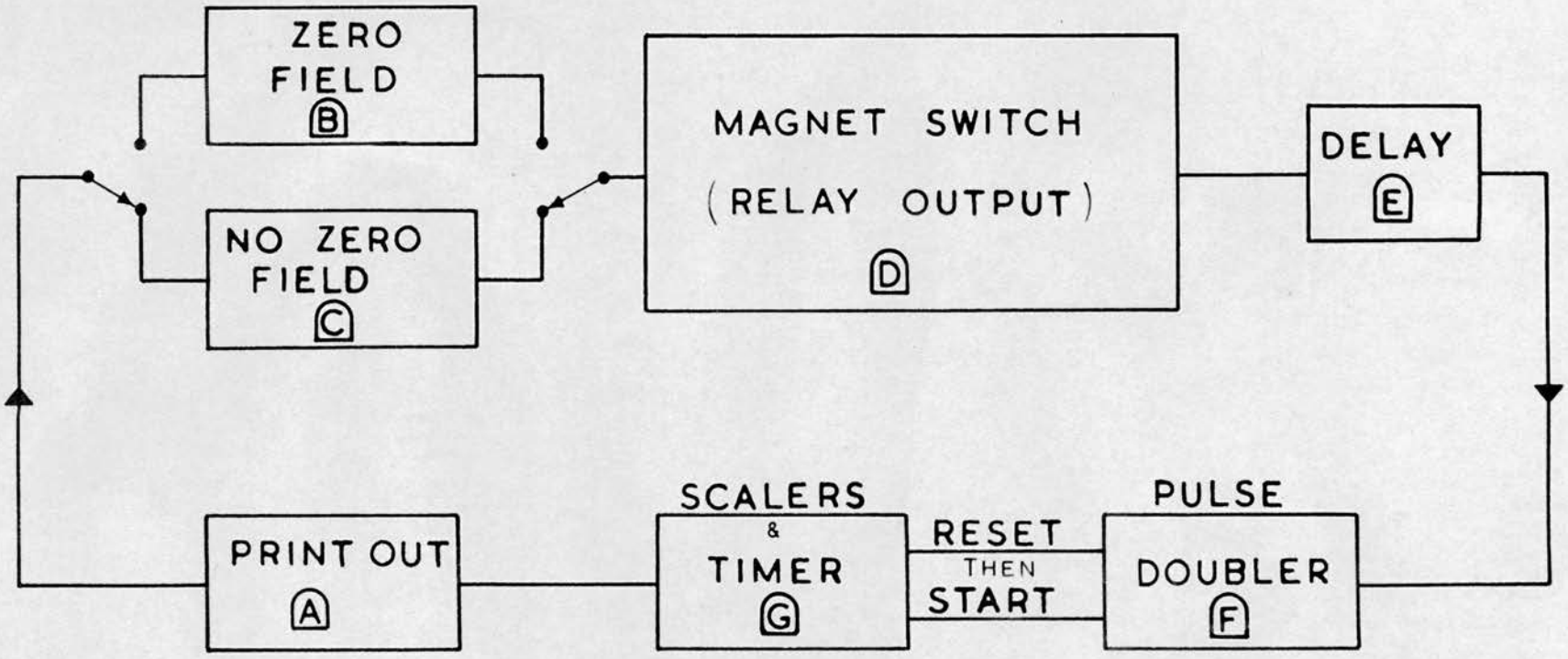
ZERO
FIELD
B
NO ZERO
FIELD
C
MAGNET SWITCH
(RELAY OUTPUT)
D
DELAY
E
PRINT OUT
A
SCALERS
&
TIMER
G
RESET
THEN
START
PULSE
DOUBLER
F

FIGURE 5.15

When the circuit is operated to include a zero field count, then the magnet cycle has four steps. The circuits B and D in series provide the necessary division by four, and also pulse routing such that each bistable with relay output receives two consecutive pulses. Correct phasing of these circuits is established at the start of an experiment by resetting the bistables with a momentary connection of points A, B, C, D, E to the +15V line.

In the other mode, when the system is set to operate without a zero field count, the magnet cycle has only two steps. The control pulse from A is fed to D along with a delayed pulse from C; the prompt pulse switches the magnet off, and the delayed pulse switches it on with opposite polarity. Circuits C and D in series then provide the necessary scale of two. The delay between the two pulses passed by C avoids short-circuiting of the magnet power supply by ensuring that both relays are never on together. In this mode of operation, the delay E, which is longer than the delay incorporated in C, suppresses the delayed pulse from C, and feeds only one control pulse to F.

The pulse doubler, F, provides the two outputs for resetting and starting the scalers, the start pulse being delayed with respect to the reset. The output pulses from a scaler or timer and from the print-out control unit are incorporated in the control pulse loop.

In order to ensure that the reset and start pulses, which are negative-going 12 volt pulses, had sufficiently fast leading edges to trigger the particular scalers used,

they were speeded up using the tunnel diode pulse shaper and amplifier shown in Fig. 5.16. The output pulse from this circuit has a rise time of 30 nanoseconds, and an amplitude of about 8 volts negative.

The power supplies required to run this control system (including the delay routing switch) are:

- 60 V	at 250 mA	none of these required to
+ 10 V	at a few μA	be stabilised or specially
+ 15 V	at 25 mA	well smoothed.

vii) An Attempt to Produce a Magnetic Field Stabilisation System

In an attempt to eliminate the γ counting rate asymmetry arising from the cycling stray magnetic field of the magnet, a magnetic field stabilisation system was designed and built. This was a feedback system using a probe sensitive to magnetic fields placed near the γ photomultiplier tube. This probe produces a signal which is amplified to provide the D.C. current flowing in the bucking coil surrounding the γ counter. Fig. 5.17 is a block diagram of the system.

The probe consists of a ferrite-cored inductor which forms part of the tuned circuit of an oscillator running at about 1 MHz. The oscillator frequency depends upon the probe inductance, which, in turn, depends upon the magnetic permeability of the ferrite core. This permeability depends quite strongly upon the state of

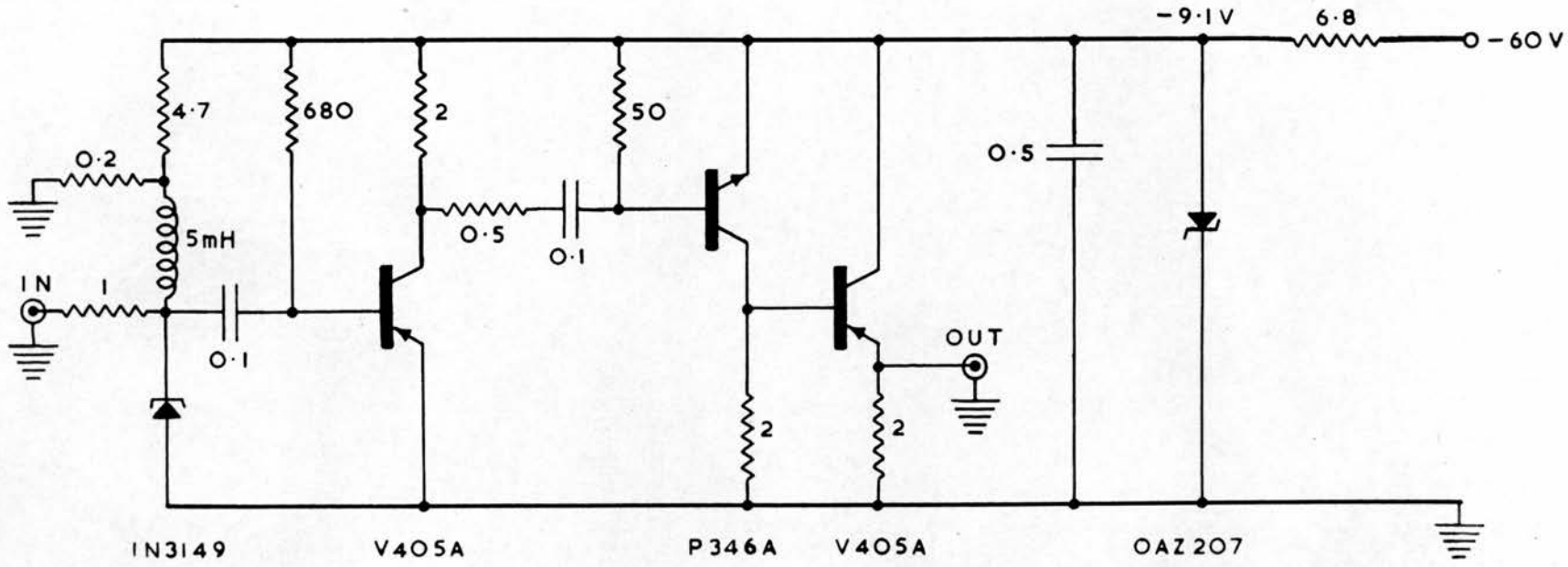

ALL RESISTORS IN KILOHMS, CAPACITORS IN μF.

FIGURE 5.16

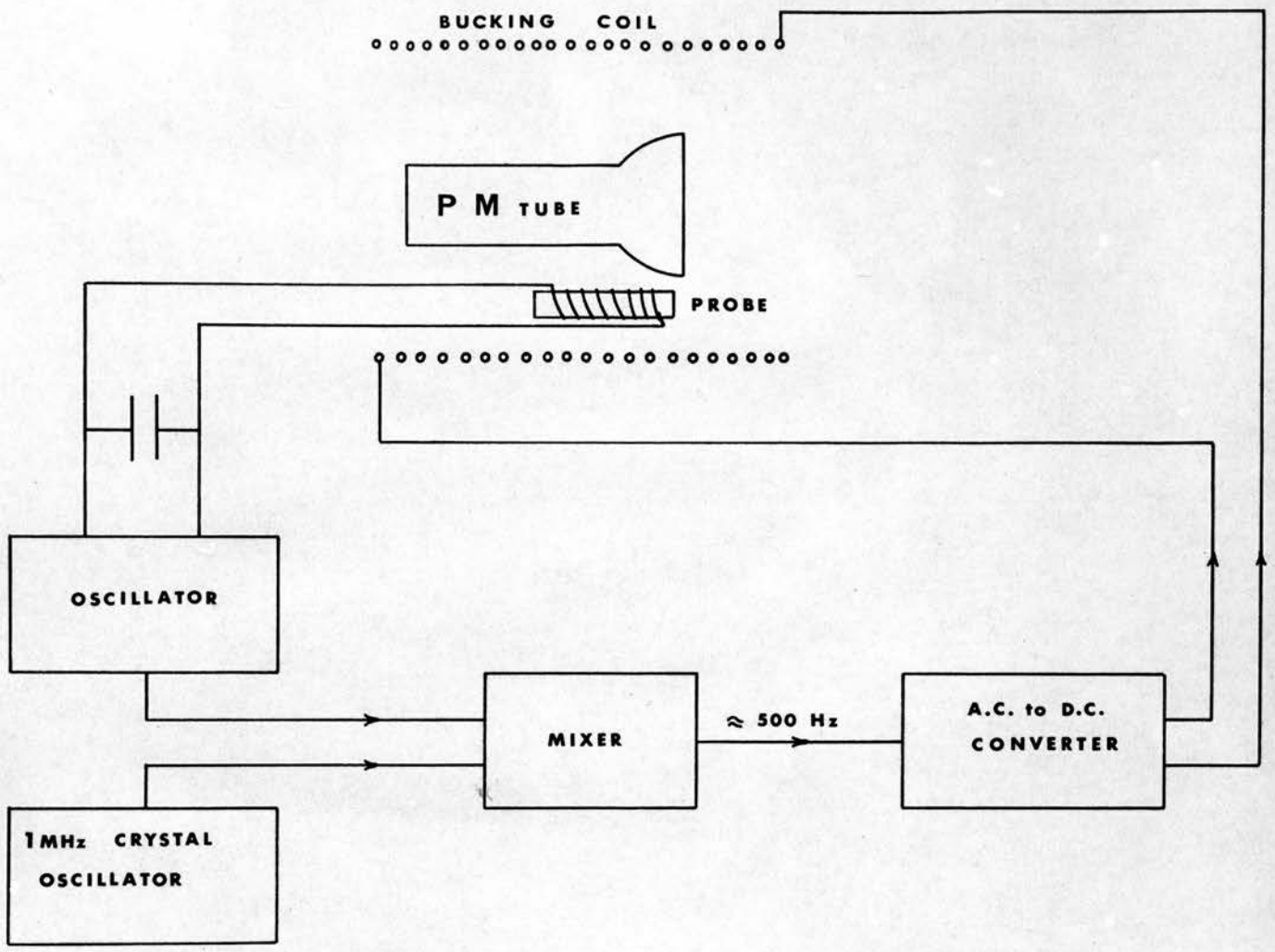
BUCKING COIL
P M TUBE
PROBE
OSCILLATOR
MIXER
≈ 500 Hz
A.C. to D.C.
CONVERTER
1MHz CRYSTAL
OSCILLATOR

FIGURE 5.17

magnetisation of the ferrite, and therefore upon the impressed magnetic field. The frequency of the oscillator is then a measure of the magnetic field at the photomultiplier. The operation of the remainder of the servo system is indicated in Fig. 5.17.

Measurements made with a tangent magnetometer replacing the photomultiplier assembly showed that the magnetic field was held constant to within about 10^{-6} weber/sq. m. when the cycling stray field was switched on. This compares very favourably with the magnitude of the uncompensated stray field fluctuations which were of the order of 10^{-4} weber/sq. m. at the position of the photomultiplier.

Although this system gave the required degree of magnetic field stabilisation, it was soon obvious that drifting of the frequency of the probe oscillator, arising from temperature fluctuations, completely outweighed the magnetic sensitivity of the probe. Various types of oscillator were tried, and it was unfortunately concluded that the required degree of frequency stability was unattainable when using a ferrite-cored inductor in the tuned circuit.

As mentioned in paragraph 4.9, a suitable stabilisation system, not suffering to such an extent from thermal drifts, should be able to be developed, from the system designed by Graham and Geiger[23].

5.4 The Source

A 6 mC source of 12.4 year half-life Eu^{152} in the chemical form Eu $C\ell_3$ was prepared at The Radiochemical Centre of the U.K.A.E.A. at Amersham by neutron bombardment of a Eu^{151} enriched target of Eu_2O_3. The extent of the Eu^{154} contamination in the final source is small and of the order of 0.5%.

The 2 mm. diameter source was mounted on a hollow perspex cylinder as shown in Fig. 5.18. The wall thickness of the cylinder was kept to a minimum to reduce scattering. The holes in the curved wall of this cylinder are to prevent source damage by relieving any pressure differences which might be developed across the source backing. The backing for the source was a 0.0005" thick (1.7 mg./sq. cm.) sheet of the melamine-based plastic, Melinex. The front of the source - the β particle exit - was protected by a layer of the epoxy lacquer Araldite PZ 820, thinned down to give a superficial density of about 300μg/sq. cm. With a specific activity of about 1C/gm., and a diameter of 2 mm., the Europium source has a superficial density of about 200 mg./sq. cm.

The source mount is held in place by a grub screw in the source holder shown in Fig. 5.19. This brass holder was specially designed to allow unimpeded γ emission towards the γ counter for all values of $\Theta_{\beta\gamma}$

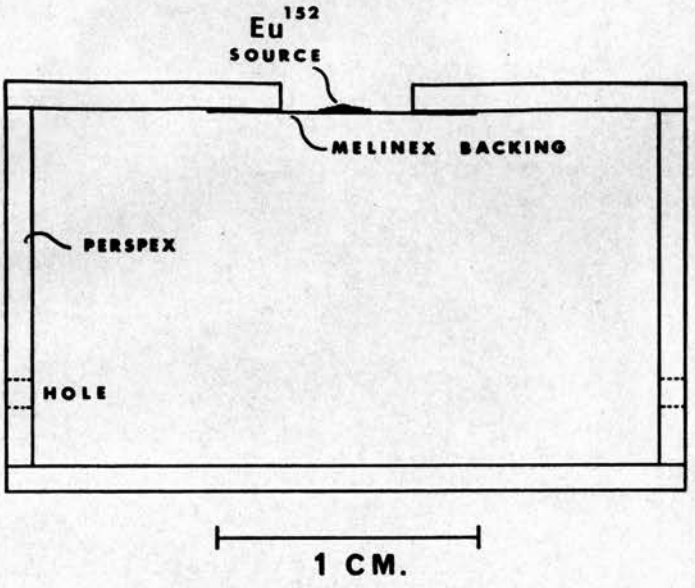

FIGURE 5.18

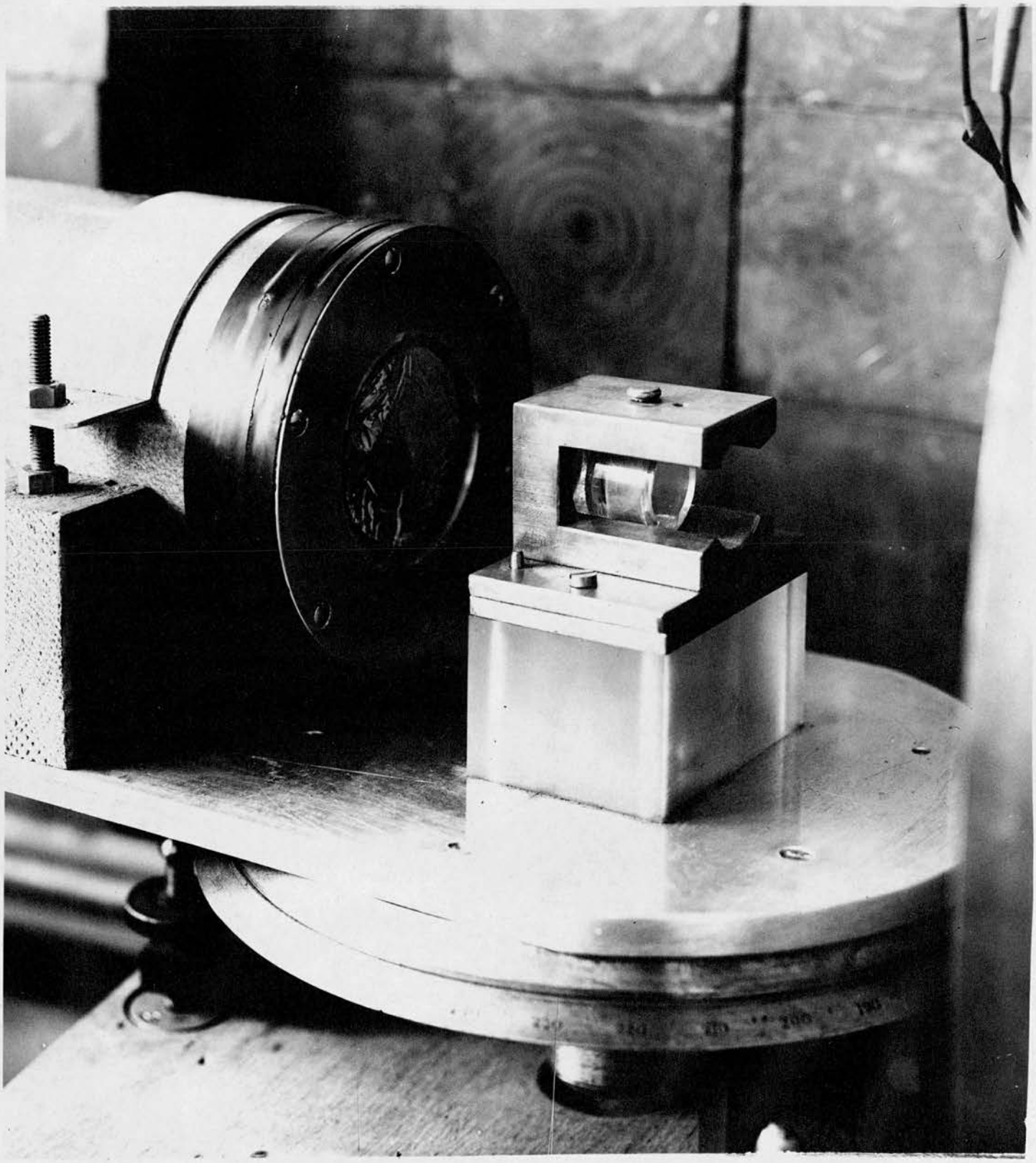

FIGURE 5.19

from $\pi/2$ to $3\pi/2$, and is accurately located on the β counter turntable by means of two tightly fitting locating pins.

It was not considered to be worthwhile evacuating the β side of the apparatus, because the path length of the β particle in air is about 5 cm. (corresponding to about 6 mg./sq. cm. at N.T.P.), while the particle kinetic energy is greater than 0.7 MeV.

CHAPTER 6

EXPERIMENTAL PROCEDURE

6.1 Centring the Source

The Eu^{152} source had to be positioned in the holder such that it lay on the axis of rotation of the turntable. This was accomplished by first of all making a rough adjustment of the location by visual inspection through a rigidly mounted telescope, ensuring that the source centre did not stray from the telescope's cross-wires as the turntable was rotated. The exact position of the centre of the active deposit is not known, however, and so the final alignment was carried out by adjusting the position of the source mount in the holder until rotation of the turntable produced a change in the γ counting rate of less than 0.2%.

6.2 Energy Calibration of Counters

Gamma Counter

The energy calibration of the γ counter was carried out using the 510 keV photons from Na^{22} and the 662 keV γ rays from Cs^{137}. The distance of each of these sources from the NaI crystal was adjusted until the total counting rates were approximately equal to the γ counting rate of the actual experiment. This was done to reduce the effect of counting rate on the gain of the γ channel. The resulting calibration is shown in Fig. 6.1, where it is seen that there appears to be no zero error in the energy calibration

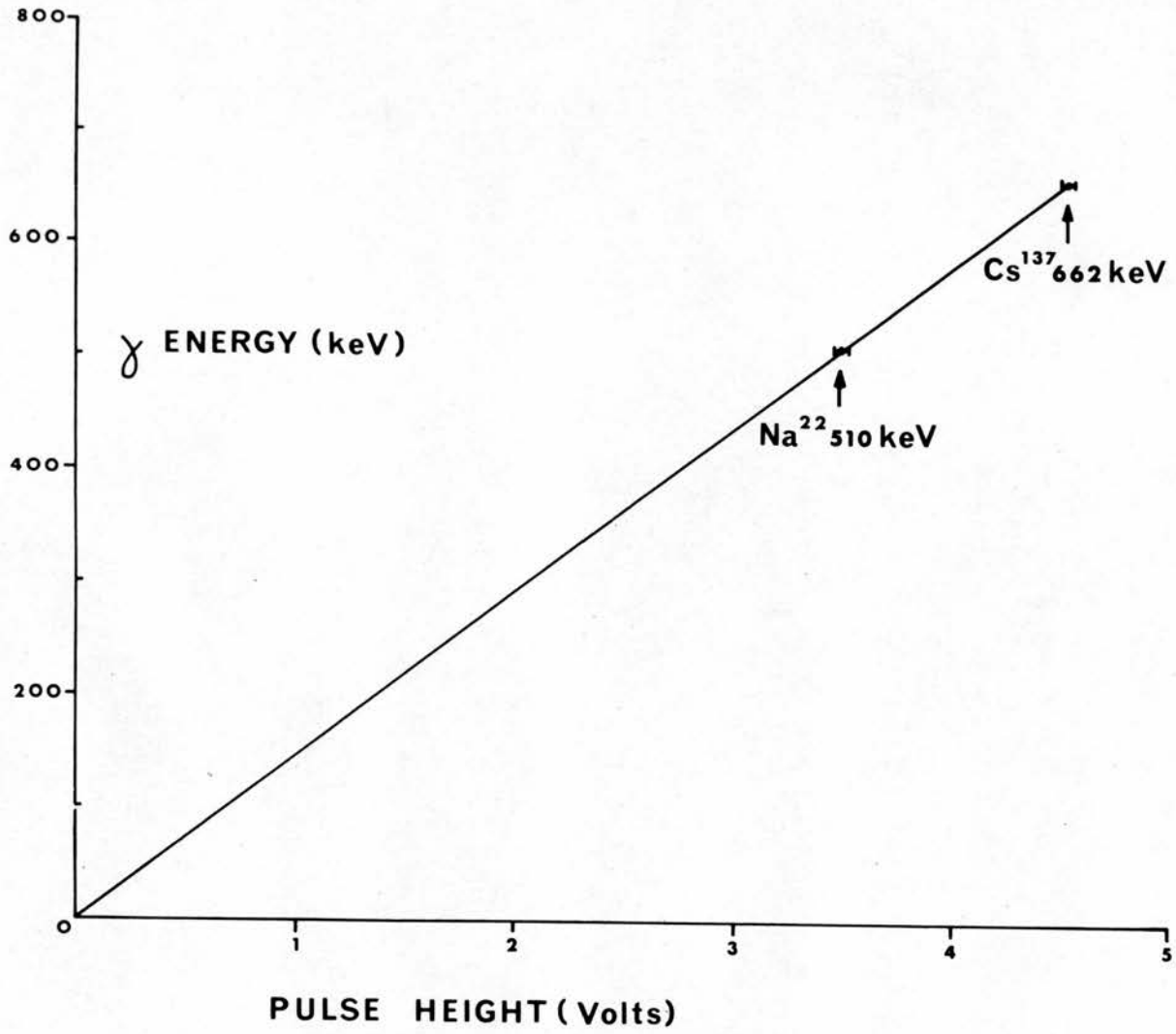
800
600
400
200
0
γ ENERGY (keV)
Cs137 662 keV
Na22 510 keV
1
2
3
4
5
PULSE HEIGHT (Volts)

FIGURE 6.1

of the γ channel ~~has no zero error~~; day-to-day energy re-calibrations of this channel were carried out using the Na^{22} source only.

Eu^{152} spectra taken with and without transmission through the magnet are shown inFig. 6.2 and Fig. 6.3, where it can be seen that the energy resolution is, as expected, severely degraded by the magnet.

Beta Counter

Since the present experiment involves measuring small asymmetries in counting rates, it is necessary to have rates as high as possible, in order to obtain reasonably small statistical uncertainty in the results. It was soon obvious that, in the present work, if sufficiently high counting rates were to be achieved, the β counter had to be operated as fast as possible, by using a large solid angle. At rates as high as these (total rate about 10^5 per second) there was considerable trouble with pulse pile-up, and the gain of the β channel was strongly dependent on counting rate. The energy calibration of the β counter, therefore, had to be carried out under an exact replica of the experimental conditions.

In fact, the β channel was calibrated by counting the β particles from the Eu^{152} source itself, under the final experimental conditions. A β spectrum, corrected for the presence of γ rays by means of a spectrum taken through a β-absorbing 0.5 inch perspex sheet, was obtained, and from this, Kurie plots were drawn using several assumed energy calibrations of the β counter. The spectrum shape cor-

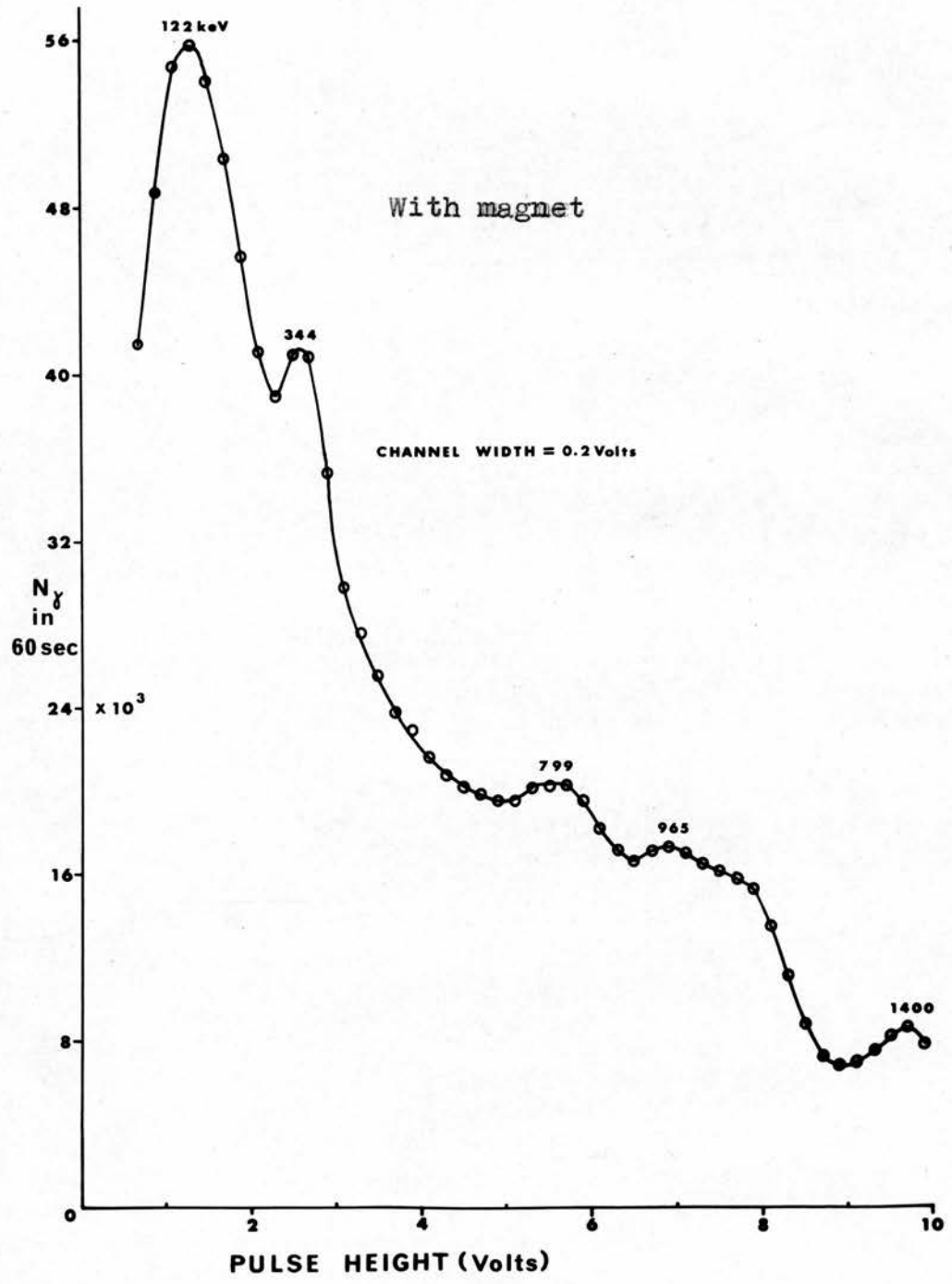
122 keV
344
799
965
1400
With magnet
CHANNEL WIDTH = 0.2 Volts
N_γ in 60 sec
x 10^3
56
48
40
32
24
16
8
0
2
4
6
8
10
PULSE HEIGHT (Volts)

FIGURE 6.2

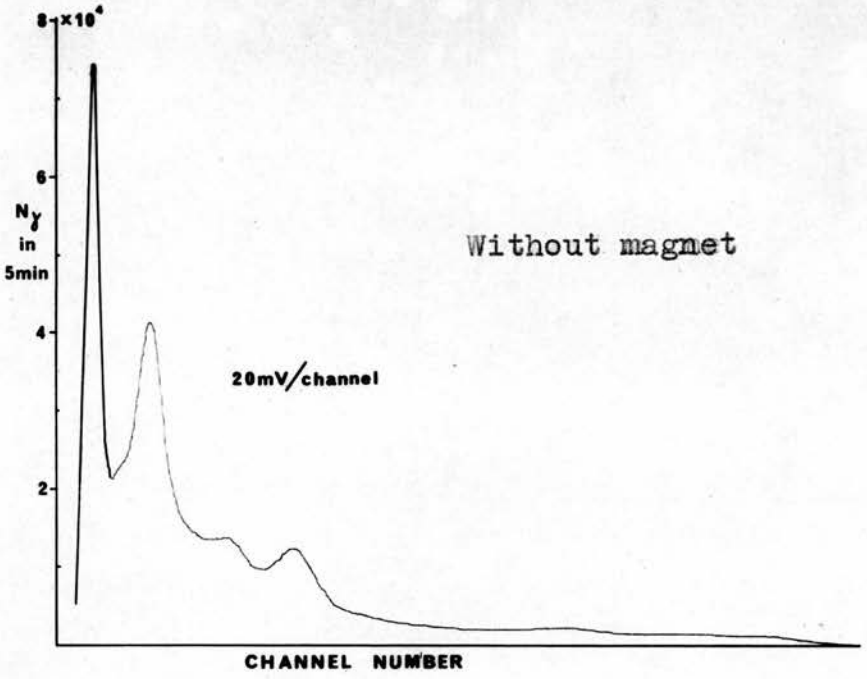
8 ×10⁴
6
Nγ in 5min
4
2
Without magnet
20mV/channel
CHANNEL NUMBER

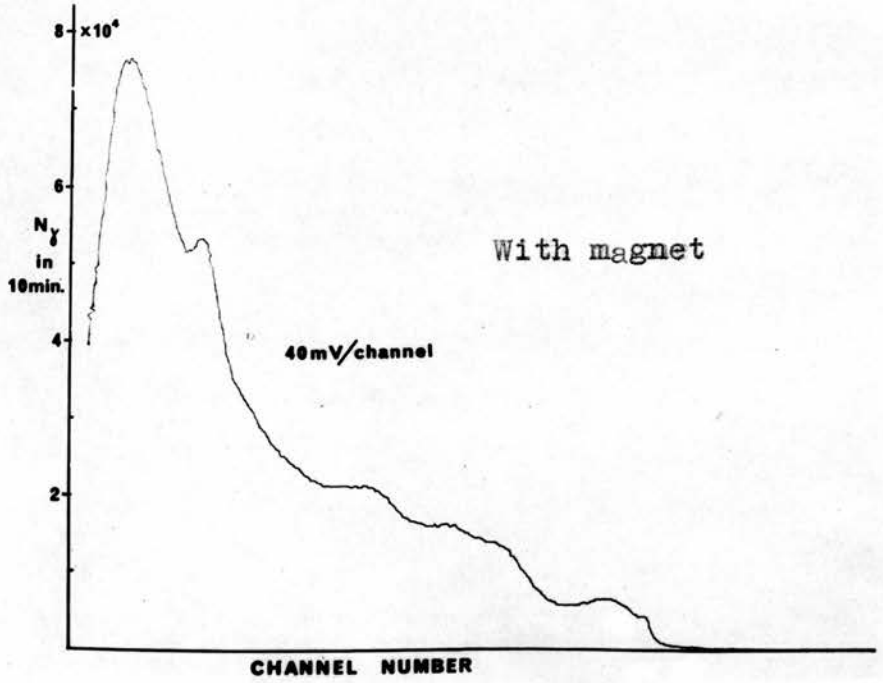
8 ×10⁴
6
Nγ in 10min.
4
2
With magnet
40mV/channel
CHANNEL NUMBER

FIGURE 6.3

rection factor of Langer and Smith[28] was used in producing these plots; the values of the Fermi function were those of Rose et al.[29]. The corrected β spectrum is shown in Fig. 6.4, and the trial Kurie plots in Fig. 6.5. These Kurie plots were examined for straightness and an extrapolated intercept at $W = 3.9\ mc^2$, which is the end-point energy of the β group being investigated. It is obvious that none of the plots is very satisfactory in these respects; at the low energy end they curve upwards due to the presence of competing β groups, whereas at the high energy end they again curve upwards due to pulse pile-up. It is possible, however, to select one plot which has, over part of its length, a straight portion which does produce an extrapolated intercept at about W = 3.9. This particular Kurie plot, the one drawn with a β spectrum calibration where 3.5 volts corresponds to 1.5 MeV, then, has been drawn with the "correct" energy calibration; and in this way, the energy calibration of the β channel can be inferred. The accuracy of this calibration selection method is rather low - possibly $\pm$ 0.3 volts in 3.5 volts, which leads to a 10% uncertainty in the β energy selection.

The β counts were divided by 16 by a prescaler, in order to avoid overflowing of the β scaler's store of 10^6.

6.3 Setting the Bucking Coil Currents

The currents through the bucking coils were bled from the magnet supply via rheostats, so that fine adjustment

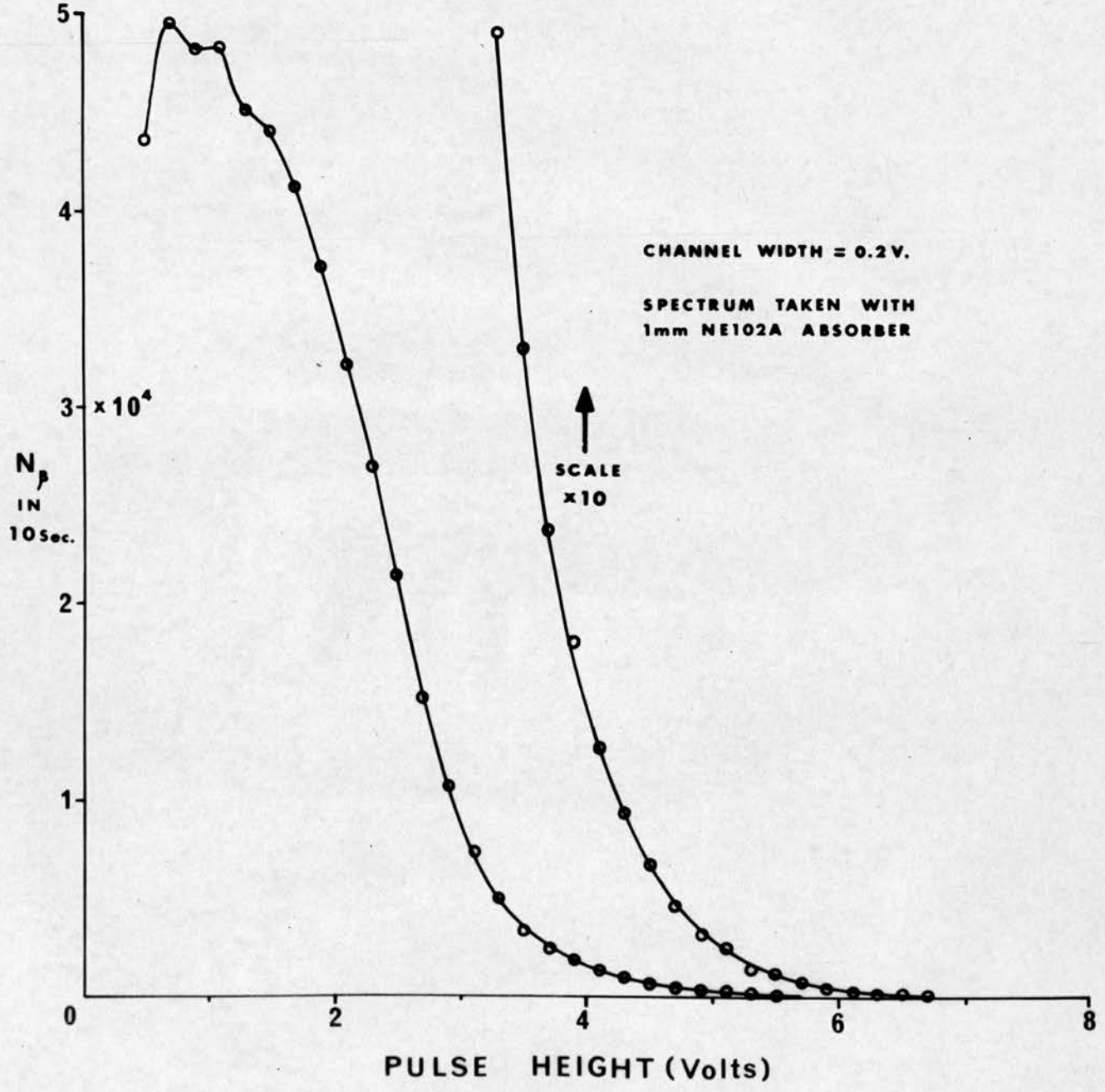
CHANNEL WIDTH = 0.2 V.
SPECTRUM TAKEN WITH
1mm NE102A ABSORBER
SCALE
x10
x 10⁴
N_β
IN
10 Sec.
PULSE HEIGHT (Volts)
0
1
2
3
4
5
6
8

FIGURE 6.4

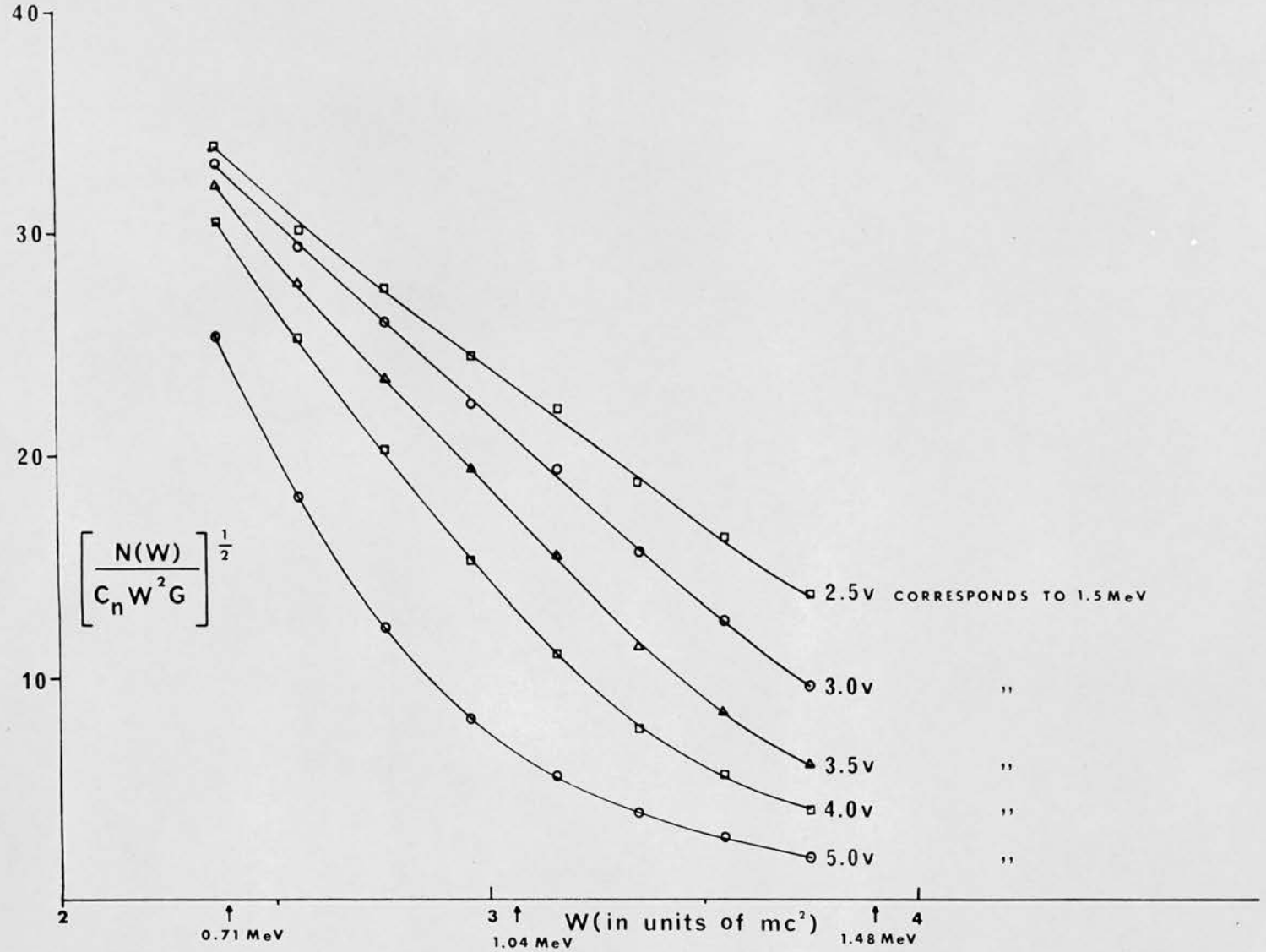
40
30
20
10
$\left[\frac{N(W)}{C_n W^2 G}\right]^{\frac{1}{2}}$
2.5v CORRESPONDS TO 1.5MeV
3.0v ,,
3.5v ,,
4.0v ,,
5.0v ,,
2
3
4
0.71 MeV
1.04 MeV
1.48 MeV
W(in units of mc^2)

FIGURE 6.5

of the stray magnetic field cancellation could be made. Each photomultiplier was replaced in turn by a tangent magnetometer, and the appropriate rheostat adjusted until there was a minimum change of deflection of the magnetometer as the magnet current was reversed. It was possible by this means to obtain an asymmetry in the stray field of a small fraction of the earth's magnetic field.

There remained, however, a considerable asymmetry in the stray magnetic field produced in the two magnet current OFF phases of the experimental cycle, due to remanence.

6.4 Setting the Fast Timing Pulse Generator Discriminator

The threshold levels of the timing pulse generators were set by adjusting their discriminators until the threshold levels were considerably below the thresholds of the corresponding energy selecting single channel analysers. This was checked by seeking a high efficiency of counting coincidences between the fast timing pulses and the corresponding single channel analyser output pulses.

6.5 Fast Pulse Delay Matching

The β and γ fast timing pulses are each delayed behind the arrival of the corresponding β particles and photons by different times which depend upon differences in decay times of the NaI and NE102A scintillators, transit time differences in the photomultiplier tubes, and different discriminator levels in the timing pulse generators. This

difference in delays must be cancelled out before true coincidences can be recorded with highest efficiency. A very accurate method of measuring this relative delay was devised, making use of the automatic cycling system and the routing circuit.

A randomising delay of 30 nS was inserted into the γ channel of the pulse routing unit, and the apparatus set cycling with all settings set as for an actual circular polarisation measurement, with the coincidence adding gate discriminator at "0". The asymmetry

$$\frac{N_c(2nS) - N_c(30nS)}{N_c(2nS) + N_c(30nS)}$$

in the coincidence counts, N_c, was measured as a function of the delay inserted into the fast β channel, and Fig. 6.6 shows the result. The delay at which this asymmetry is zero can be determined to within $\pm$ 1 nS by this method. This β delay, +5.5 nS, then matches the average of the two γ delays, 2nS and 30 nS, which is 16 nS. This shows that the fast β pulses are delayed by 10.5 nS more behind the particle arrival than are the γ pulses. Since prompt coincidences are measured through a 2 nS delay cable in the fast γ pulse routing circuit, a delay cable of 8.5 nS was inserted in the fast γ channel to match the relative delays in the fast channels.

As a check on this method of delay matching, the apparatus was cycled automatically without the matching 8.5 nS cable, and with a randomising delay of 100 nS, which

is much longer than the coincidence unit resolving time; see Fig. 5.11. The asymmetry

$$\frac{N_c(2nS) - N_c(100nS)}{N_c(2nS) + N_c(100nS)}$$

was measured as a function of the delay inserted in the fast β channel. The resulting plot in Fig. 6.7 shows that the peak is centred about -7.5nS, which is very close to the expected -8.5nS. The full width at half maximum of this peak is about 26nS, which agrees well with the coincidence resolving time measured with two random sources and shown in Fig. 5.11.

6.6 Setting the Coincidence Unit Output Delay

The apparatus was once again set cycling with all the settings as for an actual experiment, and the true coincidence counting rate was measured as a function of the coincidence output delay. It can be seen in Fig. 6.8 that an output delay of 1.2μS gives the highest coincidence counting efficiency, although this setting is not highly critical. The resolving time (2τ) of the slow coincidence circuit (slow coincidence portion of NE5704) is quoted by the makers as being 2μS, which agrees quite well with the width of the coincidence curve in Fig. 6.8.

6.7 β-γ Angular Correlation

As a check on the apparatus, a measurement of the integral β-γ angular correlation for the Eu^{152} decay

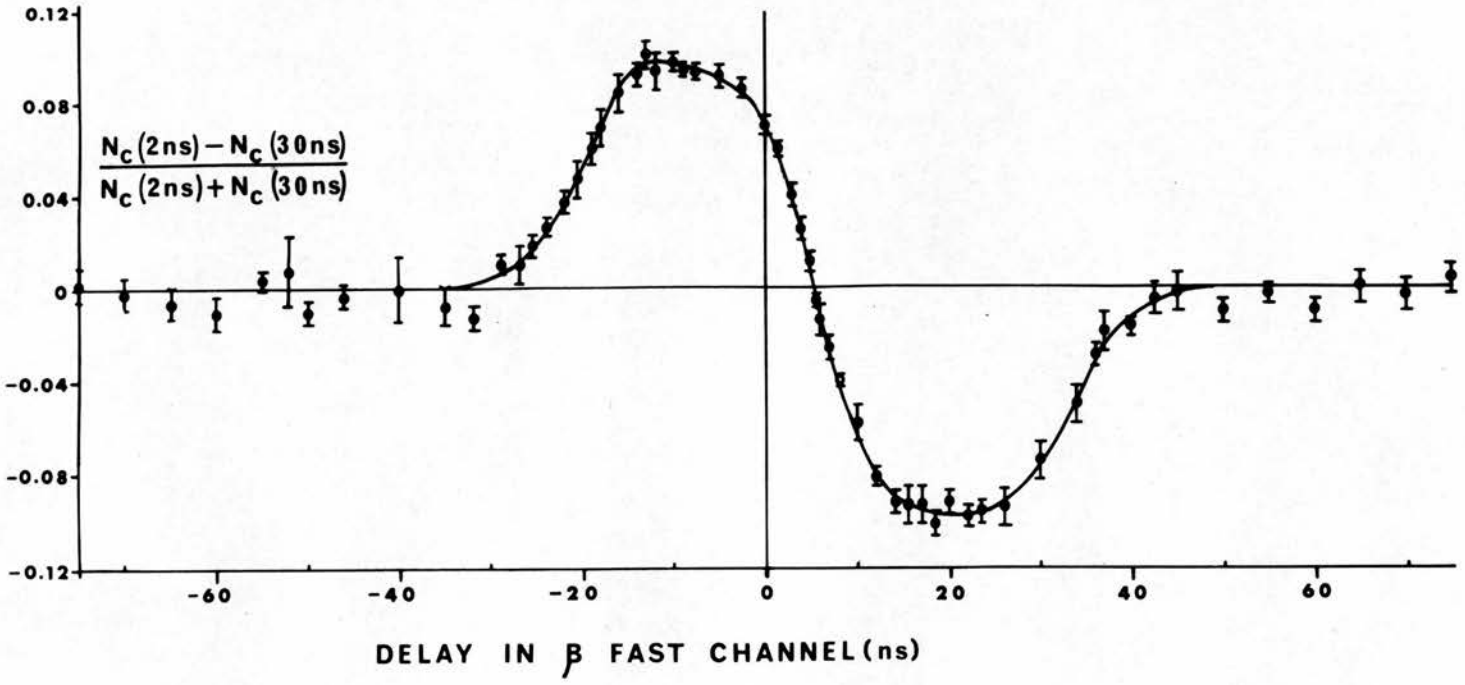
0.12
0.08
0.04
0
-0.04
-0.08
-0.12
$\frac{N_c(2ns) - N_c(30ns)}{N_c(2ns) + N_c(30ns)}$
-60
-40
-20
0
20
40
60
DELAY IN β FAST CHANNEL (ns)

FIGURE 6.6

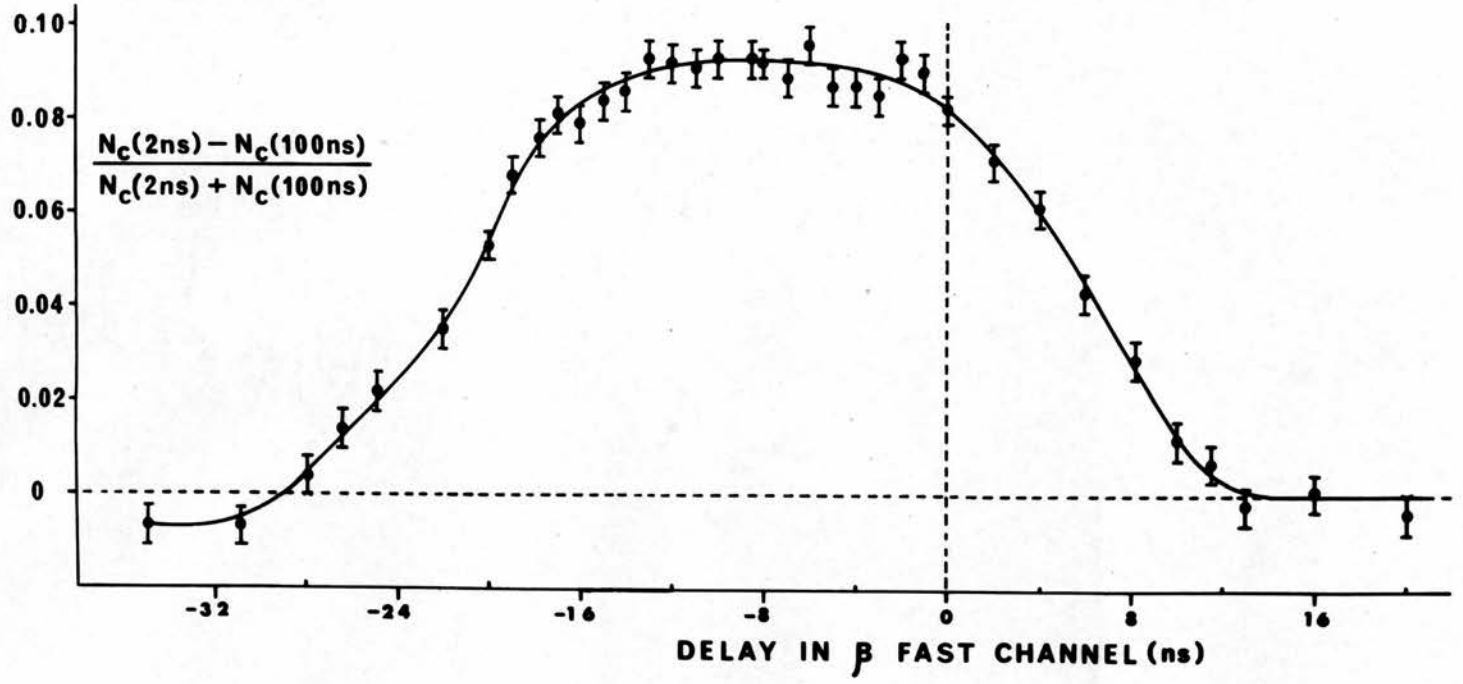
0.10
0.08
0.06
0.04
0.02
0
$\frac{N_c(2ns) - N_c(100ns)}{N_c(2ns) + N_c(100ns)}$
-32
-24
-16
-8
0
8
16
DELAY IN β FAST CHANNEL (ns)

FIGURE 6.7

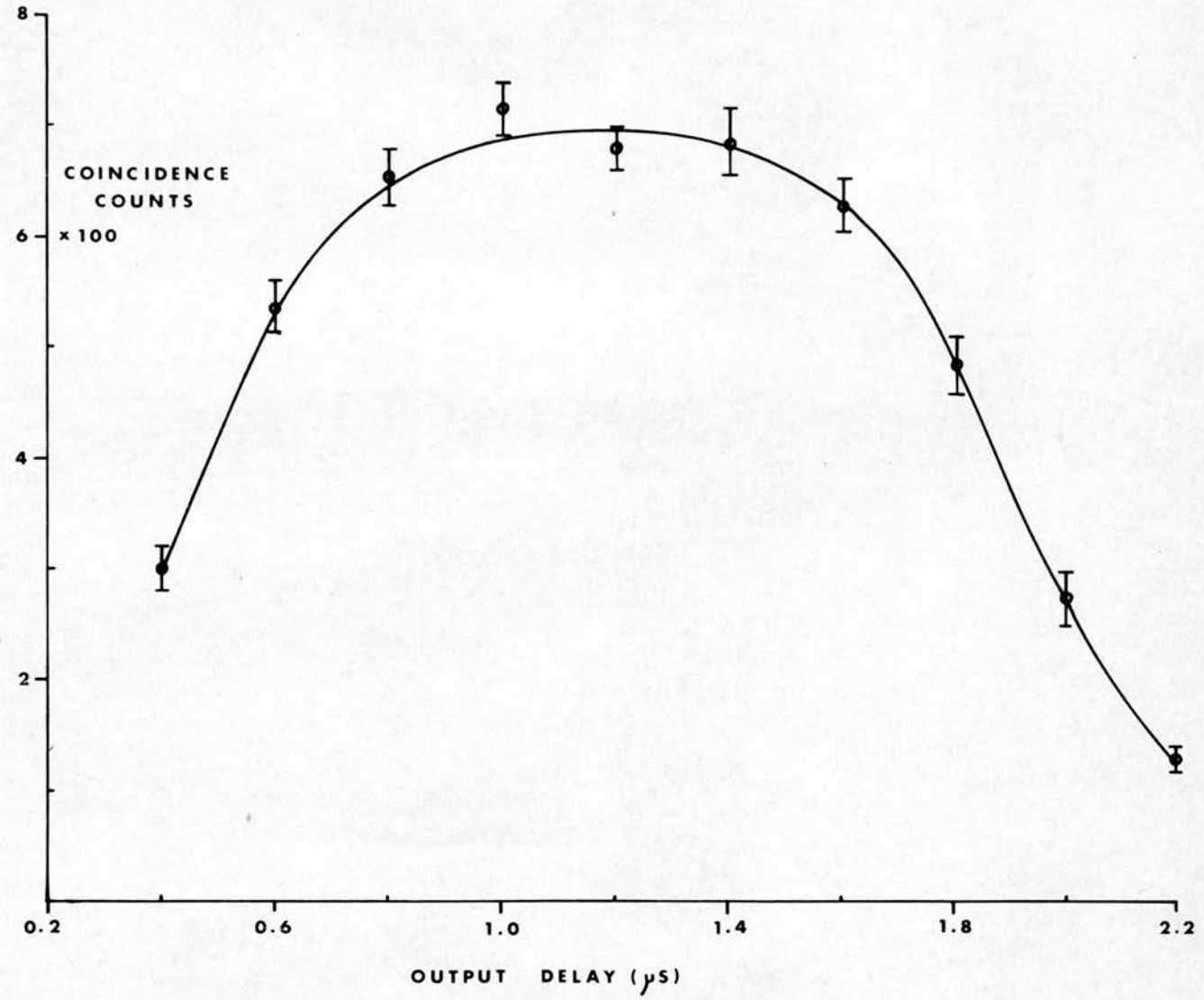
8
6
4
2
COINCIDENCE
COUNTS
x 100
0.2
0.6
1.0
1.4
1.8
2.2
OUTPUT DELAY (μS)

FIGURE 6.8

cascade 3^-(1.48 MeV β^-) 2^+(0.344 MeV γ)0^+ was made without detection of the γ circular polarisation. The integral β-γ directional correlation can be expressed

$$W(\theta_{\beta\gamma}) = 1 + \varepsilon P_2(\cos \theta_{\beta\gamma})$$

where ε is the correlation coefficient. This early experiment (April 1965) was carried out when the apparatus had rather smaller detection solid angles than those of the final version; consequently, the counting rates were rather small, and the accuracy of the correlation was correspondingly low. The γ solid angle ($\frac{\Omega}{4\pi}$) was 3.7×10^{-4}, and the β solid angle was 1.03×10^{-3}.

The γ single channel analyser window of width 60 keV was set on the 344 keV photopeak, while the β discriminator was set to accept all β particles of kinetic energy greater than 0.95 MeV. The energy calibration of the γ counter was established by means of the following γ's : 0.662 MeV from Cs^{137}, 0.51 MeV from Na^{22}, 0.122 MeV and 0.245 MeV from Eu^{152}. The β counter was calibrated using the two conversion electron lines : 0.974 MeV from Bi^{207}, and 0.624 MeV from Cs^{137}.

Counts were taken at each of the angles $\theta_{\beta\gamma}$: 60°, 90°, 105°, 120°, 135°, 150°, 165°, and 180°. At each angle, a measure of the γ-γ + random coincidences was obtained by retaking the counts after an aluminium β absorber had been placed in front of the β counter. The coincidence counts were normalised to the β and γ counts, and the

difference between these normalised counts recorded with and without the aluminium absorber provides a measure of the true β-γ coincidence counts. In practice, the counts were automatically normalised to the γ count by setting the apparatus to print out N_β, N_γ and N_c, and then restart every time the γ scaler reached 10^6. The time for this total to be reached was measured on several occasions during the course of a run, and the average counting time τ calculated. For each count, $N_c/N_\beta N_\gamma$ was worked out, and for each run, the average of this quantity was calculated. This average was converted into a dimensionless quantity by multiplication by τ^{-1}. The difference

$$\left(\frac{N_c\,\tau^{-1}}{N_\beta\,N_\gamma}\right)_{\text{without } A\ell} - \left(\frac{N_c\,\tau^{-1}}{N_\beta\,N_\gamma}\right)_{\text{with } A\ell}$$

is plotted against $P_2(\cos\theta)$ in Fig. 6.9, and the actual results are quoted in Table 6.1.

A least squares linear fit to these points gives

$$\varepsilon = (-0.31 \pm 0.10)$$

which is in agreement with the value

$$\varepsilon = (-0.289 \pm 0.003)$$

obtained by Bhattacherjee and Mitra[30] for β energies greater than 0.95 MeV, and with the value

$$\varepsilon = (-0.32 \pm 0.03)$$

obtained by Scott[31] for β's of energies $\gtrsim$ 1 MeV.

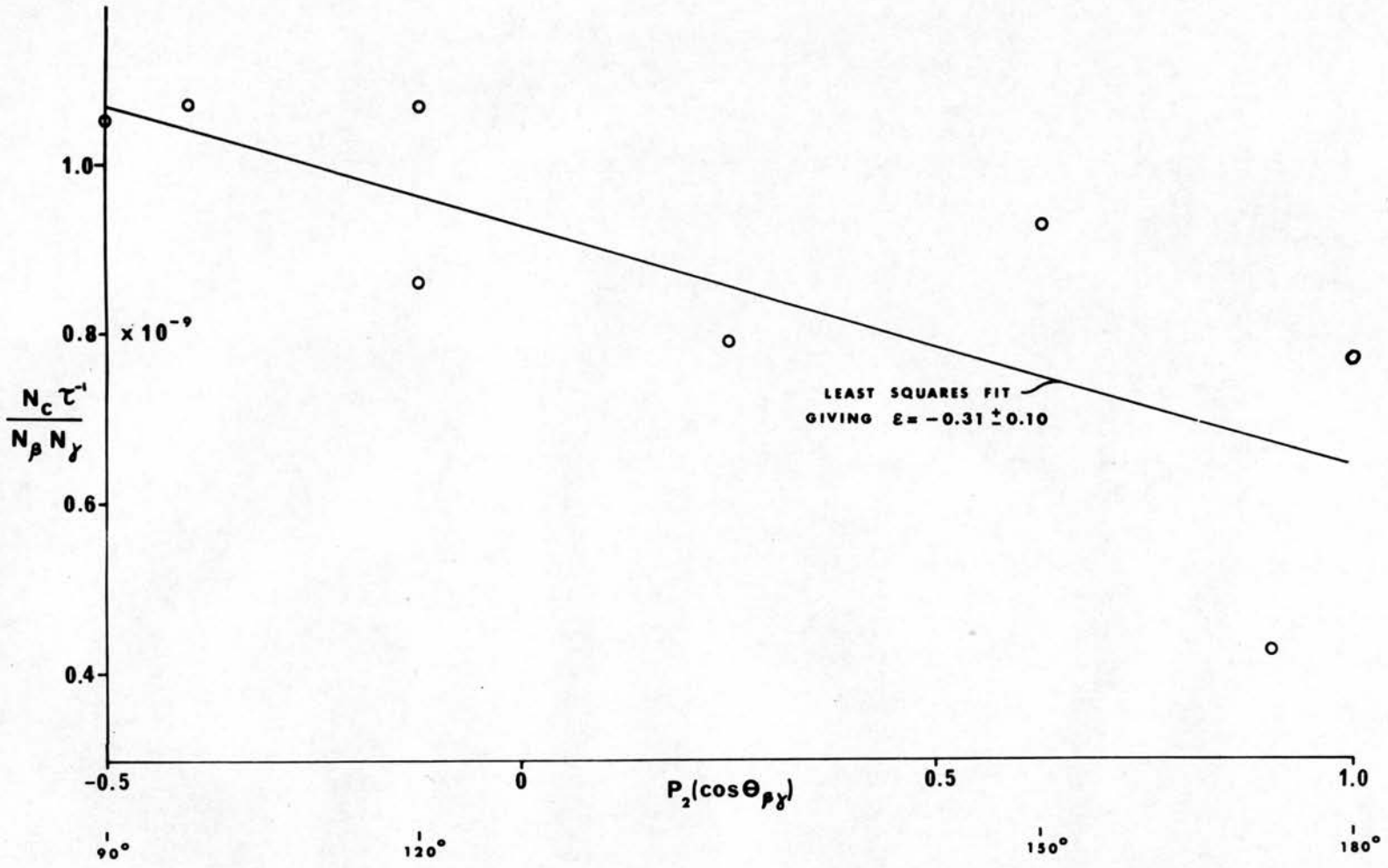
1.0
0.8
x 10⁻⁹
0.6
0.4
N_c τ⁻¹ / N_β N_γ
LEAST SQUARES FIT
GIVING ε = −0.31 ± 0.10
-0.5
0
0.5
1.0
P₂(cos Θ_βγ)
90°
120°
150°
180°

FIGURE 6.9

TABLE 6.1

$\theta_{\beta\gamma}$ °	Aluminium Absorber	N_c	τ min.	Total $\frac{N_c \tau^{-1}}{N_\beta N_\gamma} \times 10^9$	True $\beta - \gamma$ $\frac{N_c \tau^{-1}}{N_\beta N_\gamma} \times 10^9$
135	in	1275	3.98	2.54	0.79
135	out	3659	4.15	3.33	
165	in	1428	4.05	2.57	0.43
165	out	2904	4.20	3.00	
105	in	1129	4.00	2.64	1.07
105	out	4658	4.06	3.71	
60	in	1499	3.98	2.95	0.86
60	out	4026	4.00	3.81	
180	in	763	3.93	2.78	0.77
180	out	11314	3.91	3.55	
150	in	1033	3.93	2.62	0.93
150	out	7956	3.92	3.55	
120	in	1171	3.91	2.93	1.07
120	out	6307	3.88	4.00	
90	in	1264	3.98	3.08	1.05
90	out	5791	3.98	4.13	

The poor accuracy of the present result, and the small solid angles used, do not justify the application of corrections (amounting at most to a few per cent) for finite solid angles, and a β contribution from the next highest β group with end-point energy 1.05 MeV and intensity about one sixth that of the highest β group.

The present value of ε is, however, rather smaller in magnitude than the values implied by the differential results of most other workers. Since the magnitude of ε increases as the β energy increases, $|\varepsilon|$ as measured for all β's of energy greater than 0.95 MeV must be larger than the differential measurement of $|\varepsilon|$ at a β energy of 0.95 MeV. The papers of Dulaney et al.[32], Sunier et al.[33], Sunier[34], Fischbeck and Wilkinson[35], and the more recent results of Bhattacherjee and Mitra[36], quote differential values of ε measured at a β energy of 0.95 MeV ranging from - 0.29 to - 0.40.

The discrepancy between the present integral value of ε and the differential results quoted above is no doubt due to the rather oversimplified correction applied here to take account of unwanted γ-γ and accidental coincidences. The fact that a large negative correlation coefficient, not inconsistent with all other measurements, was obtained gave confidence in the apparatus and the content of the source.

6.8 Day-to-Day Running of the Apparatus

Each collection of circular polarisation data from the apparatus was limited to one day, because at the end of

this time about 100 yards of punched paper tape had been collected, and tapes much longer than this tend to give rise to reading troubles at the computer input.

The β channel was set to accept all β's of energy ≥ 0.7 MeV, and the γ channel was set with a $\pm$ 10% "window", (in other words photons with energies between 310 keV and 378 keV were accepted.). The distance between the magnet core and the NaI crystal was kept at 3 cm.

At the start of each day's run, the initial phase of the counting cycle was set so that the magnetic field pointed towards the γ counter. The system was then set running with each count (or phase of the cycle) occupying 100 seconds. After 24 hours or so, the apparatus was stopped at the end of a complete cycle, and the data tape removed for processing

If, at any time, it was noticed that the singles counting rates had changed appreciably, the apparatus was stopped at the end of a cycle, and the counters recalibrated; the γ counter by means of a Na^{22} source, and the β counter by the simple technique of altering the discriminator level until the original counting rate was restored.

The current through the magnet windings was maintained at 1.4 amps throughout the experiment - only very occasional adjustment of the series rheostat was found necessary.

CHAPTER 7

THE EXPERIMENTAL RESULTS

7.1 Counting Rates

The counting rates were made as high as possible in order to obtain a statistically significant measurement of the coincidence counting asymmetry. To this end, the β particle acceptance angle had to be increased to $\pm 48^{\circ}$, making a root mean square angle of acceptance of $\pm 34^{\circ}$. The fractional solid angle $(\frac{\Omega\beta}{4\pi})$ subtended at the source by the β counter was then 0.17, whereas the γ solid angle $(\frac{\Omega\gamma}{4\pi})$ was 1.2×10^{-3}. This meant that considerable pulse pile-up in the β channel had to be endured, as has been described in paragraph 6.2. The recorded counting rates were then of the order of

N_β	48×10^3 per second
N_γ	2.3×10^3 per second
N_c	7 per second.

7.2 Data Processing

The counts recorded on punched tape by the ASR 33 were processed daily by the KDF 9 computer of the Edinburgh Regional Computing Centre. For convenience, let the various counts be labelled as follows:

Field up : $N_\beta = A$, $N_\gamma = B$, $N_c = C$

Field off : $N_\beta = D$, $N_\gamma = E$, $N_c = F$

Field down : $N_\beta = G$, $N_\gamma = H$, $N_c = J$

Field off : $N_\beta = K$, $N_\gamma = L$, $N_c = M$

In the present apparatus, "Field up" corresponds to the magnetisation of the transmission magnet core pointing towards the γ counter; and since magnetisation and electron spin are antiparallel this counting phase corresponds to $\psi = 180^\circ$.

The computer sums these counts over all complete cycles (taking account of prescaling factors), and normalises all coincidence counts, N_c, to the simultaneously recorded singles counts, N_β and N_γ, therby eliminating instrumental asymmetries caused by gain drifts, stray magnetic fields, and misalignment of the source. The following asymmetries are calculated for every complete counting cycle (each day containing about 200 such cycles):

i) asymmetry in γ counts with field reversal

$$\frac{B - H}{B + H} \quad ;$$

ii) asymmetry in total coincidence counts with field reversal

$$\frac{\frac{C}{AB} - \frac{J}{GH}}{\frac{C}{AB} + \frac{J}{GH}}$$

because C and J are the coincidence counts recorded when the angle ψ is 180° and 0° respectively, this asymmetry is of opposite sign to the asymmetry E calculated in paragraph 4.4.

iii) ratio of true to random coincidences, $\frac{N_c\,(\text{true})}{N_c\,(\text{random})}$

$$\frac{\frac{C}{AB} + \frac{J}{GH} - \frac{F}{DE} - \frac{M}{KL}}{\frac{F}{DE} + \frac{M}{KL}} \quad ;$$

iv) The "magnetic length" of the magnet, $-\left(\frac{a_c\sqrt{L}}{2}\right)^2$

$$\frac{E + L - B - H}{E + L + B + H} \quad .$$

The average of these quantities over all complete counting cycles is then taken, and the standard deviation of the means of (ii) and (iii) calculated from the distributions of the individual results. The asymmetry of the true coincidences is then calculated according to the relation:

asymmetry in true coincidences

$$= \left(1 + \frac{N_c(\text{random})}{N_c(\text{true})}\right)\left(\begin{array}{c}\text{asymmetry in total}\\ \text{coincidences}\end{array}\right)$$

from the calculated means of the two factors. The standard deviation of this product is calculated from the standard deviation of each factor.

The computer, having summed the β, γ, and coincidence

counts recorded during each of the four phases of the counting cycles, then calculates the above four asymmetries using these total counts. If the data sampling time has been sufficiently short to eliminate the effects of instrumental drifts, then it is to be expected that the average asymmetries should agree reasonably well with the total count asymmetries. The agreement between these two daily values of the asymmetries was normally very good (they seldom differed by more than about 20%), and this was taken as showing that the sampling time of 100 seconds was sufficiently short to eliminate the effects of drifting of the electronics. Occasionally, there was a very large difference between the two values, and since these discrepancies usually arose when the laboratory temperature was abnormally high, it was concluded that the reason was malfunctioning of the electronics under such conditions.

When the counting at each angle had been completed, the daily results were compounded into mean results, and in the case of the asymmetries (ii) and (iii), which have calculated standard deviations, weighted means were calculated. The weights attached to the individual results were the inverse squares of the corresponding standard deviations, following the formulae of Topping[37].

7.3 Instrumental Results

a) Gamma Singles Asymmetry

Considerable care was taken to shield the γ photomultiplier from the cycling stray magnetic field of the

magnet, in order to aid the measurement of the magnetic length of the magnet. How successful this shielding was is shown in Table 7.1, where it can be seen that the asymmetry of the γ singles counts between the opposite magnetic field directions has been reduced to a few parts in 10^5. At 180° and 140°, where the counting times were longest, the residual asymmetry has been reduced to within the statistically expected uncertainty in the asymmetry. This statistical uncertainty is, since B is very nearly equal to H, given by

$$\frac{1}{\sqrt{B' + H'}} = 0.25 \times 10^{-4}$$

where B' and H' are the total number of gammas recorded. In Table 7.1, the quoted uncertainty is the standard deviation of the set of daily values, and the agreement with the statistically expected uncertainty is excellent.

For comparison, the following results were recorded without the bucking coil on the γ counter:

		Asymmetry in γ singles
With one magnetic shield	7 days counting	$(3.5 \pm 0.9) \times 10^{-4}$
With four magnetic shields	1 days counting	$(-5 \pm 1) \times 10^{-4}$

It appears, therefore, that increasing the number of magnetic shields had no beneficial effect; whereas, adding a bucking coil reduced the effect by at least an order of magnitude.

TABLE 7.1

$\theta'_{\beta\gamma}$ (degrees)	Date	Duration of count (days)	γ Singles Asymmetry	$-(\frac{a_c\sqrt{L}}{2})^2$ "Magnetic Length"
180	July/August 1968	23	$(+0.11 \pm 0.25)10^{-4}$	$(-0.5 \pm 0.3)10^{-4}$
160	September 1968	4	$(+0.23 \pm 0.15)10^{-4}$	$(+0.21 \pm 0.17)10^{-4}$
140	August 1968	16	$(-0.11 \pm 0.25)10^{-4}$	$(-5 \pm 3)10^{-4}$
120	September 1968	3	$(+1.5 \pm 1.2)10^{-4}$	$(-0.5 \pm 0.5)10^{-4}$
90	September 1968	3	$(-0.47 \pm 0.54)10^{-4}$	$(-0.5 \pm 0.4)10^{-4}$
140 γ-γ	September 1968	8	$(+0.21 \pm 0.45)10^{-4}$	$(-0.36 \pm 0.26)10^{-4}$

$\theta'_{\beta\gamma}$ = angle between the axes of the β and γ counters.

b) "Magnetic Length"

The conclusion reached in paragraph 4.9 that under the experimental conditions used here (in particular, a γ-ray energy of 344 keV), it is impossible to measure the magnetic length of the transmission magnet using the γ singles counts, is confirmed by the large variation in the results of such measurements quoted in Table 7.1. Once again, the quoted uncertainty is the root mean square deviation of the daily values about their weighted mean. The expected statistical uncertainty in the quantity labelled "Magnetic Length" is $\pm$ 0.2 x 10^{-4}, for 20 days counting.

c) The Polarisation-Detection Efficiency of the Magnet

The demonstration, in the preceding paragraph and in paragraph 4.9, of the failure to measure the polarisation-detection efficiency of the magnet, forces one to calculate this quantity, if the coincidence asymmetries are to be converted into γ-ray circular polarisations.

The details of the transmission magnet geometry are (see Fig. 5.2):

total length, L, = 4.1 cm. (3.3 mean free paths for 344 keV photons)

core length, ℓ, = 2.5 cm.

thickness of each cheek plate, t, = 0.8 cm.

Using Chesler's experimentally determined constant

C = 0.17, then gives:

magnetic length, LM, = 2.8 cm ;

and using $(\sigma_c)_{344\ keV} = 0.3331 \times 2\pi r_o^2$

along with the constants listed in paragraph 4.7(b), leads to:

$$a_c\sqrt{L} = 0.819 \times 10^{-2}, \text{ uncorrected for scattering.}$$

Referring to the expression

$$\psi' = \frac{\bar{b}Ln}{(1 + \bar{a}Ln)}$$

for the single scattering correction quoted in paragraph 4.7(b); since the quantity b contains the factor $\underline{k}_o \cdot \underline{S}$, on integrating over the length of the magnet some average of this factor must be inserted to take account of magnetic end effects. However, this is similar to the averaging of $p(x) \cos \psi(x)$ which occurs in the expression for the magnetic length of the magnet, and so the length, L, appearing in the numerator of the expression for ψ' should be replaced by the magnetic length, LM, when end effects are taken account of. When this substitution has been made, then, of course, $\underline{k}_o \cdot \underline{S}$ must be set equal to $k_o S$. Because the quantity a contains no spin-dependent factor, the length appearing in the denominator of ψ' remains the total length, L.

These considerations then lead to, for the transmission magnet used here, and 10% energy discrimination:

$$a_c\sqrt{L} = 0.910 \times 10^{-2} \text{ (corrected for single scattering).}$$

And when the calculations are extended to account for a multiple scattering correction:

$$\alpha_c\sqrt{L} = 0.938 \times 10^{-2} \quad \text{(corrected for multiple scattering).}$$

This latter efficiency will be taken as the calculated polarisation-detection efficiency of the transmission magnet when calculating the circular polarisation, P_c, of the γ-rays. The uncertainty in this calculation of the magnet efficiency is largely due to the uncertainty in knowing the behaviour of the magnetisation, and hence the magnetic length. With the difference between the expected value of 0.25 and the measured value of 0.17 for Chesler's constant, C, as a rough measure of the uncertainty in estimating the contribution of the magnet cheek plates to the magnetic length, the uncertainty in the magnetic length is then

$$(0.25 - 0.17)(0.8)(2) \text{ cm.} = 0.13 \text{ cm., or } 5\% .$$

A rough estimate of the uncertainty in the polarisation-detection efficiency of 10%, will then take account of the unknown fringe field effects, and also the uncertainty, due to the approximations, in the multiple scattering correction calculation.

The calculated value of $-\left(\frac{\alpha_c\sqrt{L}}{2}\right)^2$ is then -0.22×10^{-4}, which is considerably lower than the mean of the experimental "magnetic lengths".

7.4 The Circular Polarisation Results

Table 7.2 displays the coincidence asymmetry measurements, and the γ circular polarisation, P_c, obtained from these results and the calculated polarisation-detection efficiency of the magnet. Figures 7.1 and 7.2 show the daily results of the measured true coincidence asymmetry in chronological order for each angle $\theta'_{\beta\gamma}$.

The two values quoted in Table 7.2 for the asymmetry in the true coincidences are calculated from the data in different ways. The upper number is the weighted mean of the daily products of $(1 + \frac{N_{CR}}{N_{CT}})$ and (asymmetry in total coincidences), while the lower number is the result of multiplying the separately evaluated weighted means of each of these two factors. If the apparatus is working satisfactorily, then these two estimates are expected to agree. In fact, these two differently calculated values agree very well at all angles except 140°, where there is a very large discrepancy between them, suggesting malfunctioning of the apparatus. Indeed, when the daily results for 140° were examined, it was found that the random to true coincidence rate ratio showed very large variations from day to day. A range of $\frac{N_{CR}}{N_{CT}}$ from 0.3 to 15 existed, which compared very unfavourably with the spread of from 7.6 to 8.6 at 180°.

The reasons for this peculiar behaviour at 140° could be gross drifting of the coincidence resolving time,

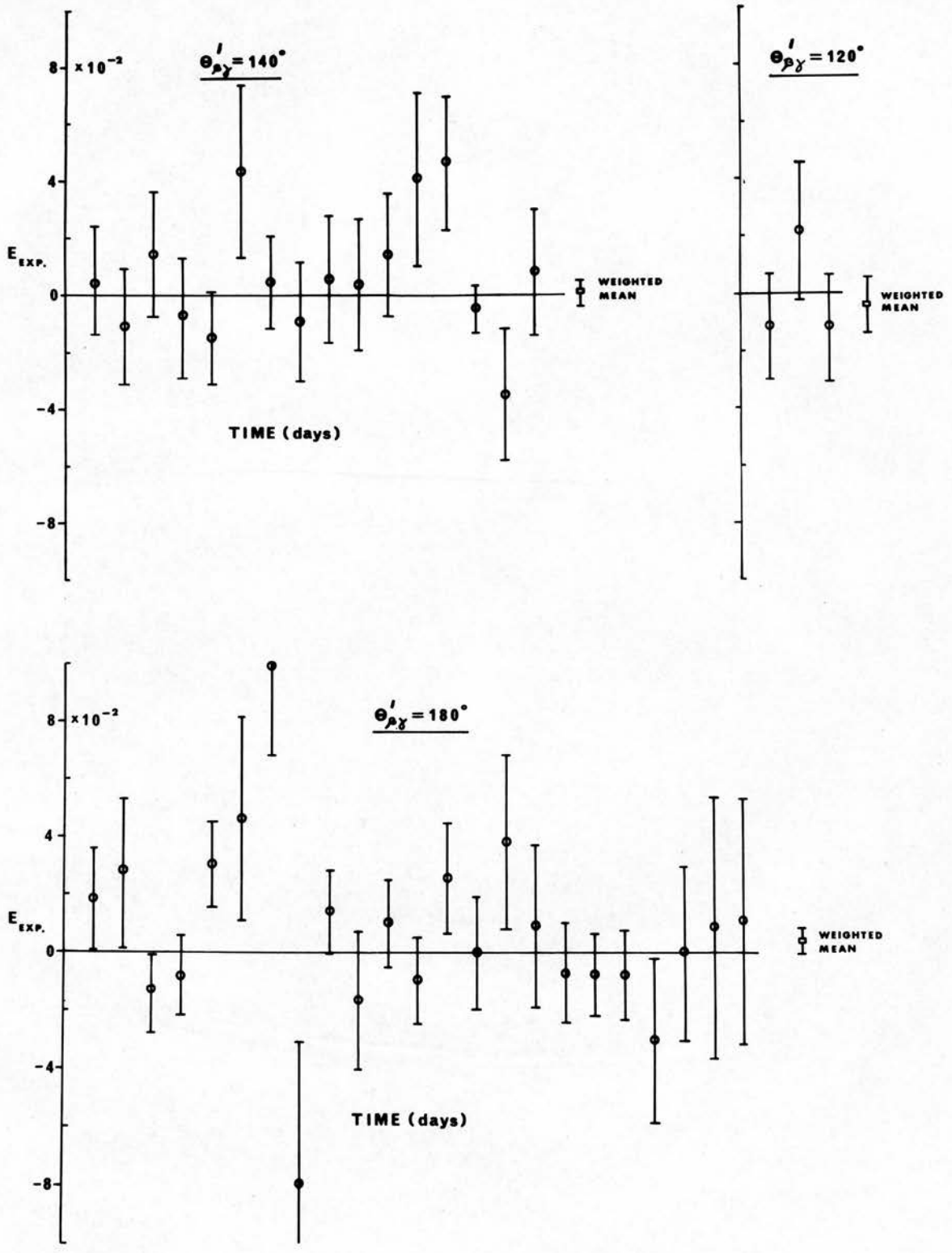
8
x10⁻²
$\theta'_{p\gamma} = 140°$
4
$E_{EXP.}$
0
-4
-8
TIME (days)
WEIGHTED MEAN
$\theta'_{p\gamma} = 120°$
WEIGHTED MEAN
8
x10⁻²
$\theta'_{p\gamma} = 180°$
4
$E_{EXP.}$
0
-4
-8
TIME (days)
WEIGHTED MEAN

FIGURE 7.1

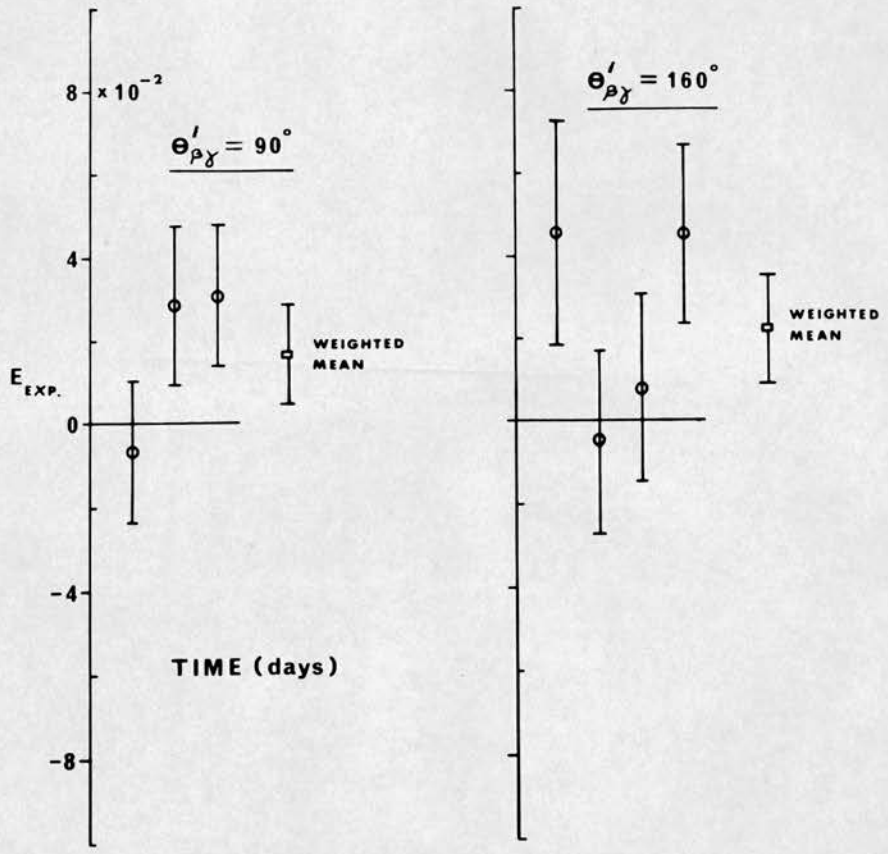
8
x 10⁻²
4
0
-4
-8
E EXP.
θ'βγ = 90°
WEIGHTED MEAN
TIME (days)
θ'βγ = 160°
WEIGHTED MEAN

FIGURE 7.2

severe gain shifts in the γ channel causing drifting of the γ window away from the 344 keV peak, or else a combination of both. The occurrence of values for $\frac{N_{CR}}{N_{CT}}$ of as low as 0.3 suggests the former suggestion. Certainly, during August, when the 140° counts were recorded, the laboratory temperature often rose abnormally high. Whatever the reason, it was decided that, in the case of the 140° measurements, the value of the asymmetry in the true coincidence counts obtained from the product of the two weighted means, i.e. the lower number, was more valid than the upper number, because at 140° each of these two weighted means and their product was typical of the corresponding values obtained at other angles, whereas the upper quoted number is highly untypical when compared with its counterparts. Complete justification of this choice must remain tentative until a thorough analysis of the 140° data has been carried out.

P_c is plotted as a function of $\theta_{\beta\gamma}$ in Fig. 7.3, where the angular error flags give the uncertainties in the mean angles $\theta_{\beta\gamma}$, which are estimated to be about $\pm$ 3 degrees.

When $\theta'_{\beta\gamma}$ was set experimentally at 180°, the presence of the large β solid angle meant that the mean angle of acceptance was about 30°; so the result listed in Table 7.2 under $\theta'_{\beta\gamma} = 180^{\circ}$ has been plotted at $\theta_{\beta\gamma} = 150^{\circ}$. The ~~dotted~~ curve in Fig. 7.3 is a typical theoretical curve given by Alexander and Steffen[10], and is drawn here for comparison, to give the expected magnitude of P_c.

TABLE 7.2

$\theta'_{\beta\gamma}$ degrees	Total Coincidences per Phase	Random to True Coincidences $\frac{N_{CR}}{N_{CT}}$	Asymmetry in Total Coincidences	Asymmetry in True Coincidences	P_c
180°	5×10^6	7.91 ± 0.05	$(+0.50 \pm 0.50) 10^{-3}$	$(+0.43 \pm 0.45) 10^{-2}$ or $(+0.45 \pm 0.45) 10^{-2}$	$+0.46 \pm 0.52$
160°	6×10^5	12.3 ± 0.3	$(+2.0 \pm 1.0) 10^{-3}$	$(2.2 \pm 1.3) 10^{-2}$ or $(2.7 \pm 1.4) 10^{-2}$	2.3 ± 1.6
140°	2×10^6	8.8 ± 0.5	$(+0.64 \pm 0.54) 10^{-3}$	$(+0.09 \pm 0.43) 10^{-2}$ or $(0.63 \pm 0.56) 10^{-2}$	0.67 ± 0.66
120°	5×10^5	9.4 ± 0.3	$(-0.38 \pm 0.96) 10^{-3}$	$(-0.41 \pm 0.99) 10^{-2}$ or $(-0.40 \pm 0.99) 10^{-2}$	0.4 ± 1.1
90°	4×10^5	8.38 ± 0.06	$(+0.18 \pm 0.13) 10^{-3}$	$(+1.7 \pm 1.2) 10^{-2}$ or $(+1.7 \pm 1.2) 10^{-2}$	$+1.8 \pm 1.3$
140° γ-γ	4×10^5	44 ± 3	$(-0.3 \pm 0.7) 10^{-3}$	$(-2.6 \pm 2.8) 10^{-2}$ or $(-1.3 \pm 3.0) 10^{-2}$	

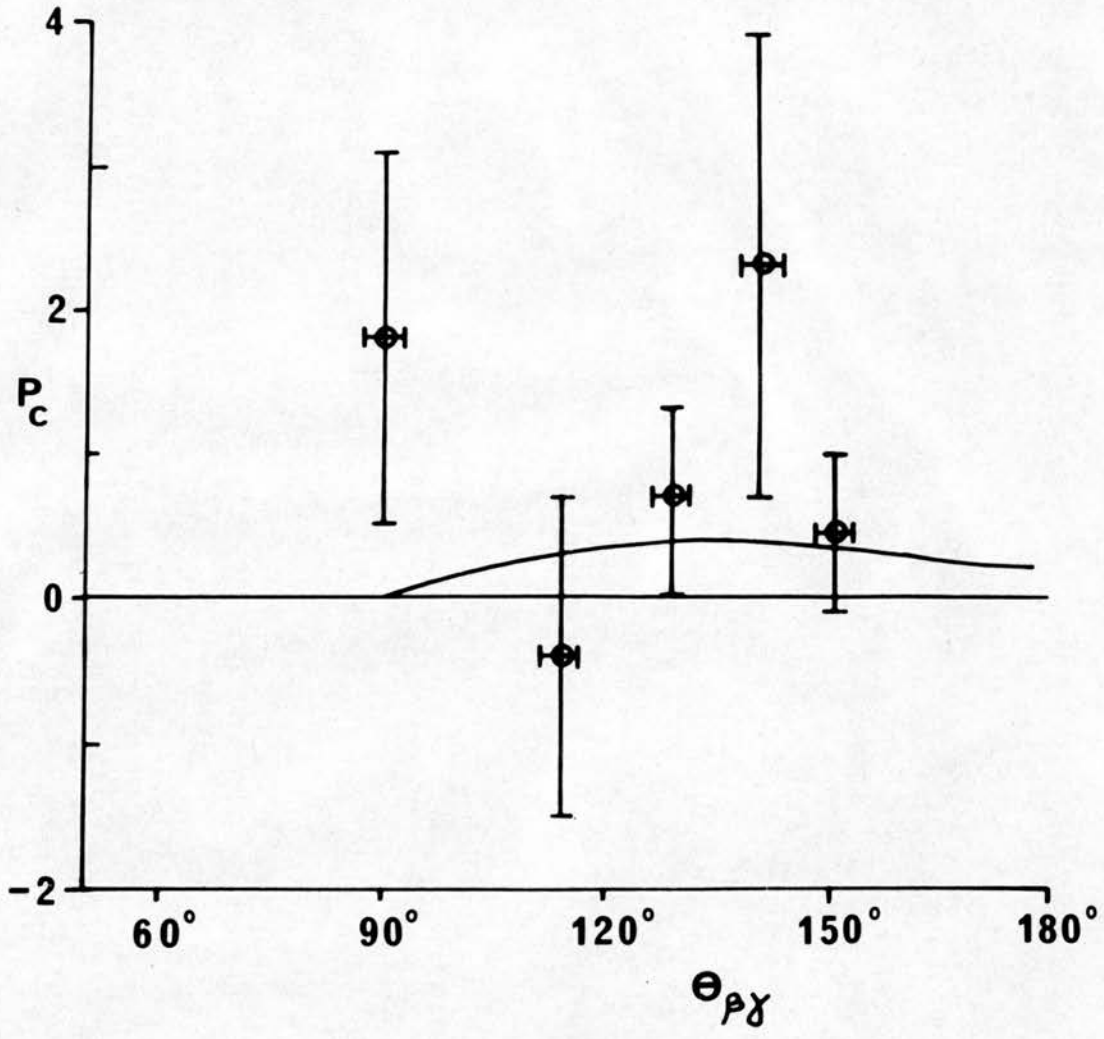

FIGURE 7.3

Table 7.2 also contains the result of an experimental estimate of the contribution to the coincidence counts from γ-γ coincidences. A $\frac{1}{2}$" thick perspex sheet placed immediately in front of the β counter filtered off all the β particles. The significance of this measurement is that from the large ratio of random to true coincidences it can be inferred that γ-γ coincidences contribute, at most, about 20% of the total coincidences.

7.5 Discussion of the Results

The very large spread and the uncertainty in the measured values of P_c, as shown in Fig. 7.3, unfortunately prevent a meaningful evaluation of the correlation coefficients $A_1(W)$ and $A_3(W)$ being carried out. This failure to be able to extract nuclear information from circular polarisation measurements on this β-γ cascade is not without precedent. Collin, Daniel and Schmitt[38] obtained rather a poor result for this measurement, and gave no satisfactory reason or any discussion. On the other hand, Alexander and Steffen[10] measured β-γ directional and β-circularly polarised γ correlations for this cascade, and from their results and the log ft value (corrected for the non-statistical spectrum shape) they were able to extract values for the matrix elements. These successful measurements of P_c carried an uncertainty of about 20 to 30%. An earlier result obtained by Berthier et al.[39], who also used the forward scattering method,

was also sufficiently accurate to enable values of the nuclear matrix elements to be extracted.

By far the largest sources of uncertainty in the results of this experiment have been due to poor counting statistics and instrumental drifts - the problem of knowing accurately the magnetic length of the magnet has proved to be relatively insignificant. From the observed coincidence counts, the uncertainty expected statistically in the asymmetry in the total coincidence rates is about 0.3×10^{-3} for 20 days counting. The standard deviations measured at 180° and 140° (where the counting time was about 20 days) are about twice this expected magnitude, showing that instrumental effects are contributing significantly to the uncertainties in the results.

Examination of the chronological plotting of the daily results in Fig. 7.1 and Fig. 7.2 suggests that there may well be some long term trends in the data. When more counts have been collected at angles other than 180°, the daily results will be scrutinised for such trends, which will then be removed using the techniques described by Cruse and Hamilton[40].

When this project was being planned, it was not fully appreciated that the superabundance of γ rays of energy greater than 344 keV emitted from a Eu^{152} source would make such a large scattered contribution to the γ count at 344 keV. Fig. 6.2 and Fig. 6.3 give an indication of the magnitude of this effect. Also, since the β group being investigated has only a 6% feed, it has been necessary to

use a strong Eu^{152} source, thus increasing this troublesome γ background. Another reason why a strong source of 6 mC was necessary is that, in the transmission method of circular polarisation measurement, severe attenuation of the γ ray beam occurs on passage through the iron. In the forward scattering method this problem does not arise to such an extent, and the collected γ intensity can therefore be much higher. In addition, the polarisation-detection efficiency of a forward scattering magnet can be as high as 8%[18], compared with about 3% for a transmission magnet; (1% in the present case).

The strong source, which had to be employed, introduced electronic problems arising from the resulting high β counting rates. The pulse pile-up problem has already been referred to in paragraph 6.2, and the large number of random coincidence counts (obvious from the measured values of $\frac{N_{CR}}{N_{CT}}$ quoted in Table 7.2) gave rise to a very large "noise" contribution to the available information. If it had been possible to reduce the coincidence resolving time, say to $2\tau = 10$ nS, then a considerable improvement in the "signal to noise ratio" could have been made. This was not possible, however, because the photomultiplier tubes, which were chosen to be of the "venetian blind" type of construction to minimise the effects of stray magnetic fields, unfortunately exhibited a large time spread.

The limitation of the coincidence counting rate due to

photon absorption in the transmission magnet is a feature of this method of measuring photon circular polarisation which makes it rather less suitable than the forward scattering method for measuring β-γ correlations in many cases. However, the transmission method has been extensively used in experiments which investigate the circular polarisation of bremsstrahlung and of γ rays emitted in transitions between nuclear levels containing parity admixtures[41,42].

ACKNOWLEDGEMENTS

I am grateful to Professor N. Feather, F.R.S., for making available the facilities of the Department of Natural Philosophy.

I am most indebted to Dr. J. Byrne, M.Sc., Ph.D., who suggested this topic for research, for his encouragement and for valuable discussions on many aspects of the work. I also wish to thank Mr. J. Kyles, O.B.E., M.A., F.R.S.E., for supervising this work from October 1966 onwards.

My thanks go to the ex-head of the workshop, Mr. A. Headridge, and his staff, for their help in constructing the mechanical parts of the apparatus; and to Dr. G. Bradford and Mr. C. McAnna, of the electronics workshop, for designing and constructing the prescaler to my specifications.

REFERENCES

1. E. Fermi, Z. f. Physik 88, 161, 1934.
2. E.J. Konopinski and G.E. Uhlenbeck, Phys. Rev. 48, 7, 1935.
3. E.J. Konopinski and G.E. Uhlenbeck, Phys. Rev. 48, 107, 1935.
4. T.D. Lee and C.N. Yang, Phys. Rev. 104, 254, 1956.
5. H.A. Weidenmüller, Rev. Mod. Phys. 33, 574, 1961.
6. R.A. Beth, Phys. Rev. 50, 115, 1936.
7. H.J. Lipkin, Beta Decay for Pedestrians, North Holland, 1962.
7. T. Kotani, Phys. Rev. 114, 795, 1959.
8. Nuclear Data Sheets 5-6-31 and 5-6-32, April 1964.
9. P. Lipnik and J.W. Sunier, Nuc. Phys. 53, 305, 1964.
10. P. Alexander and R.M. Steffen, Phys. Rev. 128, 1783, 1962.
11. O. Halpern, Nature 168, 782, 1951.
12. F.P. Clay and F.L. Hereford, Phys. Rev. 85, 675, 1952.
13. J.C. Wheatley et al., Physica 21, 841, 1955.
14. H. Schopper, Phil. Mag. 2, 710, 1957.
15. P. Saintignon, Ph.D. Thesis, University of Grenoble, 1964.
16. S.B. Gunst and L.A. Page, Phys. Rev. 92, 970, 1953.
17. A. Lundby et al., Nuovo Cimento 6, 745, 1957.
18. H. Schopper, Nuc. Inst. and Meth. 3, 158, 1958.
19. R.B. Chesler, Nuc. Inst. and Meth. 37, 185, 1965.
20. H. Schopper, Nuc. Inst. and Meth. 21, 338, 1963.
21. W.H. McMaster, Rev. Mod. Phys. 33, 8, 1961.
22. E.C. Stoner, Magnetism and Matter, Methuen, 1934.
23. R.L. Graham and J.S. Geiger, Can. J. Phys. 39, 1357, 1961.
24. L.G. Mann et al., Phys. Rev. 137, B1, 1965.

REFERENCES (Contd.)

25. C.M. Davisson, in Beta- and Gamma-Ray Spectroscopy, North Holland, 1955. Edited by K. Siegbahn.

26. R.N. Larsen and E.B. Shera, Nuc. Inst. and Meth. 32, 168, 1965.

27. B. Righini, Nuc. Inst. and Meth. 29, 89, 1964.

28. L.M. Langer and D.R. Smith, Phys. Rev. 119, 1308, 1960.

29. M.E. Rose et al. in α, β, γ Ray Spectroscopy, North Holland, 1965. Edited by K. Siegbahn.

30. S.K. Bhattacherjee and S.K. Mitra, Nuovo Cimento 16, 175, 1960.

31. R.D. Scott, Ph.D. Thesis, University of Edinburgh, 1967.

32. H. Dulaney et al., Phys. Rev. 117, 1092, 1960.

33. J.W. Sunier et al., Nuc. Phys. 19, 62, 1960.

34. J.W. Sunier, Helv. Phys. Acta, 36, 429, 1963.

35. H.J. Fischbeck and R.G. Wilkinson, Phys. Rev. 120, 1762, 1960.

36. S.K. Bhattacherjee and S.K. Mitra, Phys. Rev. 126, 1154, 1962.

37. J. Topping, Errors of Observation and their Treatment, The Institute of Physics, 1960.

38. W. Collin, H. Daniel and H. Schmitt, Z. f. Physik, 179, 528, 1964.

39. J. Berthier et al., Compt. rend. 252, 257, 1961.

40. D.W. Cruse and W.D. Hamilton, Nuc. Inst. and Meth. 57, 29, 1967.

41. F. Boehm and E. Kankeleit, Phys. Rev. Lett. 14, 312, 1965.

42. V.M. Lobashov et al., J.E.T.P. Lett. 3, 47, 1966.